Distribution Agreement

In presenting this thesis or dissertation as a partial fulfillment of the requirements for an advanced degree from Emory University, I hereby grant to Emory University and its agents the non-exclusive license to archive, make accessible, and display my thesis or dissertation in whole or in part in all forms of media, now or hereafter known, including display on the world wide web. I understand that I may select some access restrictions as part of the online submission of this thesis or dissertation. I retain all ownership rights to the copyright of the thesis or dissertation. I also retain the right to use in future works (such as articles or books) all or part of this thesis or dissertation.

Signature:

_____ _____

Yoshie Narui Date

Elucidating the Biophysical Mechanisms of Notch Activation

By

Yoshie Narui

Doctor of Philosophy

Chemistry

_____

Khalid Salaita
Advisor

_____

R. Brian Dyer
Committee Member

_____

Stefan Lutz
Committee Member

Accepted:

_____

Lisa A. Tedesco, Ph.D.
Dean of the James T. Laney School of Graduate Studies

_____

Date

Elucidating the Biophysical Mechanisms of Notch Activation

By

Yoshie Narui

B.S. The Ohio State University, 2003

M.S., California Institute of Technology, 2009

Advisor: Khalid Salaita, Ph.D.

An abstract of

A dissertation submitted to the Faculty of the

James T. Laney School of Graduate Studies of Emory University

in partial fulfillment of the requirements for the degree of

Doctor of Philosophy

in Chemistry

2013

Abstract

Elucidating the Biophysical Mechanisms of Notch Activation

By Yoshie Narui

The Notch signaling pathway is an evolutionarily conserved mechanism for cell-cell communication that regulates many aspects of development and adult tissue homeostasis. For signal transduction to occur, membrane-anchored ligand and receptor molecules make direct contact at the interface of two apposing cell surfaces and set into motion a series of proteolysis events. Aberrant Notch signaling is linked to a number of developmental diseases and cancers, but there is still much unknown regarding the molecular mechanisms of receptor activation. A proposed mechanotransduction model hypothesizes that a mechanical force is required to unfold a portion of the receptor and reveal a key cleavage site. However, methods to directly measure cell exerted tension have only recently been established and relating force to downstream biochemical signaling remains a significant challenge.

In this dissertation, surface-based activation of Notch was used to address long-standing questions regarding the role of direct mechanical intervention as well as spatial and temporal inputs in activating the signaling pathway. The second chapter of this thesis focused on the development of a new technique for disrupting receptor spatial organization. Using dip-pen nanolithography, an optically transparent polymer (PDAC) was patterned onto a glass surface. The nanoscale polymer features impeded lipid diffusion and allowed for laterally mobile ligand molecules to be located adjacent to immobilized ECM proteins. The manipulation of receptor spatial organization altered the clustering of Notch and EGFR.

The third chapter centered on understanding how Delta ligand properties influenced Notch activation. While factors such as ligand density, orientation and surface anchoring chemistry were all explored, the most important parameter influencing receptor activation was lateral ligand mobility. Intriguingly, less diffusive ligand molecules (diffusion coefficient less than 0.1 $\mu m^2/s$) resulted in significantly higher levels of downstream Notch activation.

The final chapter concentrated on modifying the tethered Delta ligand to create a DLL4 tension sensor with high sensitivity in order to detect Notch generated force and relate this to activation. The current data strongly suggest that the tension exerted by the cell is below the limit of detection as ligand-receptor dissociation is observed before extension of the linker region. There is still much to learn regarding the role of physical inputs in Notch signaling, but the development of new tools and methods continues to advance our understanding of this ubiquitous and versatile pathway.

Elucidating the Biophysical Mechanisms of Notch Activation

By

Yoshie Narui

B.S. The Ohio State University, 2003

M.S., California Institute of Technology, 2009

Advisor: Khalid Salaita, Ph.D.

A dissertation submitted to the Faculty of the

James T. Laney School of Graduate Studies of Emory University

in partial fulfillment of the requirements for the degree of

Doctor of Philosophy

in Chemistry

2013

Acknowledgements

First and foremost, I have to thank my advisor, Khalid Salaita, for allowing me the opportunity to be a part of the group when it was just getting started. He is by far one of the most optimistic and enthusiastic scientists I have ever worked with, and I am very grateful for the mentorship and guidance he has provided during my time at Emory. I also have to thank the members of my thesis committee, Dr. Brian Dyer and Dr. Stefan Lutz for always offering their advice and challenging me to think about my research from different perspectives.

For current and former members of the Salaita lab, you have made coming into lab every day an entertaining, exciting and fulfilling experience. I have to make special mention of the lab members that have been with me from the very beginning, Daniel Stabley and Kevin Yehl. I thank Carol Jurchenko for being the best cubicle-mate an ISTJ could ask for, and I know she will take great care of Master Po Ping and Audrey. I will greatly miss working with my in-lab collaborator, Yang Liu, who is an incredibly thoughtful and thorough scientist. It is impossible to survive graduate school without the support of friends and colleagues. I am very grateful for the time I was able to spend with Ashley Daugherty, Erin Schuler, Pravin Muthu, Melanie Yen, all my Lindau cohorts and so many others! I would also like to acknowledge Ann Dasher Englert, Steve Krebs and Patti Barnett for all of the work they do behind the scenes.

Thanks to my entire family for their unconditional love and support. Most importantly, I have to thank my husband, Nicholas, who inspires me to be a better scientist and better person every day.

List of Frequently Used Abbreviations

Abbreviation	Full Name
ADAM	a disintegrin and metalloprotease
AFM	atomic force microscopy
AuNP	gold nanoparticle
dsDNA	double stranded deoxyribonucleic acid
DAPT	N-[N-(3,5-difluorophenacetyl)-L-alanyl]-S-phenylglycine *t*-butyl ester
DLL1 or DLL4	Delta-like protein 1 or Delta-like protein 4
DPN	dip-pen nanolithography
ECM	extracellular matrix
EGFR	epidermal growth factor receptor
EPL	expressed protein ligation
FRET	fluorescence resonance energy transfer
k	spring constant
LNR	Lin12-Notch repeat
MTFM	molecular tension-based fluorescence microscopy
NA	numerical aperture
NECD	Notch extracellular domain
NICD	Notch intracellular domain
NRR	negative regulatory region
PEG	polyethylene glycol

PDAC	poly(diallyldimethylammonium chloride)
pN	piconewton
QE	quenching efficiency
ssDNA	single stranded deoxyribonucleic acid
SrtA	Sortase A
TACE	tumor necrosis factor-α converting enzyme

Table of Contents

List of Figures

List of Tables

Chapter 1: The Notch Signaling Pathway

1.1 Introduction

1.1.1 Historical background

In 1917, Thomas Hunt Morgan, an American geneticist and embryologist, first reported a mutant strain of fruit fly (*Drosophila melanogaster*) that displayed distinct notches at the periphery of its wing blades,[1] **Fig 1.1**. This loss-of-function phenotype was observed due to a mutation in one allele of the Notch gene. The significance of Notch in development was established in the 1930s, when it was observed that total loss of Notch activity resulted in lethal hyperplasia of the *Drosophila* embryonic nervous system.[2] In the mid-1980s, two different groups successfully cloned the Notch sequence,[3,4] and since that time its critical role in the development and differentiation of multicellular organisms has been rigorously investigated.[5]

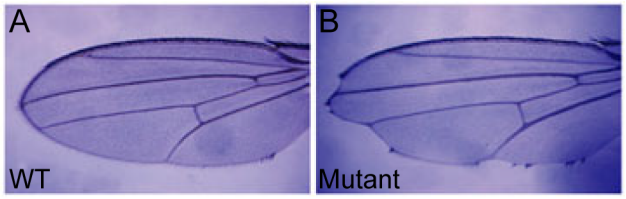

Figure 1.1. Phenotype of *Drosophila* wings. (A) Wild type and (B) mutant Notch genes result in different wing structure. Reproduced with permission from Reference 9.

At its core, the Notch signaling pathway is a classic example of juxtacrine signaling where communication between neighboring cells depends on direct cell contact. The two most common outcomes of this interaction are depicted in **Fig. 1.2**, and both result in a binary cell-fate decision. Lateral inhibition (**Fig. 1.2** *A*) occurs between two initially identical cells where over time small differences in the amount of ligand and receptor lead to different fates. This type of behavior is observed during neuronal differentiation when the Notch activated cell is inhibited from a neuronal fate.[5] Inductive

signaling (**Fig. 1.2** *B*) takes place between two non-identical cells, and the fate of the precursor cell depends on whether the adjacent cell presents the ligand on its surface. This is seen in lymphopoiesis, where precursor cells adopt a T-cell fate after interacting with thymic epithelial cells expressing the Notch ligand. In the absence of Notch signaling, the precursor cells adopt a B-cell fate.[6] Clearly, the Notch signaling pathway regulates a diverse set of cellular processes in vertebrates including neurogenesis, lymphopoiesis, somitogenesis, and vascular and kidney development.[7,8] What remains unclear is how, at the molecular level, Notch is able to carry out such complex functions using a relatively simple signaling pathway, as described below. It is evident that activation of the Notch signaling pathway leads to very different outcomes depending on where the organism is in its development and most importantly, the type of cells being studied.[9]

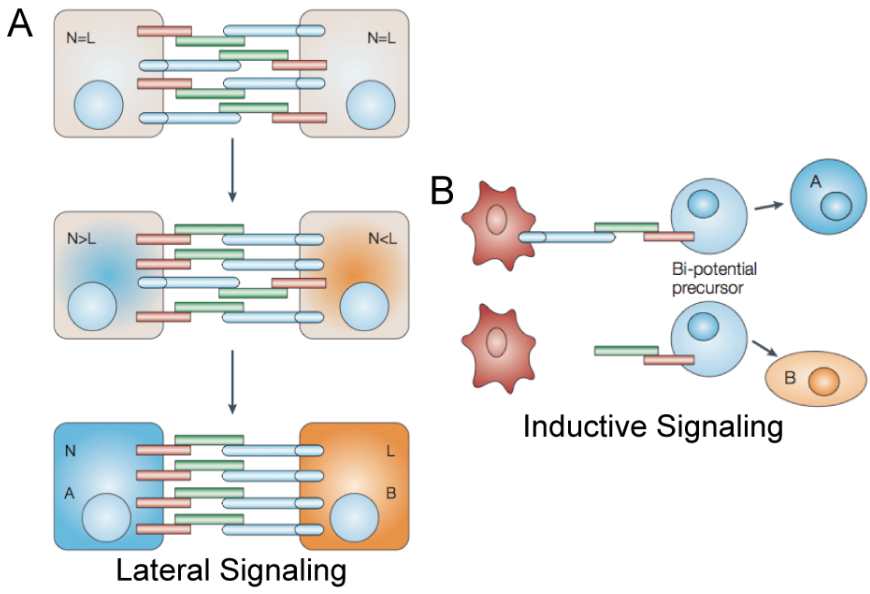

Figure 1.2. Different types of Notch function. (A) In lateral signaling, two equipotent cells expressing similar amounts of Notch (N) and ligand (L) mutually inhibit one another. Eventually, one cell commits to a specialized fate (A or B), and inhibits the neighboring cell from adopting the same fate. (B) In inductive signaling, two populations of nonequivalent cells interact with one another. If the Notch receptors on the bi-potential

precursor cell interact with ligands on a distinct neighboring cell (red), then the precursor cell adopts fate A. If there is no such interaction, then the precursor cell takes fate B. Reproduced with permission from Reference 9.

1.1.2 Biomedical relevance

As expected, dysregulation of Notch is associated with a number of human developmental disorders. This includes diseases such as Alagille Syndrome, which leads to abnormalities of the liver, heart, eye and skeleton, and CADASIL, which results in defects of brain vasculature.[10] As further evidence that the function of Notch is strongly cell context dependent, it can act as both an oncogene and a tumor suppressor gene. Gain-of-function forms of Notch are linked to certain types of cancer including breast cancer[11] and, most notably, T-cell acute lymphoblastic leukemia (T-ALL).[12] In contrast, sequencing data from primary tumors of head and neck squamous cell carcinoma revealed inactivating mutations in Notch1.[13] Even within the haematopoietic system, where Notch was thought to be strictly oncogenic (e.g., T-ALL), studies have revealed that during early stem cell differentiation Notch plays a tumor suppressor role.[14] The wide scope of diseases that exist due to errors within this signaling pathway highlight the need to better understand the molecular mechanism of Notch receptor activation. With this information, it may be possible to gain greater insight into precisely how aberrant signaling leads to diseased states and allow for the discovery of new methods to treat or prevent anomalous signaling.

1.2 What is currently known about the mechanism of Notch signaling?

1.2.1 Core components of Notch signaling

Signal transduction via the Notch pathway requires direct contact between ligand molecules on the signal sending cell and receptor molecules on the signal receiving cell.

Notch is a heterodimeric, single-pass transmembrane protein held together non-covalently in a Ca^{2+} dependent manner (**Fig. 1.3** *A*). Initially, Notch is translated as a single protein and upon transport through the trans-Golgi network to the cell membrane it is processed into a dimer by a furin-like convertase at site 1 (S1). Epidermal growth factor (EGF) repeats 11 and 12 are the regions required for binding with DSL (Delta/Serrate/LAG-2) ligand molecules. Upon ligand-receptor binding, the extracellular domain of Notch is cleaved by a disintegrin and metalloprotease (ADAM) at site 2 (S2). This proteolysis event is the key step in activation of the signaling pathway, however the precise mechanism by which the NECD is shed is still unknown. The crystal structure of the negative regulatory region (NRR), which is proximal to the membrane and composed of three Lin12/Notch repeats (LNRs) and the heterodimerization domain (HD), illustrates that the S2 site is buried within a hydrophobic pocket leading to an autoinhibited conformation (**Fig. 1.3** *B*).[15] Based upon the available NMR and crystal structures,[16, 17] activation of the receptor would likely require a significant conformational change in the NRR in order for the S2 position to be accessible for cleavage (**Fig. 1.3** *C*).

To better understand the structural changes of the NRR leading to S2 cleavage, Tiyanont et al. utilized hydrogen exchange mass spectrometry (HX MS) to replace exposed or dynamic hydrogen atoms of the intact protein with deuterium.[18] After exchange, the receptor was digested into fragments that were analyzed by mass spectrometry for deuterium content. Not surprisingly, the hydrophobic core of the HD domain in the autoinhibited form remains well protected from exchange. Following treatment with EDTA, leading to chemical activation of the receptor (as described

below), portions of the HD domain that form the interface with the LNR repeats along with other structural elements near S2 show rapid deuteration.[18]

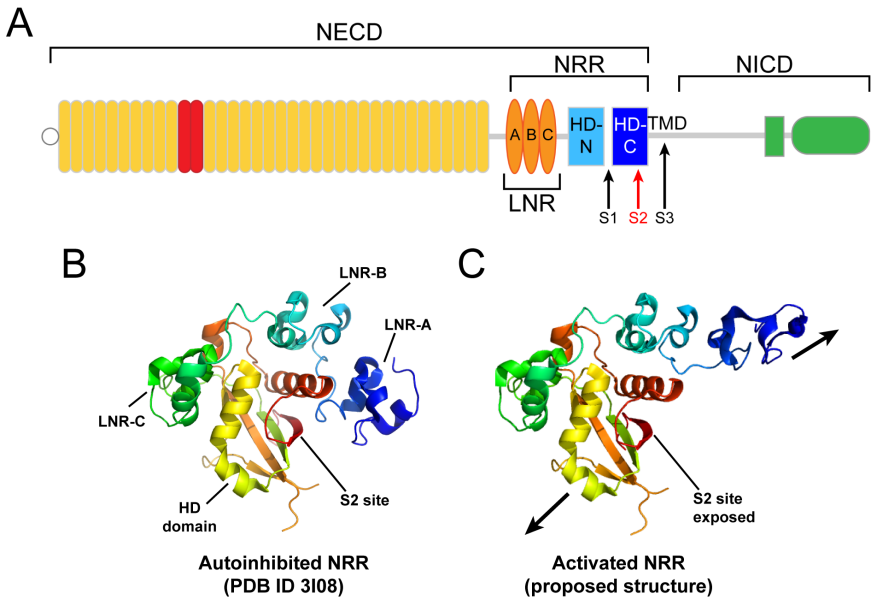

Figure 1.3 The Notch receptor. (A) Domain architecture of the Notch1 receptor. EGF repeats 1-36 are shown in yellow and EGF 11-12, which are required for ligand binding, are highlighted in red. The NRR is composed of the three LNRs and HD domain, which is shown as two halves – the N-terminal (HD-N, light blue) and the C-terminal (HD-C, dark blue) portions. The transmembrane domain (TM) indicates where the receptor spans the membrane, and the NICD is depicted in green. The three cleavage sites are marked with arrows. Adapted with permission from Reference 19. (B) Crystal structure of Notch NRR in an autoinhibited state. The S2 site is buried within a hydrophobic pocket capped by LNR-A. (C) Proposed structure of the activated NRR. Arrows indicate the direction of the mechanical force applied, which reveals the S2 site. This model was generated in PyMol using the molecular auto-sculpting mode.

Following removal of the NECD, the NICD is clipped by the γ-secretase complex at site 3 (S3) releasing it into the cytoplasm where it translocates to the nucleus and acts as a transcription factor.[19] The NICD comes together with the DNA binding protein, C promoter-binding factor/Suppressor of Hairless/LAG-1 (CSL) and recruits coactivators to activate gene expression of downstream targets in the *Hes* and *Hey* families. Unlike other pathways, Notch requires very few components to transduce the signal from the cell

surface to the transcriptional machinery (**Fig. 1.4**). While the sequence of signaling events has been elucidated, there are still many unanswered questions surrounding the Notch signaling pathway. This thesis will focus on the development and use of biophysical methods to study physical aspects such as oligomerization, surface display, lateral fluidity and mechanical tension in Notch activation.

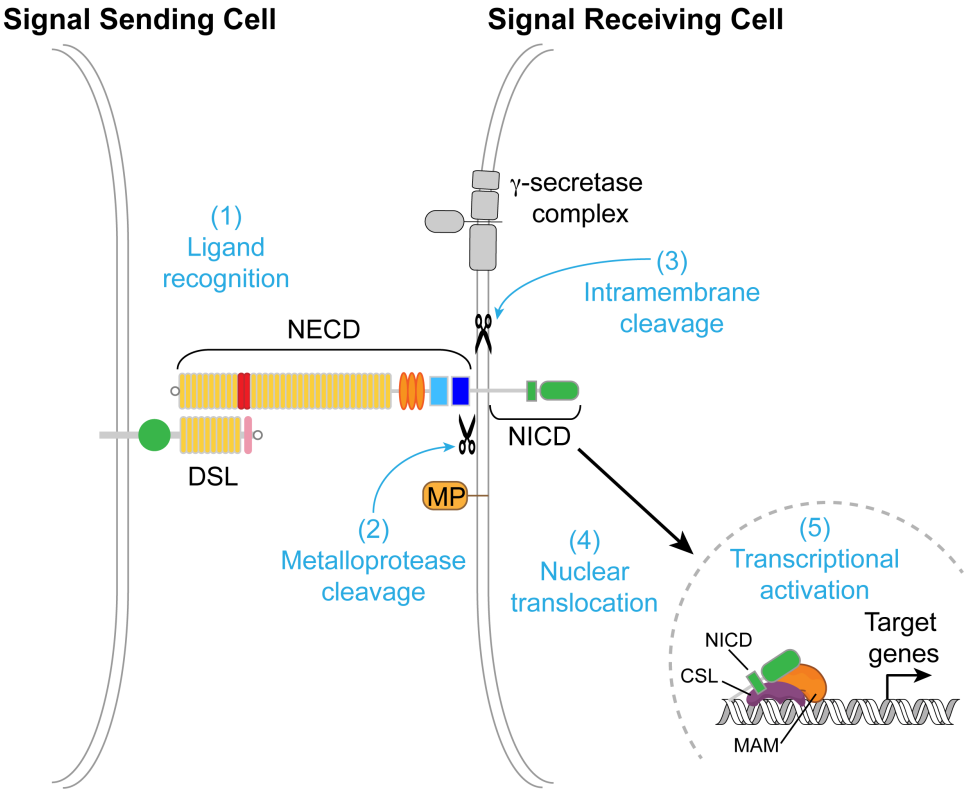

Figure 1.4. Steps in the Notch signaling pathway. (1) The Notch receptor recognizes and binds to its cognate DSL ligand on an apposing cell membrane. (2) ADAM cleaves the Notch receptor at S2 leading to removal of the NECD. (3) γ-secretase catalyzes proteolysis of the receptor at S3 releasing the NICD into the cytoplasm. (4) The NICD translocates to the nucleus. (5) This leads to transcriptional activation of target genes. Adapted with permission from Reference 19.

1.2.2 Models of activation

How does the S2 site of the Notch receptor become exposed and susceptible to cleavage? Two main theories have been proposed to explain the large conformational

change – the first is the mechanical force model and the second is the ligand recycling model. These models are not mutually exclusive, and it has been suggested that both events may be required to activate ligand and receptor.[20] In the mechanical force model, formation of the ligand-receptor complex is coupled with endocytosis in order to produce a force large enough to lead to proteolysis at S2 or physical dissociation of the NECD at S1. This model is supported by evidence that the receptor cannot be activated with soluble ligand molecules.[21] In addition, endocytosis is required for activation of Notch in both *Drosophila* and mammalian cells.[22, 23] Computational models confirm that the mechanical force exerted by endocytosis can lead to sequential disengagement of the LNR from the HD domain.[24]

In the ligand recycling model, DSL molecules are endocytosed by the signal-sending cell where they are processed and returned to the surface through an endosomal pathway, producing more potent ligand molecules, see **Fig. 1.5**. Required components of the endosomal recycling machinery, such as the GTPase, Rab11, are necessary for signaling in certain cell types.[25] The ligand molecules are primed for receptor activation through ubiquitination[26] or relocation to an area with more receptor molecules.[27] Notably, allosteric activation of Notch seems unlikely due to the fact the S2 position is located over 1000 residues away from the ligand binding region.[15] One of the main motivations for this work is to establish what role force plays in the activation of Notch. While most experiments have focused on the signal sending cell to generate force, we hypothesize that both ligand and receptor cells are actively involved in a complex interplay of events that lead to proteolysis at S2.

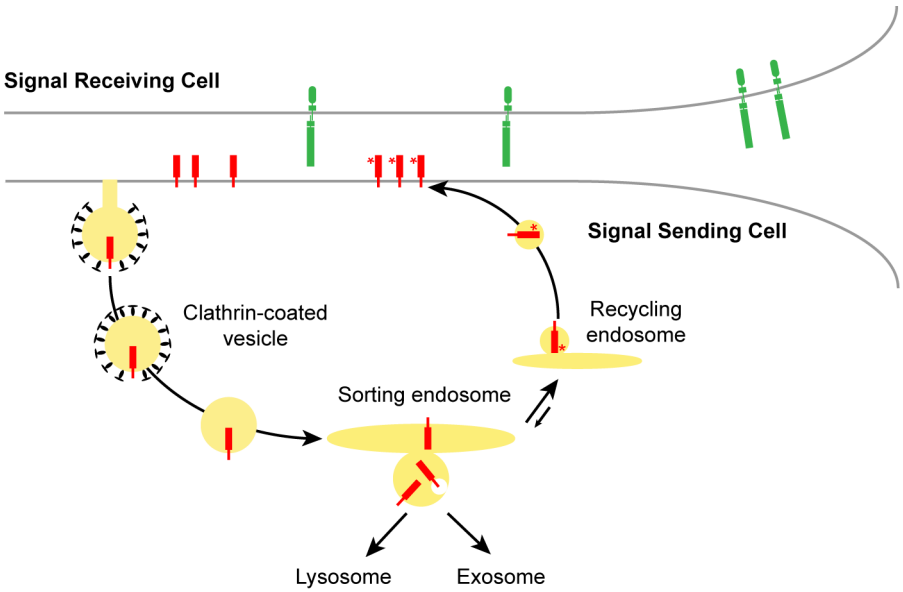

Figure 1.5. Ligand recycling model of Notch activation. Notch receptors are shown in green, and DSL ligands are red. After moving through the recycling process, the ligand molecules return to the cell surface in a more potent form (indicated with an asterisk). Only the highly potent ligands are able to bind and activate Notch receptors on the signal receiving cell.

1.2.3 Role of oligomerization

An aspect of cell signaling that has not been fully explored in the Notch signaling pathway is the role of receptor oligomerization or clustering. This behavior has been observed in other juxtracrine signaling systems such as FcεRI, cadherins and integrins.[28-31] Oligomerization is advantageous because it reduces the diffusion coefficient of receptor molecules and amplifies the signal through activation of multiple receptors.[32] Both mammalian and *Drosophila* NECD are known to form dimers due to favorable interactions between EGF repeats.[33] Studies have observed clustering of Notch, but the effect of higher-order spatial organization on the signaling pathway is still uncertain.[23, 34] Vooijs et al. found that forced oligomerization of Notch does not necessarily correlate with improved receptor activity.[35] However, it has also been shown that soluble ligand

cannot activate Notch, but pre-clustered ligand was able to restore activity suggesting that oligomerization enhances signaling.[36]

Oligomerization may have a regulatory role in the signaling pathway, but there are other justifications to support a role for clustering. The binding constant between Notch and its cognate ligand has been measured using ELISA and SPR, and the K_d varied widely from 0.7 nM to 130 μM.[37-39] If the actual value is in the micromolar range, then the binding between ligand and receptor is fairly weak. In order to activate the receptor, this interaction must be strong enough to withstand a possible cell applied force and accompanying conformation change before dissociation of the ligand and receptor interaction. One way to reinforce the strength of these interactions is through oligomerization of many complexes. It is not clear yet how the spatial organization of receptors may be used to regulate the Notch signaling pathway, but it is an intriguing concept (although not without precedent. e.g., TCR,[40] EphA2,[41] and EGFR[42]) that provides a molecular mechanism of modulating cellular response to the Notch pathway.

1.3 Current methods used to study Notch and other juxtacrine systems

Currently, there are several methods utilized to study Notch activation, however each has its own set of limitations. The most commonly used method to study the Notch signaling pathway is cellular co-culture, **Fig 1.6** *A*. Cells that only express ligand are allowed to interact with cells that exclusively express receptor molecules, often these constructs are fused with epitope tags or fluorescent proteins for imaging purposes. This method is physiologically relevant, but imaging of cell-cell junctions with high temporal and spatial resolution is difficult due to the complex membrane interface. The simplest activation method involves ligand molecules physisorbed onto a solid support with

fibronectin to activate the Notch receptor, as shown in **Fig 1.6** *B*.[43] This straightforward method is effective but the ligand molecules are oriented non-specifically and the overall distribution is not well controlled. Lastly, the Notch receptor can be activated in the absence of ligand molecules by treatment with millimolar concentrations of EDTA, **Fig. 1.6** *C*.[44] This metal chelator sequesters calcium ions, which stabilize the autoinhibited state of the NRR, and their removal leads to cleavage at the S2 site. While this strategy leads to activation of the pathway, EDTA treated receptors use ADAM17 for proteolysis while activation with ligand molecules absolutely requires ADAM10.[45] This example demonstrates that while the biological outcome may be identical, the pathways and proteins used can be context dependent. In order to fully understand the mechanism for Notch activation, new methods must be developed which allow for quantitative analysis of ligand-receptor binding in an environment composed of correctly orientated ligand molecules within a lipid membrane and introduced to signal-receiving cells.

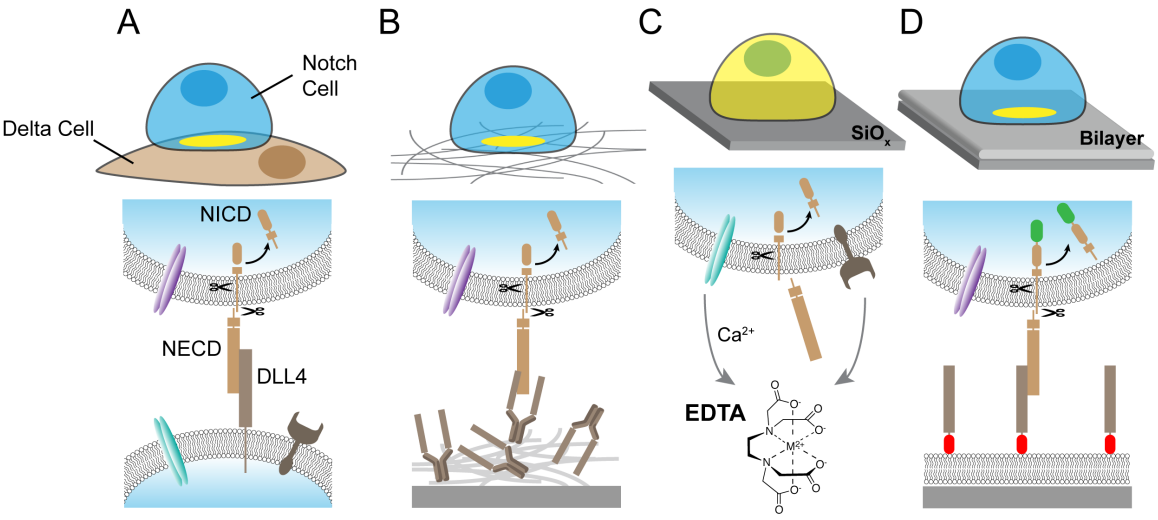

Figure 1.6. Current methods to study Notch activation. This scheme illustrates the most commonly used strategies to activate Notch, which include: (A) cellular co-culture, (B) physisorbed ligand, (C) metal depletion, and (D) supported membrane tethered ligand. The yellow regions highlighted in the top diagrams are depicted in molecular detail below.

1.4 Aim and scope of the dissertation

The current view of Notch signaling is based on conventional methods including structural biology, biochemical assays and genetic studies. These fundamental studies have provided great insight on the components and events involved in the core signaling pathway. However, new methods are needed that directly address the role of physical inputs in activation and signal regulation. This thesis intends to provide the biological community with platforms (**Fig. 1.6** *D*) that can be broadly applied to study juxtacrine signaling systems, while specifically focusing on questions related to the Notch signaling pathway. The key questions that will be addressed include:

- Does receptor clustering regulate Notch signaling?
- What is the stoichiometry of the ligand-receptor complex? Can ligand-receptor binding and activation be observed in real-time on the surface of a live cell?
- How do the mechanical properties (stability, density, lateral mobility) of the ligand molecule affect cellular response?
- What is the role of mechanical force in Notch activation? Can the cell applied force be observed and measured?

In summary, Chapter 2 addresses the role of oligomerization in signaling through the development of a new experimental method for disrupting the clustering of ligand molecules. This platform uses dip-pen nanolithography to pattern the transparent, positively charged polymer, poly(diallyldimethylammonium chloride) (PDAC) onto a glass slide. PDAC functions as a lipid barrier and allows for the juxtaposition of laterally mobile ligand molecules next to non-mobile proteins adsorbed to the polymer structures. This method was compared with standard e-beam nanopatterned grids, which were used

to disrupt the initial formation of Delta-Notch clusters. Chapter 3 closely examines the important characteristics of the ligand molecule that lead to activation of the Notch receptor. This chapter also describes in greater detail the supported membrane platform including how ligand lateral mobility and density can be readily tuned. This chapter includes a quantitative description of Notch receptor activation, and the first measurement of the stoichiometry of binding between Delta and Notch on the surface of live cells. Finally, Chapter 4 attempts to directly measure the cell applied force on the ligand molecule through the cell surface receptor. A variety of strategies were utilized including spider silk elastic linkers, PEG-based and DNA hairpin-based sensors. Unfortunately, the sensor signal remains elusive, and it must be considered that the force is much lower than initially anticipated or non-existent. In spite of this, there is still much that can be learned regarding the early moments of Delta-Notch binding, activation and oligomerization through the use of these newly developed methods.

1.5 References

1. Morgan, T. H., The theory of the gene. *Am. Nat.* **1917,** *51* (609), 513-544.
2. Poulson, D. F., The effects of certain X-chromosome deficiencies on the embryonic development of Drosophila melanogaster. *J. Exp. Zool.* **1940**.
3. Wharton, K. A.; Johansen, K. M.; Xu, T.; Artavanis-Tsakonas, S., Nucleotide sequence from the neurogenic locus notch implies a gene product that shares homology with proteins containing EGF-like repeats. *Cell* **1985,** *43* (3 Pt 2), 567-581.

4. Kidd, S.; Kelley, M. R.; Young, M. W., Sequence of the notch locus of Drosophila melanogaster: relationship of the encoded protein to mammalian clotting and growth factors. *Mol. Cell. Biol.* **1986,** *6* (9), 3094-3108.

5. Lai, E. C., Notch signaling: control of cell communication and cell fate. *Development* **2004,** *131* (5), 965-973.

6. Pear, W. S.; Radtke, F., Notch signaling in lymphopoiesis. *Sem. Immunol.* **2003**.

7. Bray, S. J.; Bernard, F., Notch targets and their regulation. *Curr. Top. Dev. Biol.* **2010,** *92*, 253-275.

8. Bray, S. J., Notch signalling: a simple pathway becomes complex. *Nat. Rev. Mol. Cell Biol.* **2006,** *7* (9), 678-689.

9. Radtke, F.; Raj, K., The role of Notch in tumorigenesis: oncogene or tumour suppressor? *Nat. Rev. Cancer* **2003,** *3* (10), 756-767.

10. Hansson, E. M.; Lendahl, U.; Chapman, G., Notch signaling in development and disease. *Semin. Cancer Biol.* **2004,** *14* (5), 320-328.

11. Yamaguchi, N.; Oyama, T.; Ito, E.; Satoh, H.; Azuma, S.; Hayashi, M.; Shimizu, K.; Honma, R.; Yanagisawa, Y.; Nishikawa, A.; Kawamura, M.; Imai, J.-i.; Ohwada, S.; Tatsuta, K.; Inoue, J.-I.; Semba, K.; Watanabe, S., NOTCH3 signaling pathway plays crucial roles in the proliferation of ErbB2-negative human breast cancer cells. *Cancer Res.* **2008,** *68* (6), 1881-1888.

12. Weng, A. P.; Ferrando, A. A.; Lee, W.; Morris, J. P.; Silverman, L. B.; Sanchez-Irizarry, C.; Blacklow, S. C.; Look, A. T.; Aster, J. C., Activating mutations of NOTCH1 in human T cell acute lymphoblastic leukemia. *Science* **2004,** *306* (5694), 269-271.

13. Agrawal, N.; Frederick, M. J.; Pickering, C. R.; Bettegowda, C.; Chang, K.; Li, R. J.; Fakhry, C.; Xie, T.-X.; Zhang, J.; Wang, J.; Zhang, N.; El-Naggar, A. K.; Jasser, S. A.; Weinstein, J. N.; Treviño, L.; Drummond, J. A.; Muzny, D. M.; Wu, Y.; Wood, L. D.; Hruban, R. H.; Westra, W. H.; Koch, W. M.; Califano, J. A.; Gibbs, R. A.; Sidransky, D.; Vogelstein, B.; Velculescu, V. E.; Papadopoulos, N.; Wheeler, D. A.; Kinzler, K. W.; Myers, J. N., Exome sequencing of head and neck squamous cell carcinoma reveals inactivating mutations in NOTCH1. *Science* **2011,** *333* (6046), 1154-1157.

14. Klinakis, A.; Lobry, C.; Abdel-Wahab, O.; Oh, P.; Haeno, H.; Buonamici, S.; van De Walle, I.; Cathelin, S.; Trimarchi, T.; Araldi, E.; Liu, C.; Ibrahim, S.; Beran, M.; Zavadil, J.; Efstratiadis, A.; Taghon, T.; Michor, F.; Levine, R. L.; Aifantis, I., A novel tumour-suppressor function for the Notch pathway in myeloid leukaemia. *Nature* **2011,** *473* (7346), 230-233.

15. Gordon, W. R.; Vardar-Ulu, D.; Histen, G.; Sanchez-Irizarry, C.; Aster, J. C.; Blacklow, S. C., Structural basis for autoinhibition of Notch. *Nat. Struct. Mol. Biol.* **2007,** *14* (4), 295-300.

16. Cordle, J.; Johnson, S.; Tay, J. Z. Y.; Roversi, P.; Wilkin, M. B.; de Madrid, B. H.; Shimizu, H.; Jensen, S.; Whiteman, P.; Jin, B.; Redfield, C.; Baron, M.; Lea, S. M.; Handford, P. A., A conserved face of the Jagged/Serrate DSL domain is involved in Notch trans-activation and cis-inhibition. *Nat. Struct. Mol. Biol.* **2008,** *15* (8), 849-857.

17. Gordon, W. R.; Roy, M.; Vardar-Ulu, D.; Garfinkel, M.; Mansour, M. R.; Aster, J. C.; Blacklow, S. C., Structure of the Notch1-negative regulatory region:

implications for normal activation and pathogenic signaling in T-ALL. *Blood* **2009,** *113* (18), 4381-4390.

18. Tiyanont, K.; Wales, T. E.; Aste-Amezaga, M.; Aster, J. C.; Engen, J. R.; Blacklow, S. C., Evidence for Increased Exposure of the Notch1 Metalloprotease Cleavage Site upon Conversion to an Activated Conformation. *Structure* **2011,** *19* (4), 546-554.

19. Gordon, W. R.; Arnett, K. L.; Blacklow, S. C., The molecular logic of Notch signaling - a structural and biochemical perspective. *J. Cell Sci.* **2008,** *121* (Pt 19), 3109-3119.

20. Heuss, S. F.; Ndiaye-Lobry, D.; Six, E. M.; Israël, A.; Logeat, F., The intracellular region of Notch ligands Dll1 and Dll3 regulates their trafficking and signaling activity. *Proc. Natl. Acad. Sci. U. S. A.* **2008,** *105* (32), 11212-11217.

21. Varnum-Finney, B.; Wu, L.; Yu, M.; Brashem-Stein, C.; Staats, S.; Flowers, D.; Griffin, J. D.; Bernstein, I. D., Immobilization of Notch ligand, Delta-1, is required for induction of notch signaling. *J. Cell Sci.* **2000,** *113* (23), 4313-4318.

22. Parks, A.; Klueg, K. M.; Stout, J.; Muskavitch, M. A., Ligand endocytosis drives receptor dissociation and activation in the Notch pathway. *Development* **2000,** *127* (7), 1373-1385.

23. Nichols, J. T.; Miyamoto, A.; Olsen, S. L.; D'Souza, B.; Yao, C.; Weinmaster, G., DSL ligand endocytosis physically dissociates Notch1 heterodimers before activating proteolysis can occur. *J. Cell Biol.* **2007,** *176* (4), 445-458.

24. Chen, J.; Zolkiewska, A., Force-induced unfolding simulations of the human Notch1 negative regulatory region: possible roles of the heterodimerization domain in mechanosensing. *PLoS One* **2011,** *6* (7), e22837.

25. Emery, G.; Hutterer, A.; Berdnik, D.; Mayer, B.; Wirtz-Peitz, F.; Gaitan, M. G.; Knoblich, J. A., Asymmetric Rab 11 endosomes regulate delta recycling and specify cell fate in the Drosophila nervous system. *Cell* **2005,** *122* (5), 763-773.

26. Pitsouli, C.; Delidakis, C., The interplay between DSL proteins and ubiquitin ligases in Notch signaling. *Development* **2005,** *132* (18), 4041-4050.

27. Nichols, J. T.; Miyamoto, A.; Weinmaster, G., Notch signaling - constantly on the move. *Traffic* **2007,** *8* (8), 959-969.

28. Wilson, B. S.; Pfeiffer, J. R.; Oliver, J. M., Observing FcepsilonRI signaling from the inside of the mast cell membrane. *J. Cell Biol.* **2000,** *149* (5), 1131-1142.

29. Sheets, E. D.; Holowka, D.; Baird, B., Membrane organization in immunoglobulin E receptor signaling. *Curr. Opin. Chem. Biol.* **1999,** *3* (1), 95-99.

30. Yap, A. S.; Niessen, C. M.; Gumbiner, B. M., The juxtamembrane region of the cadherin cytoplasmic tail supports lateral clustering, adhesive strengthening, and interaction with p120ctn. *J. Cell Biol.* **1998,** *141* (3), 779-789.

31. Hantgan, R. R.; Lyles, D. S.; Mallett, T. C.; Rocco, M.; Nagaswami, C.; Weisel, J. W., Ligand binding promotes the entropy-driven oligomerization of integrin alpha IIb beta 3. *J. Biol. Chem.* **2003,** *278* (5), 3417-3426.

32. Bethani, I.; Skånland, S. S.; Dikic, I.; Acker-Palmer, A., Spatial organization of transmembrane receptor signalling. *The EMBO Journal* **2010,** *29* (16), 2677-2688.

33. Kelly, D. F.; Lake, R. J.; Middelkoop, T. C.; Fan, H.-Y.; Artavanis-Tsakonas, S.; Walz, T., Molecular structure and dimeric organization of the Notch extracellular domain as revealed by electron microscopy. *PLoS One* **2010,** *5* (5), e10532.

34. Luty, W. H.; Rodeberg, D.; Parness, J.; Vyas, Y. M., Antiparallel segregation of notch components in the immunological synapse directs reciprocal signaling in allogeneic Th : DC conjugates. *J. Immunol.* **2007,** *179* (2), 819-829.

35. Vooijs, M.; Schroeter, E. H.; Pan, Y.; Blandford, M.; Kopan, R., Ectodomain shedding and intramembrane cleavage of mammalian Notch proteins is not regulated through oligomerization. *J. Biol. Chem.* **2004,** *279* (49), 50864-50873.

36. Hicks, C.; Ladi, E.; Lindsell, C. E.; Hsieh, J. J. D.; Hayward, S. D.; Collazo, A.; Weinmaster, G., A secreted Delta1-Fc fusion protein functions both as an activator and inhibitor of Notch1 signaling. *J. Neurosci. Res.* **2002,** *68* (6), 655-667.

37. Shimizu, K.; Chiba, S.; Kumano, K.; Hosoya, N.; Takahashi, T.; Kanda, Y.; Hamada, Y.; Yazaki, Y.; Hirai, H., Mouse Jagged1 physically interacts with Notch2 and other Notch receptors. *J. Biol. Chem.* **1999,** *274* (46), 32961-32969.

38. Pei, Z.; Baker, N. E., Competition between Delta and the Abruptex domain of Notch. *BMC Dev. Biol.* **2008,** *8*, 4.

39. Cordle, J.; Redfieldz, C.; Stacey, M.; van der Merwe, P. A.; Willis, A. C.; Champion, B. R.; Hambleton, S.; Handford, P. A., Localization of the delta-like-1-binding site in human Notch-1 and its modulation by calcium affinity. *J. Biol. Chem.* **2008,** *283* (17), 11785-11793.

40. Manz, B. N.; Jackson, B. L.; Petit, R. S.; Dustin, M. L.; Groves, J. T., T-cell triggering thresholds are modulated by the number of antigen within individual T-cell receptor clusters. *Proc. Natl. Acad. Sci. U. S. A.* **2011,** *108* (22), 9089-9094.

41. Salaita, K. S.; Nair, P. M.; Petit, R. S.; Neve, R. M.; Das, D.; Gray, J. W.; Groves, J. T., Restriction of receptor movement alters cellular response: physical force sensing by EphA2. *Science* **2010,** *327* (5971), 1380-1385.

42. Stabley, D. R.; Retterer, S.; Marshall, S.; Salaita, K. S., Manipulating the lateral diffusion of surface-anchored EGF demonstrates that receptor clustering modulates phosphorylation levels. *Integr. Biol.* **2013,** *5* (4), 659-668.

43. Mattheyses, A. L.; Simon, S. M.; Rappoport, J. Z., Imaging with total internal reflection fluorescence microscopy for the cell biologist. *J. Cell Sci.* **2010,** *123* (21), 3621-3628.

44. Rand, M. D.; Grimm, L. M.; Artavanis-Tsakonas, S.; Patriub, V.; Blacklow, S. C.; Sklar, J.; Aster, J. C., Calcium depletion dissociates and activates heterodimeric notch receptors. *Mol. Cell. Biol.* **2000,** *20* (5), 1825-1835.

45. Bozkulak, E. C.; Weinmaster, G., Selective use of ADAM10 and ADAM17 in activation of Notch1 signaling. *Mol. Cell. Biol.* **2009,** *29* (21), 5679-5695.

Chapter 2: Nanoscale Patterning for Manipulating the Spatial Organization of Proteolipid Membranes

Adapted from Narui, Y.; Salaita, K. S., Dip-pen Nanolithography of Optically Transparent Cationic Polymers to Manipulate Spatial Organization of Proteolipid Membranes. *Chem. Sci.* **2012**, *3* (3), 794-799, with permission from The Royal Society of Chemistry.

2.1 Introduction

The lateral movement of lipids and associated biomolecules within the cell membrane is one of the hallmarks of living cells.[1] These motions allow cells to dynamically respond to their surrounding environment, converting extracellular signals into internal chemical responses. Often, this can lead individual receptors to associate within the cell membrane forming hierarchical organizations that alter the kinetics and thermodynamics of their functions.[2-4] For example, specific receptors have been observed in microdomains separated by "picket-fences" or semi-permeable lipid diffusion barriers on the surface of many cells.[5, 6] Nano- or microscale membrane corrals alter the higher order organization of receptor assemblies and subsequently influence the transmission of information across the cell membrane.[7, 8] Given the importance of these protein assemblies, it is imperative that new methods are developed to investigate the role of protein and lipid compartmentalization in the surface of live cells.[5, 9-15]

To address this need, nanopatterned supported lipid membranes have been introduced to direct the lateral diffusion of specific receptors in live cells.[16, 17] Supported lipid bilayers are formed by the self-assembly of phospholipids onto an appropriate solid surface, such as silicon oxide or mica.[18, 19] On these supporting materials, lipid molecules adopt a fully fluid membrane bilayer structure with molecular adlayers of water separating the substrate and lipid membrane.[19] This thin film of water maintains the membrane structure and allows for lateral fluidity of the lipids. Ligands that are conjugated to the lipid headgroups are confined to the plane of the membrane and also display two-dimensional diffusion across the substrate. When nanoscale metal and metal oxide structures (100-500 nm lateral dimensions and 10 nm height) are fabricated onto

the solid support using e-beam lithography, lipid molecules are unable to move across these nanostructures, and ligand mobility is restricted to specific pre-defined geometries.[7, 9, 20] Importantly, when cell surface receptors encounter their cognate ligands on the supported membrane, they too become subject to the constraints of the substrate diffusion barriers. The transport of ligand-receptor complexes and associated signaling molecules is only influenced through their interactions with the nanopatterned glass coverslip, which provides molecular specificity in cell manipulations.

While conventional metal nanostructures are excellent lipid diffusion barriers, there are several challenges to address when using them to investigate the role of receptor organization in cell signaling. The first relates to the relatively large extinction coefficient of metallic structures within the UV and visible range of wavelengths,[21] see **Fig. 2.1**. This limits the use of fluorescence microscopy as a characterization tool because the metal barriers selectively absorb a portion of the excitation and emission intensity. For example, in our hands, we find that 10 nm Cr nanopatterns reduce the measured fluorescence intensity of a 1 μM fluorescein solution by ~15% (**Fig. 2.1**). Therefore, the optical properties of metallic nanostructures pose a challenge because imaging fluorescent proteins is a fundamental technique used in cell biology investigations. The second issue relates to the serial nature of e-beam lithography.[22] Biological studies require statistically significant data sets, and, as such, high-throughput nanopatterning approaches are required to increase the utility of the nanopatterned supported membrane technique. The third feature of metallic nanostructures pertains to their size, most importantly their height, which is typically 10 nm.[10] While the cell membrane may not be directly influenced by nanoscale topographical features, some theoretical and

experimental data suggest that ligand-receptor sorting may be influenced by nanoscale topography.[23, 24] Ideally, a biomimetic membrane should present minimal topographical features to the cell except for the ligand molecules whose interactions with cell receptors are being investigated. Finally, thin-film deposited Cr structures are difficult to chemically functionalize, and it would be desirable to generate nanoscopic structures to control lipid diffusion that are amenable to chemical modification.[25]

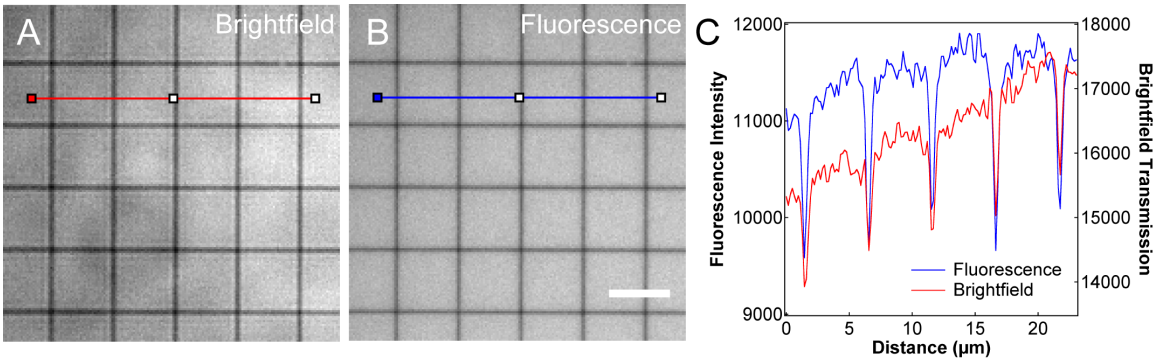

Figure 2.1. E-beam patterned chromium grid with 5 μm squares. The substrate was prepared with a 100 mol% DOPC bilayer followed by BSA blocking to prevent non-specific binding. The grid was imaged in a 1 μM fluorescein solution using (A) brightfield illumination and (B) epifluorescence. (C) Line scans taken from (A) and (B) reveal a steep drop-off in measured brightfield transmission and fluorescence intensity in areas where chromium was deposited. Scale bar represents 5 μm.

DPN is a scanning probe-based lithographic technique that generates maskless patterns by directly transferring ink molecules from the tip of a scanning probe to the underlying substrate.[26, 27] Recent advances in tip parallelization have led to high-throughput printing capabilities across centimeter length scales with sub-50 nm resolution, including the development of corollary techniques such as hard-tip soft spring lithography and polymer pen lithography techniques.[28, 29] DPN is compatible with a wide range of ink and substrate combinations, and there are several examples demonstrating

the deposition of polymer inks such as proteins,[30, 31] dendrimers,[32] and polydimethylsiloxane (PDMS).[33]

The Mirkin group has further shown that DPN can be used for patterning conducting polymers, poly(aniline sulfonic acid) and polypyrrole, onto modified silicon surfaces for use in nanoscale electronic devices, demonstrating that electrostatic forces stabilize the charged polymer ink onto the surface.[34] In our study, we extend the functionality of poly(diallyldimethylammonium chloride) PDAC nanopatterns beyond the fields of molecular electronics and layer-by-layer assembly,[35] showing that these structures obstruct lipid diffusion and are mechanically robust enough to withstand cellular forces. Thus, they may be used to manipulate the spatial organization of ligand-receptor complexes.

Herein, we identify PDAC (**Fig. 2.2** *A*) as an optically transparent polymer that hinders the lateral diffusion of lipid molecules, adheres strongly to silicon oxide substrates, and is amenable for nanopatterning using the DPN technique. We find that DPN-generated PDAC structures guide the organization of laterally mobile and anchored cell surface receptors into specific geometries. This method is compared with conventional e-beam generated nanopatterns to investigate formation and translocation of Delta-Notch clusters. Other groups have directly used atomic force microscopy-based lithography to selectively deposit or remove lipids in a range of applications.[12-15, 36] However, to the best of our knowledge, this is the first report of direct writing and rapid prototyping of micro- and nanoscale structures for controlling lipid diffusion and for patterning protein ligands within a proteolipid membrane.

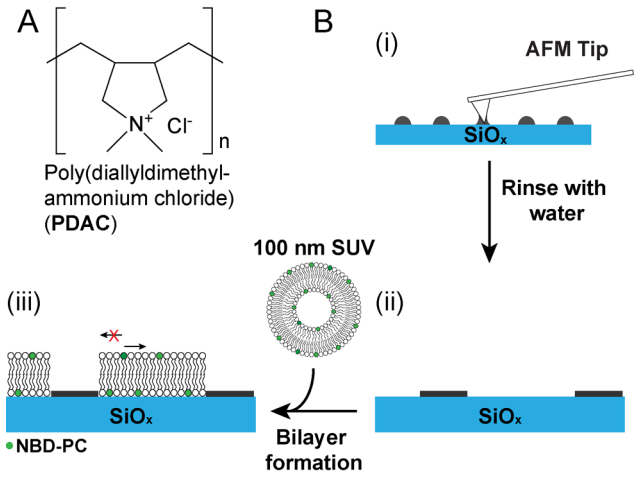

Figure 2.2. Description of PDAC patterning. (A) Chemical structure of PDAC polymer (n~500). (B) Scheme of the DPN procedure: (i) deposition of PDAC on a silica substrate using an AFM tip, (ii) removal of excess polymer to form a thin film and (iii) formation of the supported lipid membrane. The lipids are laterally mobile except in the regions where the nanopatterned PDAC is located.

2.2 Results and discussion

2.2.1 Selection of polymer "ink" and procedure for patterning

Aside from metal or metal oxides, there are a limited number of materials that can prevent lipid membrane spreading and that are also compatible with nanoscale patterning approaches. Predicting molecular species that can function in this capacity is not straightforward; moreover, to the best of our knowledge, there are no reports of molecular nanostructures that can hinder the diffusion of lipid membranes. For example, the most commonly used inks in DPN or PDMS-based microcontact printing (μCP)[22] are functionalized alkanethiols that are known to support the formation of hybrid lipid monolayers.[37] To address this challenge, we empirically tested a range of molecular inks that were amenable to patterning on silica. This included silanes terminated with polyethylene glycol, alkanes and perfluorinated alkanes, and poly(ethyleneimine), but only PDAC was effective at impeding lipid diffusion. We suspect that PDAC confers

these capabilities based on its propensity to adsorb multilayers of intact vesicles that do not support the formation of fluid bilayers.[38-41]

In a typical DPN experiment as depicted in **Fig. 2.2** *B*, etched glass coverslips were dried under a stream of N_2 and immediately used for DPN with an NScriptor system (see Materials and Methods). The PDAC polymer solution was applied to a one-dimensional, 24-tip F type pen array by immersing the tips into a small droplet of PDAC located on a nearby glass coverslip. The tips were subsequently blotted to remove excess ink, and then the tip array was brought into contact with the glass surface and leveled by observing changes in tip reflectivity.[27, 29, 42, 43] In order to generate PDAC line structures, the tips contacted the surface and moved at a speed of 100 nm/sec using an automated stage controller. After generating a set of lines, the stage was rotated by 90° where a second set of lines was deposited creating a grid pattern. The initial layer of polymer was tens of nanometers thick (data not shown), and the excess polymer layers were rinsed off with Nanopure water. The electrostatic interactions between the positively charged polymer and negatively charged glass surface were highly stable and allowed the patterns to remain robustly adhered under vigorous washes and across a range of ionic solution strengths. The formation of uniform PDAC lines was favored at low writing speeds, at or below 100 nm/s, and low polymer concentrations, 1 wt% PDAC. The polymer ink included 20% by vol ethylene glycol to reduce solvent evaporation and 58% by vol ethanol to assist transport of polymer from the tip to the glass surface.

2.2.2 PDAC impedes lipid diffusion

To test the ability of the PDAC patterns to impede lipid diffusion, a lipid bilayer was allowed to form by incubating the patterned glass substrate with a solution of small

unilamellar vesicles in PBS at pH 7.4, as shown schematically in **Fig. 2.2** *B*. In order to visualize lipid membrane diffusion with fluorescence microscopy, the lipid vesicles were doped with 2 mol% of fluorescent lipid, NBD-PC. Fluorescence recovery after photobleaching (FRAP) experiments were performed on the grid, where a defined region of the lipid bilayer was photobleached and allowed to recover, see **Fig. 2.3** *A*. Fluorescence images of the as-fabricated structures before photobleaching (**Fig. 2.3** *B*) shows a series of 2 vertical and 3 horizontal polymer lines surrounded by a uniform lipid bilayer. The fluorescence image in **Fig. 2.3** *C* shows the same patterned lipid membrane region immediately after photobleaching. After 2.5 min, the lipid membrane underwent lateral diffusion such that the fluorescence intensity reached an equilibrium value within each corral, but intermixing across the polymer structures was hindered (**Fig. 2.3** *D*). The FRAP data demonstrate that DPN-generated PDAC lines structures can inhibit lipid diffusion.

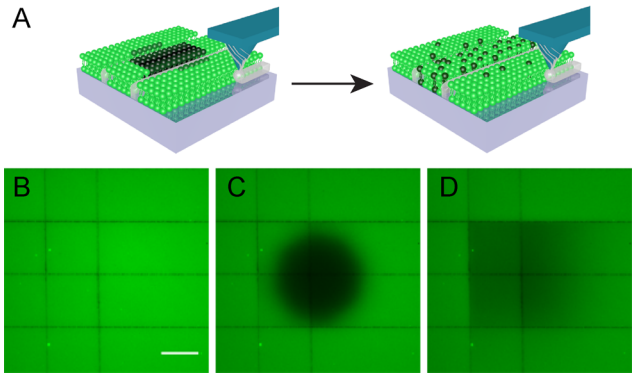

Figure 2.3 FRAP analysis of polymer patterns. (A) Schematic illustration of the FRAP experiment. (B) Representative fluorescence microscopy image of a supported lipid membrane doped with NBD-PC, and patterned with PDAC line structures deposited by DPN. Fluorescence images of the same region immediately after photobleaching (C), and 2.5 min after photobleaching (D). Scale bar = 25 μm.

In some cases, intermittent line patterns formed where incomplete polymer deposition occurred. Disjointed lines of PDAC were clearly observed with reflection interference contrast microscopy (RICM) (**Fig. 2.4**). Importantly, such structures act as semi-permeable barriers that lower the effective diffusion rate but do not completely prevent lateral diffusion. Such structures mimic restricted diffusion in cells[6] and are desirable to study non-Brownian diffusion behavior of membrane bound molecules.[9]

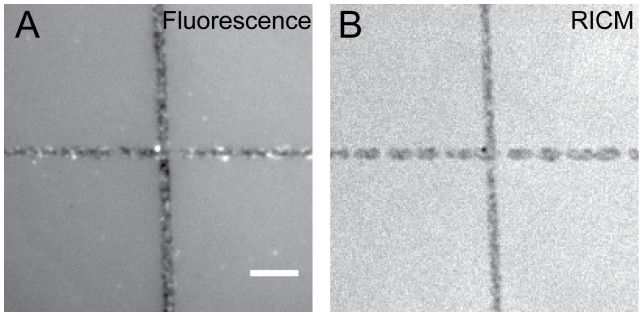

Figure 2.4. Deposition of partially formed PDAC lines. (A) Fluorescence image of NBD lipids surrounding intersecting polymer lines. (B) RICM image showing clear gaps in the patterned horizontal line. However, the vertical line contains no breaks. Scale bar represents 5 μm.

2.2.3 Characterization of patterned polymer

In order to describe the structure of PDAC adsorbates, dot arrays of the polymer were deposited onto an etched glass substrate and the remaining regions backfilled with a lipid membrane doped with NBD-PC (**Fig. 2.5**). Such fluorescence images provided an indirect description of the size of the PDAC dot arrays. Using this analysis, we found that the optimum ink concentration for generating dot arrays consisted of a higher polymer concentration of 15.8 wt% PDAC (see **Table 2.1**). In addition, we found that high spring constant tip arrays (1 N/m) with pre-fabricated ink channels, were ideally suited for generating dot arrays. This is in agreement with the conditions that were recently employed to pattern PDMS dot arrays.[33]

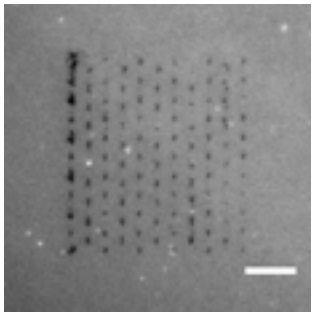

Figure 2.5. PDAC dot array. Representative fluorescence image of NBD-PC membrane formed on a PDAC dot array patterned glass coverslip. Patterning conditions were the same as those in Fig. 2.6 below. Scale bar = 5 μm.

Tip Array	PDAC (by wt)	Ethanol	Water	Ethylene Glycol	Relative Humidity	Pattern
F Type	1%	57.9%	21.1%	20%	Ambient	Lines
F Type	5%	49.3%	25.7%	20%	Ambient	Lines
F Type	10%	38.6%	31.4%	20%	Ambient	Lines
F Type	20%	6.5%	48.5%	20%	Ambient	Lines
F Type	10%	38.6%	31.4%	20%	75%	Lines
F Type	1%	10%	69%	20%	Ambient	Lines
F Type	5%	10%	65%	20%	Ambient	Lines
F Type	10%	10%	60%	20%	Ambient	Lines
F Type	5%	10%	65%	20%	75%	Lines
M Type	15.8%	10%	29.2%	45%	Ambient	Dots
M Type	10%	10%	60%	20%	Ambient	Dots

Table 2.1. PDAC ink composition. Summary of the different PDAC ink compositions tested for this study including the type of tip array used and the pattern written.

Using these conditions, a dot array was designed and fabricated in force-feedback mode under the InkCad software, where the dot-to-dot spacing was 2 mm and the total tip dwell time was 60 s. Given that the PDAC adsorbates are optically transparent, see **Fig. 2.6**, dot arrays were immersed in a fluorescein solution to aid in rapid inspection and identification of the regions for AFM imaging (**Fig. 2.6** *A*). The fluorescent PDAC dot array was imaged in AC mode with a clean, premounted AC probe tip in order to avoid deforming the deposited structures. The phase image (**Fig. 2.6** *C*) indicated that the

average dot diameter was 300 nm, but the topographical scan (**Fig. 2.6** *D*) showed no detectable features. To verify this observation, two line scans are plotted over identical regions across the center of a single dot in the phase and height AFM channels in **Fig. 2.6** *B*. Phase imaging has often been used for mapping differences in chemical composition, adhesion or viscoelasticity.[44] This result implies that the PDAC layers are chemically distinct, but their thickness cannot be distinguished from the root-mean-square roughness of the glass surface (~8 Å). Previous AFM studies of PDAC multilayer films agree with these findings and indicate that PDAC layers deposited at low ionic strength (< 0.1 M NaCl) tend to adopt an extended rod-like conformation.[45, 46] The thickness of polyelectrolyte multilayer films (10 bilayers) range from 6-9 nm, thus indicating that the thickness of a single layer of polyelectrolyte ranges from 3-4.5 Å.[45, 47] Taken together, this data indicate that DPN-deposited films consist of 1-3 molecular layers of PDAC and are responsible for hindering lipid mobility.

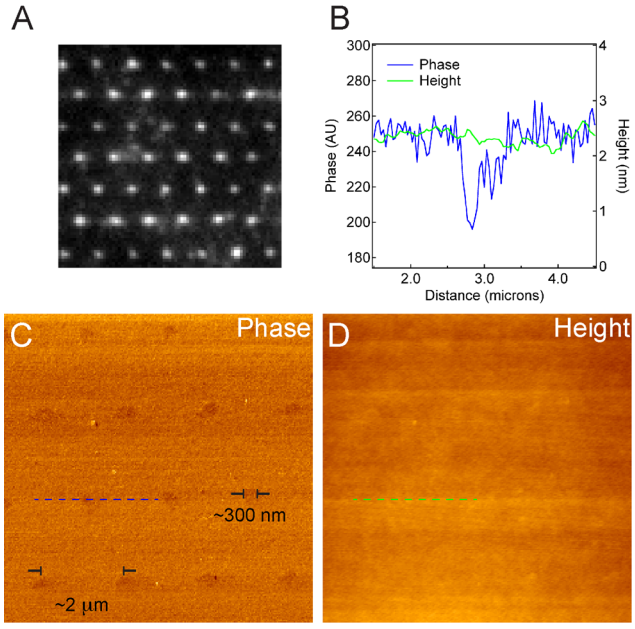

Figure 2.6. AFM characterization of PDAC dot array. (A) Representative fluorescence image of fluorescein-doped PDAC dot-array generated on a glass substrate (Fig.2.2 Bii).

The image is 12 μm x 12 μm. (B) Plots of tapping-mode AFM height and AFM phase of line scans taken from a single 300 nm dot from the array shown in (A). (C) AFM phase image, and (D) AFM height image of the PDAC dot array in (A). The dashed lines indicate the location of the regions that were plotted in (B). AFM images were collected with a scan size of 7.5 μm x 7.5 μm and scan rate of 1.0 Hz.

2.2.4 Cell response to ligand functionalized nanopatterns

One of the major challenges in the area of supported membranes pertains to the ability to juxtapose mobile proteins and lipid alongside immobile proteins. The PDAC patterns created by DPN address this issue, as they provide a template for protein adsorption, while the phospholipid membrane prevents non-specific adsorption of biomolecules. To target protein binding to the PDAC lines, the nanopatterned supported membrane was exposed to a solution of 100 μg/mL bovine serum albumin (BSA) fluorescently tagged with Cy3 (BSA-Cy3). The BSA-Cy3 localized to the polymer lines and was not observed to adhere to the supported lipid membrane, as seen in **Fig. 2.7**.

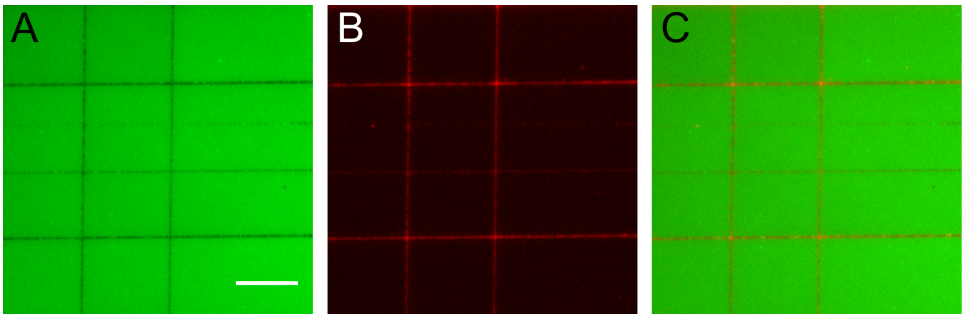

Figure 2.7. Selective localization of BSA-Cy3 onto PDAC lines. (A) NBD lipids on a glass surface patterned with a PDAC grid. Scale bar = 25 μm. (B) BSA-Cy3 was selectively adsorbed onto the polymer lines. (C) Image overlay of (A) and (B), which shows that BSA-Cy3 adheres specifically to the polymer regions and not the lipid corrals.

To demonstrate that the PDAC molecular layers can engage and manipulate the organization of cell surface receptors, we generated nanopatterned lipid membranes and coupled these to live cells. In particular, we sought to spatially immobilize integrin

adhesions to the nanopatterned regions while allowing the molecular assembly of a free-floating cell receptor, such as the epidermal growth factor receptor (EGFR), within the fluid membrane surface. This was important because EGF-EGFR complexes are known to dynamically form higher-order oligomers at the cell surface.[48-52] Fibronectin conjugated to Cy3 fluorescent dye (FN-Cy3) was immobilized onto the PDAC regions, while the epidermal growth factor (EGF-Alexa Fluor 647) ligand was tethered to the upper leaflet of a supported lipid membrane as shown in **Fig. 2.8** *A*.

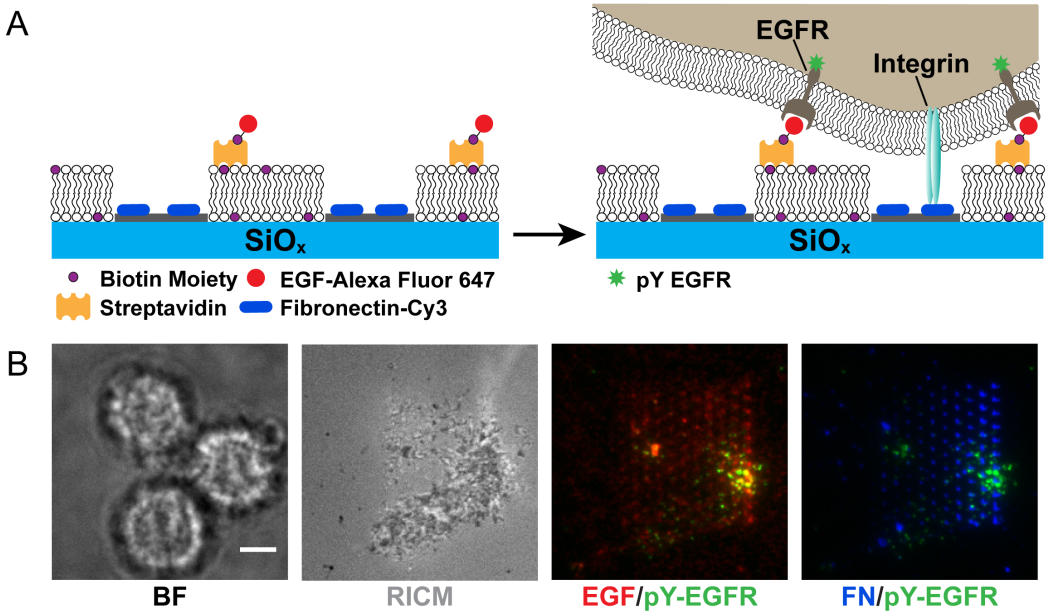

Figure 2.8. Live cell binding to PDAC pattern. (A) Scheme illustrating the binary ligand system that presents immobilized FN-Cy3 and laterally mobile EGF-647. The EGF and fibronectin ligands bind EGFR and integrins, respectively, when the substrate is interfaced with a live cell. (B) Representative brightfield, RICM, and fluorescence microscopy images of three cells that are engaged to a nanopatterned supported membrane. The overlaid images are false colored to aid in visualizing EGF/pY-EGFR and FN/pY-EGFR. Scale bar = 5 μm.

The breast cancer cell line, HCC1143, was selected for this experiment because it is an adherent cell line known to overexpress EGFR. Initially, the dot array was patterned and rinsed, followed by vesicle fusion to form the biotin functionalized

membrane bilayer. The surface was incubated with 50 μg/mL FN-Cy3 for 30 min and then blocked with 100 μg/mL BSA to minimize any non-specific adsorption to the PDAC pattern. Streptavidin at 1 μg/mL and EGF-647 at 1 μg/mL were added sequentially to the bilayer to complete the surface preparation. Finally, RPMI media with 10% fetal bovine serum was exchanged into the sample chamber and 600,000 cells, in two aliquots, were incubated on the surface for 30 minutes at 37° C and 5% CO_2. After 30 minutes of live cell imaging, the samples were fixed and stained for activation of EGFR through phosphorylation of the tyrosine residue at position 1068 (pY-1068).

A representative set of brightfield and fluorescence microscopy images show three cells adhered to a nanoscale dot array (**Fig. 2.8** *B*). RICM, which provides a measure of the distance between a cell membrane and the underlying support,[53] shows that the cells were tightly adhered to the dots presenting fibronectin. Note that the dot array maintained strong attachment to the glass slide despite cell adhesion and the application of tension across dots. Additional experiments indicated that polymer lines were able to withstand interactions with the cell (**Fig. 2.9**). Fluorescence imaging of EGF-647 reveals the formation of EGF-EGFR clusters that translocate to the center of the cell-surface junction, presumably though a retrograde flow mechanism.[51] Importantly, some of the EGF clusters remain constrained by the immobilized fibronectin dots, indicating that these PDAC-FN-Cy3 adsorbates serve to restrict the motions of the EGFR in the cell membrane. There is a small amount of non-specific binding of EGF-647 onto the PDAC implying that BSA blocking was not complete, though it is possible that other compounds such as PEG or casein may be more effective at preventing undesired protein binding to the polyelectrolyte. In spite of this, the pY antibody stain revealed that ~84%

of the total pY signal, representing activated EGFR, is found in the fluid regions of the membrane and not over the immobilized fibronectin, thus suggesting that the non-specifically bound EGF-647 is notably less biologically active in comparison to the membrane-bound EGF species.

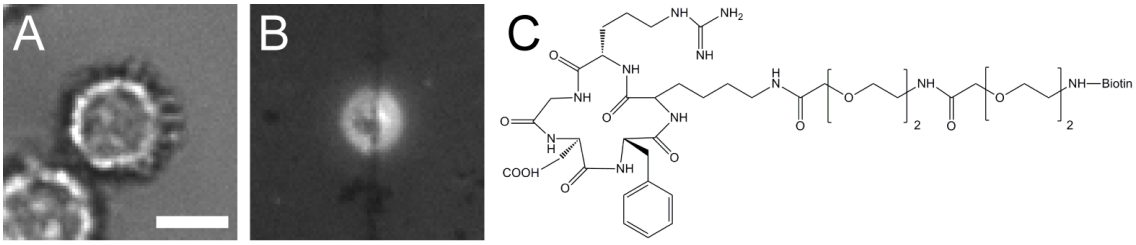

Figure 2.9. Effect of cell binding on PDAC line. Image of live cells on a biotinylated lipid surface functionalized with Alexa Fluor 647 labeled streptavidin (Streptavidin-647). Biotinylated cyclic RGD (cRGD) was placed onto the surface, and the cells were incubated onto the supported lipid membrane for 30 min. (A) Brightfield image of a cell that adhered to a DPN-generated PDAC line. Scale bar = 10 μm. (B) Epifluorescence image revealing the location of the streptavidin-647 and cRGD. (C) Chemical structure of biotinylated cRGDfK.

2.2.5 E-beam nanopatterns to restrict Delta-Notch movement

The current standard for nanopatterning technology is e-beam lithography because of its ability to produce highly consistent and precise metal patterns on the nanoscale. While these metal barriers are currently unable to accommodate both mobile and non-mobile ligands, they have been shown to be very effective diffusion barriers that can modulate cellular response of membrane spanning receptors such as EphA2 and EGFR.[10, 54] The Notch receptor is a compelling candidate to study using these nanopatterned grids due to the potential significance of mechanical inputs in triggering activation of the signaling pathway. For this reason, biotin-modified DLL4 ligand was tethered to the biotin-DPPE membrane using streptavidin. Notch1-eGFP expressing cells were introduced to the substrate, which contained several different types of patterns, as

seen in **Fig. 2.10**. Typical ligand-receptor binding and clustering was observed for cells that landed in the area with no grid. Although not captured in static images, the clusters are highly dynamic and do not exhibit signs of directed movement. Interestingly, on the 3 μm grid, a single cell imaged after 1 h showed accumulation of ligand-receptor complexes near the edges of the squares. Similar to the PDAC patterns, the lines and dots show that the metal nanostructures confine lateral motion of the Notch receptor.

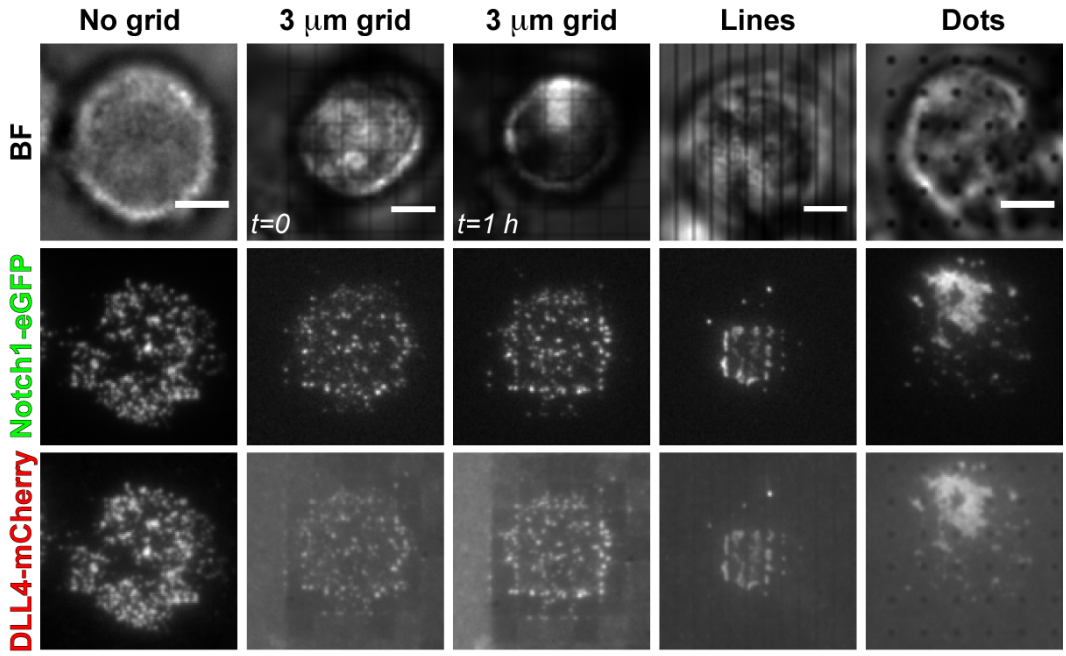

Figure 2.10. Interaction of Notch1-eGFP cells with chromium nanostructures. The type of pattern captured is indicated at the top of the figure, and the channel or molecule imaged is labeled on the left. Scale bar represents 5 μm.

Although not fully investigated in this study, the results shown in **Fig. 2.10** suggest that the receptor is actively transported towards the metal nanostructures. One potential reason for this behavior is that the barrier provides resistance to the cell and as a consequence the receptor. This physical interaction could be enough to result in the conformational change needed to activate the Notch receptor. In order to make such a

conclusion, a direct measurement of receptor activation is required. Current methods to measure receptor activation require at least 24 h for signal readout (discussed in Chapter 3). Based upon the preliminary data, no difference in activation levels could be measured for cells located on and off grid areas. It should be taken into account that the readout of the reporter cell line is relatively noisy and only a small number of cells (<200) per grid area were measured.

2.3 Conclusions

We have developed a new method for controlling ligand spatial organization in synthetic membranes and cells by using DPN to pattern PDAC, an optically transparent polyelectrolyte. We have shown that PDAC effectively impedes lipid diffusion, although its precise mechanism of lipid membrane interaction remains unclear. Based upon our AFM measurements, we rule out the possibility that the polymer acts as a topographical barrier, since the film thickness is below ~8 Å. This system can be used to understand the role of altered receptor spatial organization in the Notch signaling pathway, as well as force transduction in adhesion contacts when coupled with recently developed force sensing methods at membranes.[55] Using this platform, one protein of interest was immobilized onto the PDAC pattern while a second protein was tethered to the laterally mobile lipid surface, recapitulating a biological membrane and avoiding the introduction of distinct topographical features. Our preliminary data with laterally mobile EGF and immobilized fibronectin is one of hundreds of possible ligand pairs that can be investigated using this approach. The technique offers significant advantages in terms of throughput, simplicity, and biological relevance compared to many previous approaches

for receptor manipulations and especially given the recent development of massively parallel DPN-based patterning capabilities.

2.4 Materials and methods

2.4.1 Materials

PDAC (M_w = 100,000 g mol^{-1}), 35 wt% in water, paraformaldehyde and Triton X-100 were purchased from Sigma Aldrich, USA. Ethanol, ethylene glycol, 25 mm diameter #2 glass coverslips and BSA were acquired from VWR, USA. F- and M-type pen arrays and premounted AC mode tips were purchased from NanoInk, Inc., USA. All lipids were obtained from Avanti Polar Lipids, USA. Human fibronectin was purchased from Innovative Research, USA and labeled with reactive Cy3 dye from GE Healthsciences, USA. Recombinant human EGF was purchased from R&D Systems, USA. Alexa Fluor 647 carboxylic acid, succinimidyl ester and the secondary goat anti-rabbit IgG antibody conjugated with Alexa Fluor 488 were from Invitrogen, USA. Streptavidin was acquired from Rockland Immunochemicals, Inc., USA. Primary rabbit monoclonal antibody for pY (D7A5) was purchased from Cell Signaling Technology, USA.

2.4.2 DPN and AFM experiments

All DPN and AFM experiments were performed using the NScriptor DPNWriter nanolithography platform from NanoInk, Inc., USA, and the dot arrays were patterned using the InkCad software. The ink solution typically used to generate grid arrays consisted of a mixture of 1 wt% PDAC, 21% water, 58% ethanol, and 20% ethylene glycol by vol. The following ink solution mixture was typically prepared to generate dot arrays: 15.8 wt% PDAC, 29.2% water, 10% ethanol, and 45% ethylene glycol by vol. In

order to load the tip with ink, the AFM cantilever was brought into contact with a 0.5 mL drop of the appropriate ink solution that was pipetted onto a clean glass slide. All glass substrates for DPN were piranha etched (H_2O_2:H_2SO_4; 1:3; v:v) for 15 min and rinsed 3 times with copious amounts of NanoPure water (Caution: piranha solution is an extremely strong oxidant and can become explosive if mixed with organics). DPN was carried out under ambient conditions of 22-25° C and 25-40% relative humidity. AFM images were recorded in AC mode with the NScriptor.

2.4.3 Supported bilayer formation

After PDAC pattern fabrication, samples were rinsed with copious amount of NanoPure water. Substrates were then incubated with a 30 μL solution consisting of 15 μL of PBS and 15 μL of a 2 mg/mL solution of lipid vesicles. For FRAP experiments, the lipid vesicle solution was composed of 98 mol% 1,2-dioleoyl-*sn*-glycero-3-phosphocholine (DOPC) and 2 mol% NBD-PC. For cell experiments, the solution was comprised of 99.9 mol% DOPC and 0.1 mol% 1,2-dioleoyl-*sn*-glycero-3-phosphoethanolamine-N-(cap biotinyl) (biotin DPPE). The vesicles were prepared according to previously published methods.[52] Note that each incubation step was followed by rinsing with 50 mL of 1 x PBS.

2.4.4 Fluorescence imaging

All fluorescence images were collected on a Nikon Ti Eclipse microscope featuring an Evolve EM CCD (Photometrics), an Intensilight epifluorescence source (Nikon), and a TIRF launcher with two laser lines: 488 nm (10 mW) and 638 nm (20 mW). The microscope also includes the Nikon Perfect Focus System, an interferometry-based focus lock. The microscope is equipped with Chroma filter cubes, of which the

following were used for experiments in this paper: TIRF 488, TIRF 647, Cy5, TRITC, FITC, and RICM. Images were collected using Nikon's NIS Elements software and analyzed using ImageJ software from NIH. For FRAP experiments, the samples were illuminated in an epifluorescence configuration while the cells were imaged in total internal reflection fluorescence (TIRF) mode to minimize autofluorescence and image the interface between the cell membrane and the supported lipid membrane. The exception to this was the FN-Cy3, which was imaged in epifluorescence.

2.4.5 Cell experiments

Cells were fixed by rinsing with cold PBS to remove media and treated with a 4% paraformaldehyde solution for 12 min. After rinsing with 1 x PBS, the cells were permeated with 0.1% Triton X-100 for 5 min, rinsed, and stored overnight in a 1% BSA in 1 x PBS solution. The primary antibody was diluted 1:200 in 1% BSA and incubated for 1 h. The sample was thoroughly rinsed and incubated with the secondary antibody at a dilution of 1:1000 for 30 min. After a final rinse, the fixed cells were ready for imaging.

2.4.6 Determination of pY levels of EGFR

To quantify activation levels, a region of interest (ROI) was selected around each cell based on the bright field image, **Fig. 2.11**. Using the fluorescence signal from the physisorbed fibronectin, the PDAC dots were located using the particle analysis function in ImageJ, as seen in (1). The integrated signal from the pY channel excluding the dots was measured and divided by the total pY intensity under the cellular ROI (2). This allowed for a direct measurement of EGFR that was activated by fluid, membrane-bound EGF.

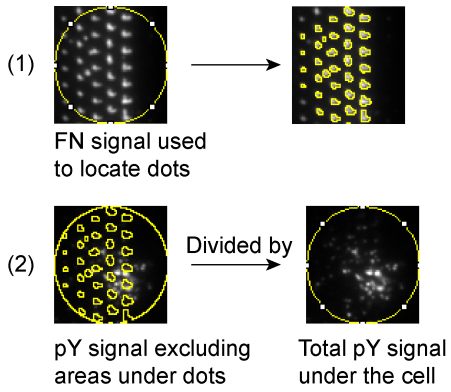

Figure 2.11. Summary of image analysis used to determine the pY levels of EGFR.

2.5 References

1. Singer, S. J.; Nicolson, G. L., The fluid mosaic model of the structure of cell membranes. *Science* **1972,** *175* (23), 720-731.

2. Gureasko, J.; Galush, W. J.; Boykevisch, S.; Sondermann, H.; Bar-Sagi, D.; Groves, J. T.; Kuriyan, J., Membrane-dependent signal integration by the Ras activator Son of sevenless. *Nat. Struct. Mol. Biol.* **2008,** *15* (5), 452-461.

3. Holowka, D. A.; Gosse, J. A.; Hammond, A. T.; Han, X.; Sengupta, P.; Smith, N. L.; Wagenknecht-Wiesner, A.; Wu, M.; Young, R. M.; Baird, B., Lipid segregation and IgE receptor signaling: a decade of progress. *Biochim. Biophys. Acta* **2005,** *1746* (3), 252-259.

4. Bromley, S.; Burack, W.; Johnson, K.; Somersalo, K.; Sims, T.; Sumen, C.; Davis, M.; Shaw, A.; Allen, P.; Dustin, M. L., The immunological synapse. *Annu. Rev. Immunol.* **2001,** *19*, 375-396.

5. Wu, M.; Holowka, D. A.; Craighead, H. G.; Baird, B., Visualization of plasma membrane compartmentalization with patterned lipid bilayers. *Proc. Natl. Acad. Sci. U. S. A.* **2004,** *101* (38), 13798-13803.

6. Andrews, N. L.; Lidke, K. A.; Pfeiffer, J. R.; Burns, A. R.; Wilson, B. S.; Oliver, J. M.; Lidke, D. S., Actin restricts FcepsilonRI diffusion and facilitates antigen-induced receptor immobilization. *Nat. Cell Biol.* **2008,** *10* (8), 955-963.

7. Mossman, K. D.; Campi, G.; Groves, J. T.; Dustin, M. L., Altered TCR signaling from geometrically repatterned immunological synapses. *Science* **2005,** *310* (5751), 1191-1193.

8. Manz, B. N.; Groves, J. T., Spatial organization and signal transduction at intercellular junctions. *Nat. Rev. Mol. Cell Biol.* **2010,** *11* (5), 342-352.

9. Tsai, J.; Sun, E.; Gao, Y.; Hone, J. C.; Kam, L. C., Non-Brownian diffusion of membrane molecules in nanopatterned supported lipid bilayers. *Nano Lett.* **2008,** *8* (2), 425-430.

10. Salaita, K. S.; Nair, P. M.; Petit, R. S.; Neve, R. M.; Das, D.; Gray, J. W.; Groves, J. T., Restriction of receptor movement alters cellular response: physical force sensing by EphA2. *Science* **2010,** *327* (5971), 1380-1385.

11. Nair, P. M.; Salaita, K. S.; Petit, R. S.; Groves, J. T., Using patterned supported lipid membranes to investigate the role of receptor organization in intercellular signaling. *Nat. Protoc.* **2011,** *6* (4), 523-539.

12. Shi, J.; Chen, J.; Cremer, P. S., Sub-100 nm patterning of supported bilayers by nanoshaving lithography. *J. Am. Chem. Soc.* **2008,** *130* (9), 2718-2719.

13. Lenhert, S.; Brinkmann, F.; Laue, T.; Walheim, S.; Vannahme, C.; Klinkhammer, S.; Xu, M.; Sekula, S.; Mappes, T.; Schimmel, T.; Fuchs, H., Lipid multilayer gratings. *Nature Nanotech.* **2010,** *5* (4), 275-279.

14. Sekula, S.; Fuchs, J.; Weg-Remers, S.; Nagel, P.; Schuppler, S.; Fragala, J.; Theilacker, N.; Franzreb, M.; Wingren, C.; Ellmark, P.; Borrebaeck, C. A. K.; Mirkin, C. A.; Fuchs, H.; Lenhert, S., Multiplexed lipid dip-pen nanolithography on subcellular scales for the templating of functional proteins and cell culture. *Small* **2008,** *4* (10), 1785-1793.

15. Lenhert, S.; Sun, P.; Wang, Y.; Fuchs, H.; Mirkin, C. A., Massively parallel dip-pen nanolithography of heterogeneous supported phospholipid multilayer patterns. *Small* **2007,** *3* (1), 71-75.

16. Groves, J. T.; Boxer, S. G., Micropattern formation in supported lipid membranes. *Acc. Chem. Res.* **2002,** *35* (3), 149-157.

17. Yu, C.-h.; Groves, J. T., Engineering supported membranes for cell biology. *Med. Biol. Eng. Comput.* **2010,** *48* (10), 955-963.

18. Czolkos, I.; Jesorka, A.; Orwar, O., Molecular phospholipid films on solid supports. *Soft Matter* **2011,** *7* (10), 4562-4576.

19. Sackmann, E., Supported membranes: scientific and practical applications. *Science* **1996,** *271* (5245), 43-48.

20. DeMond, A. L.; Mossman, K. D.; Starr, T.; Dustin, M. L.; Groves, J. T., T cell receptor microcluster transport through molecular mazes reveals mechanism of translocation. *Biophys. J.* **2008,** *94* (8), 3286-3292.

21. Sennett, R.; Scott, G., The Structure of Evaporated Metal Films and Their Optical Properties. *J. Opt. Soc. Am.* **1950,** *40* (4), 203-211.

22. Gates, B. D.; Xu, Q.; Stewart, M.; Ryan, D.; Willson, C. G.; Whitesides, G. M., New approaches to nanofabrication: molding, printing, and other techniques. *Chem. Rev.* **2005,** *105* (4), 1171-1196.

23. Alakoskela, J.-M.; Koner, A. L.; Rudnicka, D.; Koehler, K.; Howarth, M.; Davis, D. M., Mechanisms for Size-Dependent Protein Segregation at Immune Synapses Assessed with Molecular Rulers. *Biophys. J.* **2011,** *100* (12), 2865-2874.

24. Krobath, H.; Różycki, B.; Lipowsky, R.; Weikl, T. R., Line tension and stability of domains in cell-adhesion zones mediated by long and short receptor-ligand complexes. *PLoS One* **2011,** *6* (8), e23284.

25. Lohmüller, T.; Triffo, S. B.; O'Donoghue, G. P.; Xu, Q.; Coyle, M. P.; Groves, J. T., Supported membranes embedded with fixed arrays of gold nanoparticles. *Nano Lett.* **2011,** *11* (11), 4912-4918.

26. Piner, R.; Zhu, J.; Xu, F.; Hong, S.; Mirkin, C. A., "Dip-Pen" nanolithography *Science* **1999,** *283* (5402), 661-663.

27. Salaita, K. S.; Wang, Y.; Mirkin, C. A., Applications of dip-pen nanolithography. *Nature Nanotech.* **2007,** *2* (3), 145-155.

28. Shim, W.; Braunschweig, A. B.; Liao, X.; Chai, J.; Lim, J. K.; Zheng, G.; Mirkin, C. A., Hard-tip, soft-spring lithography. *Nature* **2011,** *469* (7331), 516-521.

29. Huo, F.; Zheng, Z.; Zheng, G.; Giam, L. R.; Zhang, H.; Mirkin, C. A., Polymer pen lithography. *Science* **2008,** *321* (5896), 1658-1660.

30. Lee, K.-B.; Park, S.; Mirkin, C. A.; Smith, J.; Mrksich, M., Protein nanoarrays generated by dip-pen nanolithography. *Science* **2002,** *295* (5560), 1702-1705.

31. Wilson, D. L.; Martin, R.; Hong, S.; Cronin-Golomb, M.; Mirkin, C. A.; Kaplan, D. L., Surface organization and nanopatterning of collagen by dip-pen nanolithography. *Proc. Natl. Acad. Sci. U. S. A.* **2001,** *98* (24), 13660-13664.

32. McKendry, R.; Huck, W.; Weeks, B. L.; Florini, M.; Abell, C.; Rayment, T., Creating nanoscale patterns of dendrimers on silicon surfaces with dip-pen nanolithography. *Nano Lett.* **2002,** *2* (7), 713-716.

33. Hernandez-Santana, A.; Irvine, E.; Faulds, K.; Graham, D., Rapid prototyping of poly(dimethoxysiloxane) dot arrays by dip-pen nanolithography. *Chem. Sci.* **2011,** *2* (2), 211-215.

34. Lim, J.-H.; Mirkin, C. A., Electrostatically driven dip-pen nanolithography of conducting polymers. *Adv. Mater.* **2002,** *14* (20), 1474-1477.

35. Yu, M.; Nyamjav, D.; Ivanisevic, A., Fabrication of positively and negatively charged polyelectrolyte structures by dip-pen nanolithography. *J. Mater. Chem.* **2005,** *15* (6), 649-652.

36. Jackson, B. L.; Groves, J. T., Scanning probe lithography on fluid lipid membranes. *J. Am. Chem. Soc.* **2004,** *126* (43), 13878-13879.

37. Silin, V.; Wieder, H.; Woodward, J.; Valincius, G.; Offenhausser, A.; Plant, A., The role of surface free energy on the formation of hybrid bilayer membranes. *J. Am. Chem. Soc.* **2002,** *124* (49), 14676-14683.

38. Kohli, N.; Vaidya, S.; Ofoli, R. Y.; Worden, R. M.; Lee, I., Arrays of lipid bilayers and liposomes on patterned polyelectrolyte templates. *J. Colloid Interface Sci.* **2006,** *301* (2), 461-469.

39. Luo, G.; Liu, T.; Zhao, X.; Huang, Y.; Huang, C.; Cao, W., Investigation of polymer-cushioned phospholipid bilayers in the solid phase by atomic force microscopy. *Langmuir* **2001,** *17* (13), 4074-4080.

40. Zhang, L.; Longo, M.; Stroeve, P., Mobile phospholipid bilayers on a polyion/alkylthiol layer pair. *Langmuir* **2000,** *16* (11), 5093-5099.

41. Ma, C.; Srinivasan, M.; Waring, A.; Lehrer, R.; Longo, M.; Stroeve, P., Supported lipid bilayers lifted from the substrate by layer-by-layer polyion cushions on self-assembled monolayers. *Colloids Surf., B* **2003,** *28* (4), 319-329.

42. Salaita, K. S.; Wang, Y.; Fragala, J.; Vega, R. A.; Liu, C.; Mirkin, C. A., Massively parallel dip-pen nanolithography with 55 000-pen two-dimensional arrays. *Angew. Chem. Int. Ed.* **2006,** *45* (43), 7220-7223.

43. Liao, X.; Braunschweig, A. B.; Mirkin, C. A., "Force-feedback" leveling of massively parallel arrays in polymer pen lithography. *Nano Lett.* **2010,** *10* (4), 1335-1340.

44. Garcia, R.; Perez, R., Dynamic atomic force microscopy methods. *Surf. Sci. Rep.* **2002,** *47*, 197-301.

45. McAloney, R.; Sinyor, M.; Dudnik, V.; Goh, M., Atomic force microscopy studies of salt effects on polyelectrolyte multilayer film morphology. *Langmuir* **2001,** *17* (21), 6655-6663.

46. Dahlgren, M.; Claesson, P.; Audebert, R., Highly-Charged Cationic Polyelectrolytes on Mica - Influence of Polyelectrolyte Concentration on Surface Forces. *J. Colloid Interface Sci.* **1994,** *166* (2), 343-349.

47. Dubas, S.; Schlenoff, J. B., Factors controlling the growth of polyelectrolyte multilayers. *Macromolecules* **1999,** *32* (24), 8153-8160.

48. Costa, M. N.; Radhakrishnan, K.; Edwards, J. S., Monte Carlo simulations of plasma membrane corral-induced EGFR clustering. *J. Biotechnol.* **2011,** *151* (3), 261-270.

49. Hofman, E. G.; Bader, A. N.; Voortman, J.; van den Heuvel, D. J.; Sigismund, S.; Verkleij, A. J.; Gerritsen, H. C.; Henegouwen, P. M. P. v. B. E., Ligand-induced EGF Receptor Oligomerization Is Kinase-dependent and Enhances Internalization. *J. Biol. Chem.* **2010,** *285* (50), 39481-39489.

50. Chung, I.; Akita, R.; Vandlen, R.; Toomre, D.; Schlessinger, J.; Mellman, I., Spatial control of EGF receptor activation by reversible dimerization on living cells. *Nature* **2010,** *464* (7289), 783-787.

51. Lidke, D. S.; Lidke, K. A.; Rieger, B.; Jovin, T. M.; Arndt-Jovin, D. J., Reaching out for signals: filopodia sense EGF and respond by directed retrograde transport of activated receptors. *J. Cell Biol.* **2005,** *170* (4), 619-626.

52. Nam, J.-M.; Nair, P. M.; Neve, R. M.; Gray, J. W.; Groves, J. T., A fluid membrane-based soluble ligand-display system for live-cell assays. *ChemBioChem* **2006,** *7* (3), 436-440.

53. Theodoly, O.; Huang, Z. H.; Valignat, M. P., New modeling of reflection interference contrast microscopy including polarization and numerical aperture effects: application to nanometric distance measurements and object profile reconstruction. *Langmuir* **2010,** *26* (3), 1940-1948.

54. Stabley, D.; Retterer, S.; Marshall, S.; Salaita, K. S., Manipulating the lateral diffusion of surface-anchored EGF demonstrates that receptor clustering modulates phosphorylation levels. *Integr. Biol.* **2013,** *5* (4), 659-668.

55. Stabley, D. R.; Jurchenko, C.; Marshall, S. S.; Salaita, K. S., Visualizing mechanical tension across membrane receptors with a fluorescent sensor. *Nat. Methods* **2012,** *9* (1), 64-67.

Chapter 3: Membrane Tethered Delta Activates Notch and Reveals a Role for Spatio-Mechanical Regulation of the Signaling Pathway

Adapted from Narui, Y.; Salaita, K. S., Membrane Tethered Delta Activates Notch and Reveals a Role for Spatio-Mechanical Regulation of the Signaling Pathway. *Biophys. J.* **2013**, *105* (12), 2655-2665.

3.1 Introduction

Cell-cell communication is essential for the development, proliferation, and survival of multicellular organisms. To coordinate complex events within multicellular organisms, certain signals need to be short-ranged and confined to a cell's nearest neighbors. One general strategy for short-range cellular communication employs membrane anchored ligands and receptors such that direct physical contact between adjacent cells is required for pathway activation. This type of interaction is commonly found in cell-adhesion junctions, neuronal and immunological synapses, and during cellular patterning and development.[1] Despite the importance of these juxtacrine interactions, the role of receptor oligomerization, spatial organization, membrane topography, and physical forces in signal modulation remains poorly understood. The fundamental challenge pertains to the lack of methods to characterize ligand-receptor interactions in the confined and dynamic two-dimensional environment of the cell-cell junction. Therefore, new experimental strategies are needed to better understand the role of chemo-mechanical couplings in short-range, juxtacrine signaling pathways.

One important example of short range cellular signaling is the Notch pathway, which is universally conserved and critical to development and differentiation in metazoa. The Notch receptors are a family of heterodimeric membrane proteins that bind directly to Delta/Serrate/Lag-2 ligand molecules expressed on the surface of an apposing cell.[2] Ligand-induced activation of Notch receptors is characterized by a series of regulated intramembrane proteolysis events. The key proteolysis step in activation of the signaling pathway is cleavage of Notch at site 2 (S2) by a disintegrin and metalloprotease (ADAM) that results in shedding of the Notch extracellular domain (NECD). Following

S2 cleavage, the Notch intracellular domain (NICD) is released from the membrane by γ-secretase proteolysis at site 3 (S3), which is located within the transmembrane domain of Notch. The NICD translocates to the nucleus where it functions as a transcription factor and upregulates gene expression of targets in the Hes and Hey families.

NMR and x-ray crystallography studies have revealed that a large conformational change is required to expose S2 for attack by ADAM.[3, 4] The ligand binding domain is nearly 1000 amino acid residues away from the cleavage site, and thus a mechanical force model has been proposed as a mechanism for this long range conformational change [5-8]. This mechanotransduction model suggests that the formation of ligand-receptor complexes is coupled with endocytosis to generate mechanical tension that opens up the S2 site and renders it susceptible to proteolysis. This model is supported by evidence that the receptor cannot be activated with soluble ligand molecules and that endocytosis is required for activation in both *Drosophila* and mammalian cells.[6, 7, 9-12] Interestingly, one recent study found that Notch activation requires between 0 and 12 pN of mechanical tension, but the direct observation of force exerted by a cell has yet to be observed.[13]

In addition to the mechanical forces applied by cells, altering the physical properties of ligand molecules may significantly influence signaling. For example, the activity of chemically identical ligand molecules can be modulated by adjusting factors such as density, spatial organization, and lateral mobility within the membrane environment. This effect has been observed in a wide variety of signaling pathways involving immunorecognition receptors, E-cadherins and receptor tyrosine kinases.[14-17]

Current strategies for studying Delta-Notch interactions have been unable to distinguish a role for ligand density, diffusion and oligomerization in activation of the Notch receptor, as summarized in **Fig. 1.6**. Herein, we use a supported lipid membrane functionalized with DLL4 to observe ligand-induced activation of Notch in live cells. The key advantages of this method include: (i) fine control and quantification of ligand composition and concentration; (ii) ability to adjust the lateral mobility of ligand molecules and the rate at which Notch and Delta molecules interact and form clusters; (iii) proper orientation of the Delta ligand on the membrane through site-specific anchoring; (iv) absolute number density determination of ligand and receptor molecules and clusters, and their stoichiometry within an intermembrane junction; and (v) direct observation of dynamics of Delta-Notch complex formation and internalization events in real-time. By frustrating the lateral motions of Notch receptors in the cell membrane, we increase activation levels by 2.6-fold compared to chemically identical ligand that is laterally mobile. Finally, we determine the stoichiometry of ligand:receptor binding to be 1:1 when approximated to the nearest integer value, in agreement with accepted structural models.[3]

3.2 Results and discussion

3.2.1 Delta-Notch binding on fluid membranes

Supported lipid membranes were prepared as illustrated in **Fig. 3.1** *A*, and two types of DLL4 ligand (residues Ser27-Pro524) were tethered to the membrane surfaces, see Material and Methods. The first was a DLL4 tagged with 2-3 molecules of an amine-reactive Alexa Fluor 568 or 647 (DLL4-568 or DLL4-647), and the second was a DLL4-mCherry fusion, where the fluorescent protein was inserted at the C-terminus. It is

important to note that the poly-histidine tag is the final element of the C-terminus for both proteins ensuring that the ligand is oriented in the correct conformation for binding with Notch [2]. Fluorescence recovery after photobleaching (FRAP) demonstrates that surface anchored DLL4 is fluid within the membrane (**Fig. 3.1** *B-D*). A small area of the bilayer was photobleached (**Fig. 3.1** *B*) and after ~5 min non-photobleached ligand molecules diffused into the area and restored fluorescence intensity to pre-bleached levels (**Fig. 3.1** *C*). A line scan over the photobleached spot (**Fig. 3.1** *D*) showed near complete recovery of the ligand fluorescence and verified the fluid nature of the supported lipid membrane tethered DLL4.

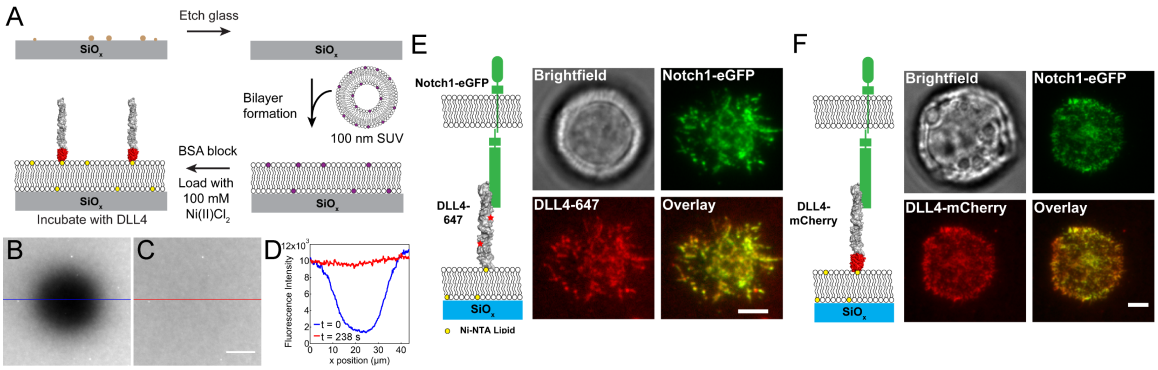

Figure 3.1. Preparation of membrane tethered DLL4. (A) Outline of the procedure used to fabricate supported lipid membranes containing tethered DLL4 molecules. Rendering of the extracellular domain of DLL4 is based upon the crystal structure of a fragment of human Jagged1, residues 187-335, which includes the DSL domain and the first 3 EGF repeats (PDB ID: 2VJ2). (B-C) Fluorescence recovery after photobleaching of the DLL4-647 bilayer surface verifying the lateral mobility of the fluorophore labeled ligand. Scale bar = 10 μm. (D) Line scans over the indicated areas of images (B) and (C). Representative live cell images demonstrating binding between Notch1-eGFP and membrane tethered (E) DLL4-647 and (F) DLL4-mCherry following a 30 min incubation period. Overlay images indicate a high degree of colocalization between Notch1 and DLL4. Scale bar = 5 μm.

To demonstrate that the membrane-bound ligand molecules function biologically, stably transfected Notch1-eGFP C2C12 mouse myoblasts were incubated with the

membrane surfaces for 30 min to bind to DLL4. Live cell images of single cells showed that both DLL4-647 and DLL4-mCherry formed ligand-receptor complexes, **Fig. 3.1** *E* and *F*, respectively. These representative images show near complete colocalization between the DLL4 and Notch1 fluorescence signal as seen in the overlay images, thus suggesting that Notch1 is the primary binding partner for DLL4. As a control, parental C2C12 cells were incubated onto DLL4-mCherry functionalized bilayers and showed low levels of ligand-receptor binding (**Fig. 3.2**). Based on quantitative single cell intensity analysis, the amount of parental cell binding to DLL4 ligand was calculated to be 28% of Notch1-eGFP binding. It is important to note that this percentage reflects binding of all types of endogenous Notch receptors in the parental cell line compared with Notch1-eGFP and endogenous Notch binding in the transfected cell line. To verify the specificity of the DLL4-Notch1 interaction, Notch1-eGFP expressing cells were incubated with soluble DLL4/Fc (185 nM) and then placed onto the DLL4 membrane. In this case, binding of the Notch1-eGFP expressing cells to the ligand-presenting membrane was completely blocked after treatment with soluble ligand, as seen in **Fig. 3.3**. Note that the soluble DLL4/Fc-treated cells very weakly attached to the membrane, therefore a small amount (0.1% by molar ratio) of cyclic Arg-Gly-Asp-d-Phe-Lys (cRGDfK) was incorporated into the bilayer to anchor cells and facilitate imaging (see Supporting Material). We found that cRGDfK-integrin binding does not upregulate the downstream marker of Notch activation, Hey1 (also known as Herp2), as determined by RT-PCR (data not shown). Taken together, this data confirms that Notch1-eGFP specifically binds to membrane bound DLL4.

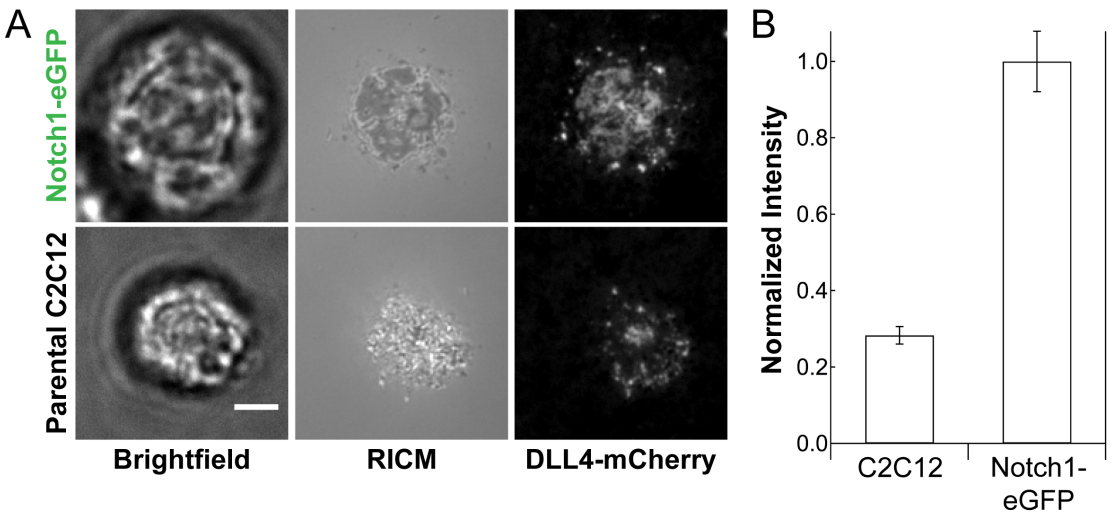

Figure 3.2. DLL4 binding of Notch receptors on parental C2C12 cells compared with Notch1-eGFP expressing cells. (A, Top panel) Representative images of Notch1-eGFP receptor binding to DLL4-mCherry on a supported membrane after 30 min reveal the formation of ligand-receptor clusters. (A, Bottom panel) Representative images of endogenous Notch receptors in parental C2C12 cells show binding to the DLL4-mCherry surfaces and formation of clusters that are smaller and less dense. Scale bar = 5 μm. (B) Quantitative comparison of the amount of ligand-receptor binding for Notch1-eGFP and C2C12 cells, error bars represent SEM for n = 60 C2C12 cells and n = 35 Notch1-eGFP cells.

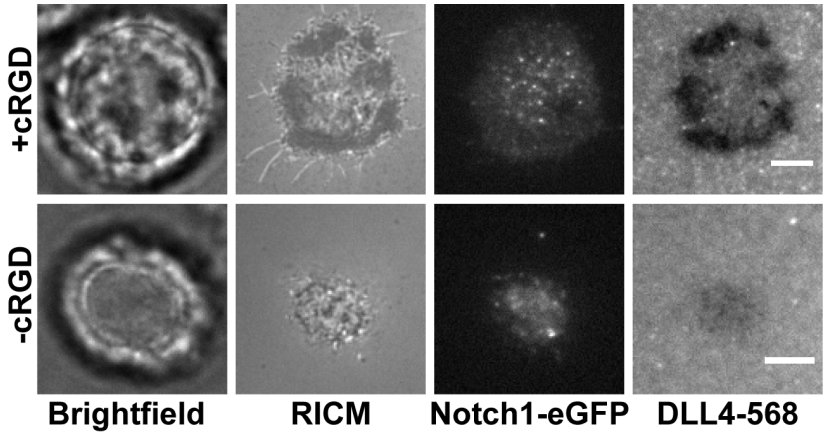

Figure 3.3. Specificity of DLL4 binding to Notch1. Notch1-eGFP cells were treated with soluble DLL4/Fc (185 nM) for 20 min before incubating on a DLL4-568 membrane surface. In order to facilitate imaging of cells, cRGD was added to the supported lipid membrane (top) to promote cell adhesion. Without cRGD-integrin binding, the Notch1-eGFP expressing cells very weakly associated with the supported lipid membrane (bottom).

3.2.2 Formation and dynamics of Delta-Notch clusters

In addition to DLL4-Notch1 binding, we observed the formation of clusters of ligand-receptor complexes, in agreement with previous studies.[11, 18] To determine if clustering is Notch cell-driven, DLL4 supported lipid membrane surfaces were incubated with recombinant human Notch1 extracellular domain/Fc labeled with Alexa Fluor 647 (NECD-647), **Fig. 3.4**. This NECD construct is composed of the first 13 EGF repeats of the Notch receptor including the 11th and 12th repeats that are known to be necessary and sufficient for ligand binding.[19] NECD-647 binds to both types of DLL4 surfaces, however the receptor had an enhanced affinity for DLL4-mCherry compared to DLL4-568 as evidenced by higher overall fluorescence signal in the NECD channel. One potential reason for reduced ligand potency of DLL4-568 arises as a result of fluorophore conjugation to lysine residues (K189, K190) found in the Notch receptor binding site.[3] This highlights an important difference between the two ligands tested as DLL4-mCherry possesses a single fluorescent protein located at the C-terminus of the ligand, far from the Notch binding domain. Regardless of ligand affinity, when receptor ectodomain fragments were exposed to a DLL4 supported membrane no significant clustering of the ligand was observed and the membrane remained fluid as verified by FRAP (**Fig. 3.4**). These results illustrate that the Notch expressing cell is sufficient in driving ligand-induced receptor clustering.

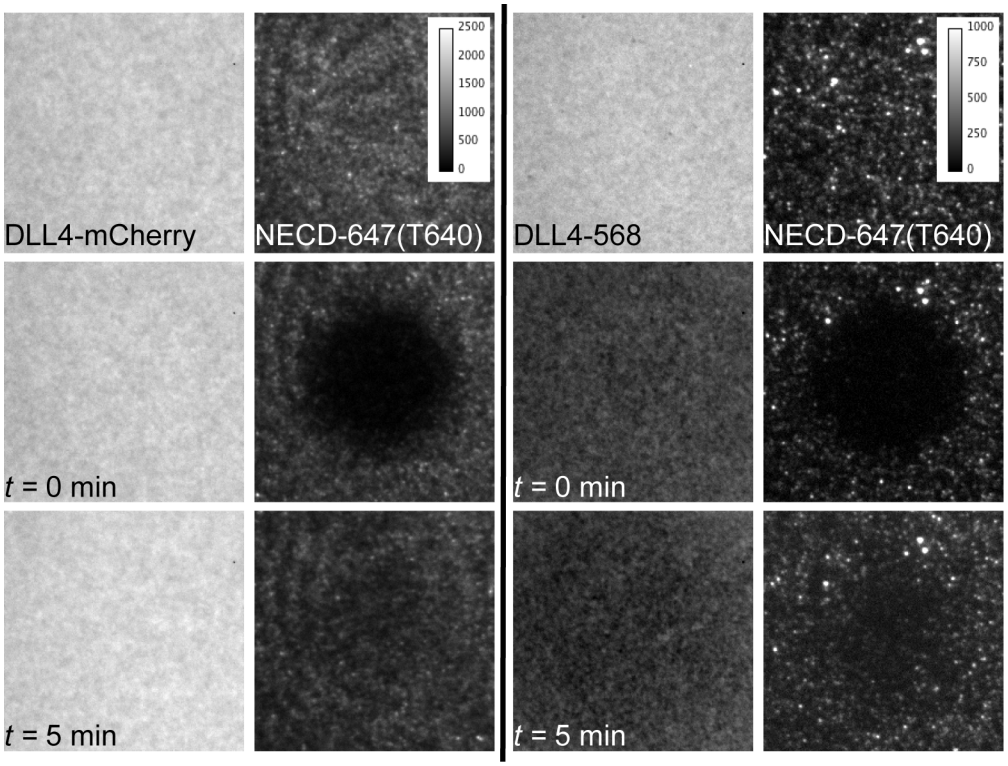

Figure 3.4. Clustering of DLL4 is Notch-cell driven. Binding of NECD-647 to DLL4 supported lipid membrane surface alone does not result in observable clustering. Note that the NECD-647 displays different affinity for the two types of ligand tested as indicated by the differences in intensity (calibration bars). FRAP assay shows that the NECD-647 is still laterally mobile when bound to DLL4.

To gain insight into the formation of ligand-receptor clusters, the dynamics of individual Notch1-eGFP cells on a DLL4 supported lipid membrane were observed using time-lapse microscopy. Interestingly, these movies revealed the depletion of Notch1-eGFP signal through two distinct routes. The first type of receptor depletion was gradual loss in Notch1-eGFP intensity on the timescale of minutes (**Fig. 3.5** *A*-*B*, Movie S1). These clusters were comprised of hundreds of receptor molecules, and the reduction in intensity was distinct from eGFP photobleaching (**Fig. 3.6**). In **Fig. 3.5** *A*, two clusters labeled 1 and 2 were tracked for a total of 60 min. The eGFP intensity of cluster 1 steadily decreased over a 12 min interval while the overall signal never reached zero.

Cluster 2 served as a control and showed that the depletion of specific clusters was coordinated by cellular inputs and not due to fluctuations in excitation intensity or photobleaching. The second depletion behavior was represented in **Fig. 3.5** *C-D* and Movie S2 where a Notch1-eGFP cluster disappeared abruptly between two frames (t ~ less than 1 min). In both types of Notch1-eGFP depletion, loss of the ligand signal was correlated with eGFP loss.

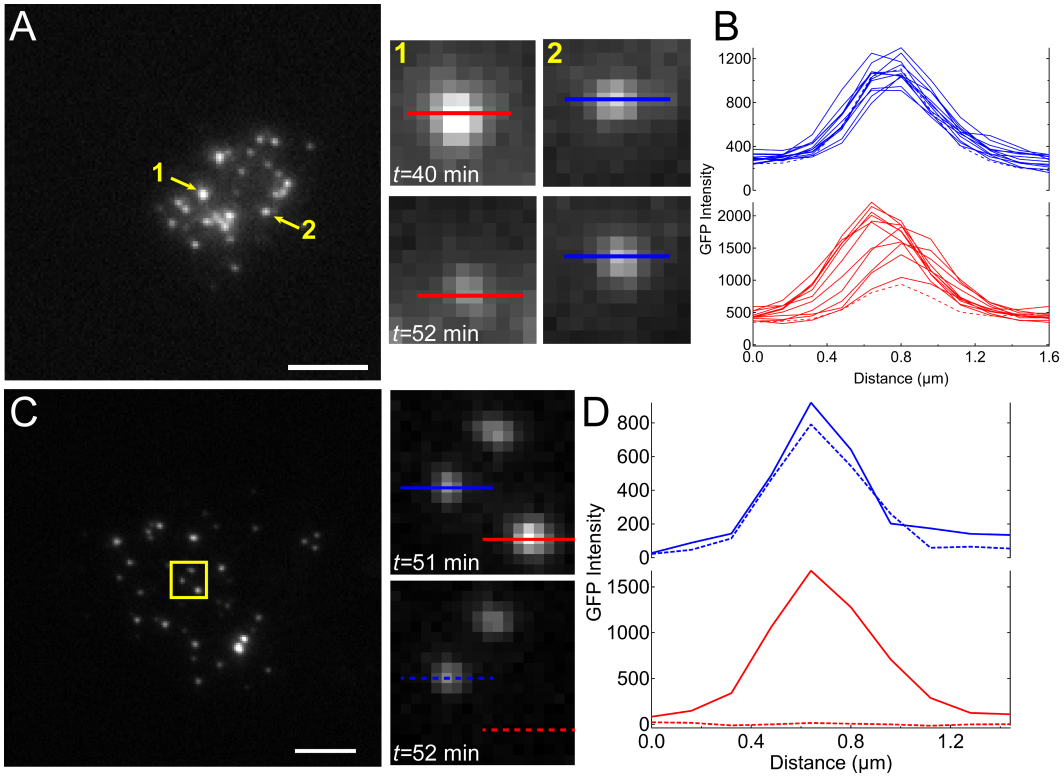

Figure 3.5. Dynamics of Notch1-eGFP cluster depletion. (A) Representative TIRFM image of Notch1-eGFP taken from a time-lapse series showing the depletion dynamics from a single cell. Two clusters are highlighted: position 1 shows attenuation of eGFP signal while position 2 shows only small fluctuations in signal intensity. (B) Signal quantification using line scans taken through both clusters. Dashed line indicates intensity profile at t = 52 min. (C) Representative fluorescence image demonstrating sudden loss of an entire Notch1-eGFP cluster and (D) line scans taken through two clusters to highlight this event. Scale bar = 5 μm.

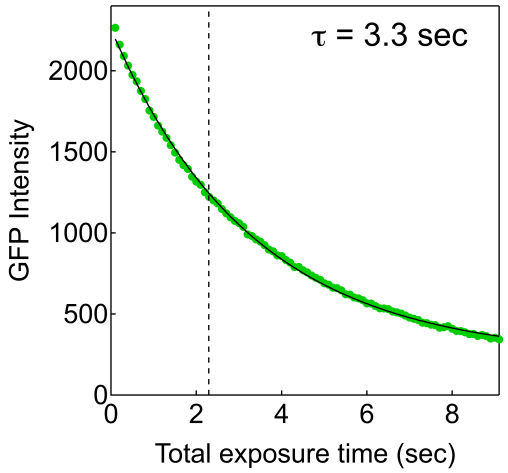

Figure 3.6. Photobleaching profile of eGFP physisorbed onto a glass surface. The experimentally measured values were fit to an exponential decay (solid line), and the half-life was calculated to be 2.3 sec or 23 frames taken at 100 msec exposure time (dashed line).

Within each set of time-lapse images, the loss of fluorescence intensity in the TIRFM illumination field corresponds to either cleavage of the NICD from the cell membrane, activation of the Notch receptor, or internalization of the receptor. It is important to state that the ligand is rarely observed inside the cell, which suggests that the intact ligand-bound receptor complex is not internalized. To see if this coordinated signal loss is due to a mechanism independent of receptor activation, we conducted a set of live cell experiments with Notch1-eGFP cells that were DAPT treated. In one of these control cells, we observed simultaneous loss of DLL4 and Notch1 signal, which must be due to an internalization mechanism and not cleavage at S3 (**Fig. 3.7**). However, it is still possible that the receptor is internalized before being cleaved from the membrane and progressing to the nucleus. Therefore, the coordination between ligand and receptor depletion suggests that we are viewing either S3 cleavage, an intermediate regulatory step that takes place prior to S3 proteolysis or an alternate receptor internalization process.

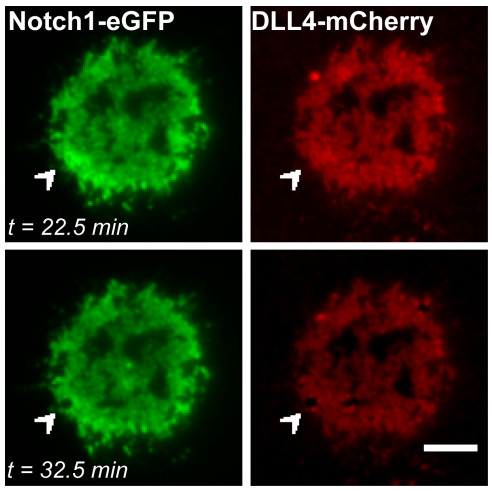

Figure 3.7. Time-lapse analysis of an individual DAPT treated cell. Arrow highlights an area where concerted loss of Notch1-eGFP and DLL4-mCherry was observed. Scale bar = 5 μm.

Given that the NICD is a potent transcription factor that translocates from the membrane to the nucleus, we employed an approach developed by Toomre et al. to localize the *z*-position of the Notch1-eGFP through tandem imaging with epifluorescence and TIRF microscopy.[20, 21] By switching between these two excitation configurations, it was possible to determine the lateral location of the clusters and their proximity to the cell membrane.[22] Live cell imaging of a Notch1-eGFP expressing cell on a DLL4-568 surface resulted in the formation of ligand-receptor clusters as evidenced by colocalization of the ligand and receptor signals (**Fig. 3.8** *A*). After binding, one of the formed clusters (arrowhead, **Fig. 3.8** *A*) vanished from the TIRF channel at a rate that was faster than can be expected for photobleaching (**Fig. 3.6**). There was also noticeable loss of the DLL4-568 signal indicating that the unbound ligand molecules diffused away (**Fig. 3.8** *B*). Strikingly, the epifluorescence channel revealed that the receptor cluster remained near the plasma membrane and had not yet translocated to the nucleus. Our data

suggest that after ligand-induced S2 cleavage occurs at the cell-supported lipid membrane junction, the NICD cluster moves at least 100 nm away from the plasma membrane.

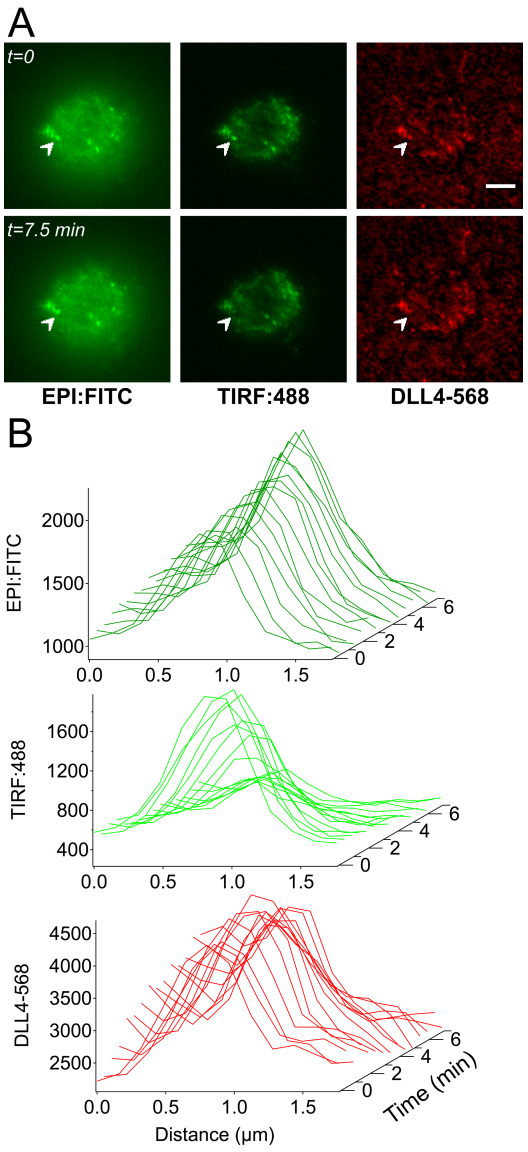

Figure 3.8. Observation of DLL4-Notch1 complexes using alternating epifluorescence-TIRFM. (A) Localization of the Notch1-eGFP at different time points is monitored with both epifluorescence and TIRFM (green) while DLL4 position is visualized in epifluorescence only (red). The highlighted cluster remains in the epifluorescence channel, but is diminished in TIRFM, suggesting translocation away from the membrane. Scale bar = 10 μm. (B) Waterfall plots indicate the changes in fluorescence intensity of the ligand-receptor complex (white arrow) as a function of time for each channel.

To explain this series of events, it is important to emphasize that the precise cellular location of S3 cleavage is still unknown. There are studies that demonstrate that proteolysis at the S3 site occurs at the plasma membrane.[23, 24] In contrast, Gupta-Rossi et al. show that monoubiquitination and endocytosis of the Notch receptor are necessary to trigger S3 cleavage.[25] Alternatively, there is evidence to support that S3 cleavage may occur at both the plasma membrane and early endosomes but produce different forms of the NICD as a way to regulate Notch signaling.[26] Currently, our results suggest that the cell has different ways to process the NICD and supports the hypothesis that the S3 cleavage event occurs at either the plasma membrane or early endosomes.

3.2.3 Determination of DLL4-Notch1 binding ratio

Given that receptor clustering is thought to play a role in signal activation,[27] we were interested in determining the absolute molecular density of ligands and receptors and their stoichiometry within DLL4-Notch1 complexes of live cells. This is a general question that pertains to all juxtacrine pathways. Using a method developed by Galush et al., the fluorescence intensity of the ligand and the receptor was calibrated using a spectrally similar lipid-fluorophore conjugate as a standard.[28] In the case of the DLL4 ligand molecules, the calibration curve was constructed with TRITC-DHPE, while for the receptor molecules, NBD-PC lipid molecules were selected, as seen in **Fig. 3.9** *A-C*. The second component of this analysis required that the fluorescence intensity of the ligand molecules be directly compared with the lipid-fluorophore standards. This comparison produced a unitless scaling factor, *F* factor, which is unique to each ligand/lipid pair, and these values are provided in **Fig. 3.9** *A-C*. Based on the calibration data, the average ligand density of DLL4-568 on the membrane surface was determined to be 3700 ± 200

molecules per μm^2 while the DLL4-mCherry density was lower at 1400 ± 300 molecules per μm^2. This variation in surface packing density may be explained by the differences in protein dimension and possible interactions between the deca-histidine tag and ligand C-terminus. To calibrate the Notch1 receptor signal, a surface was prepared with dodeca-histidine eGFP, and its protein density was measured at 4800 ± 300 molecules per μm^2. All calculated values were consistent with previously published results for histidine-tagged proteins on membrane surfaces, thus validating the calibration method for quantifying ligand and receptor molecular densities.[29]

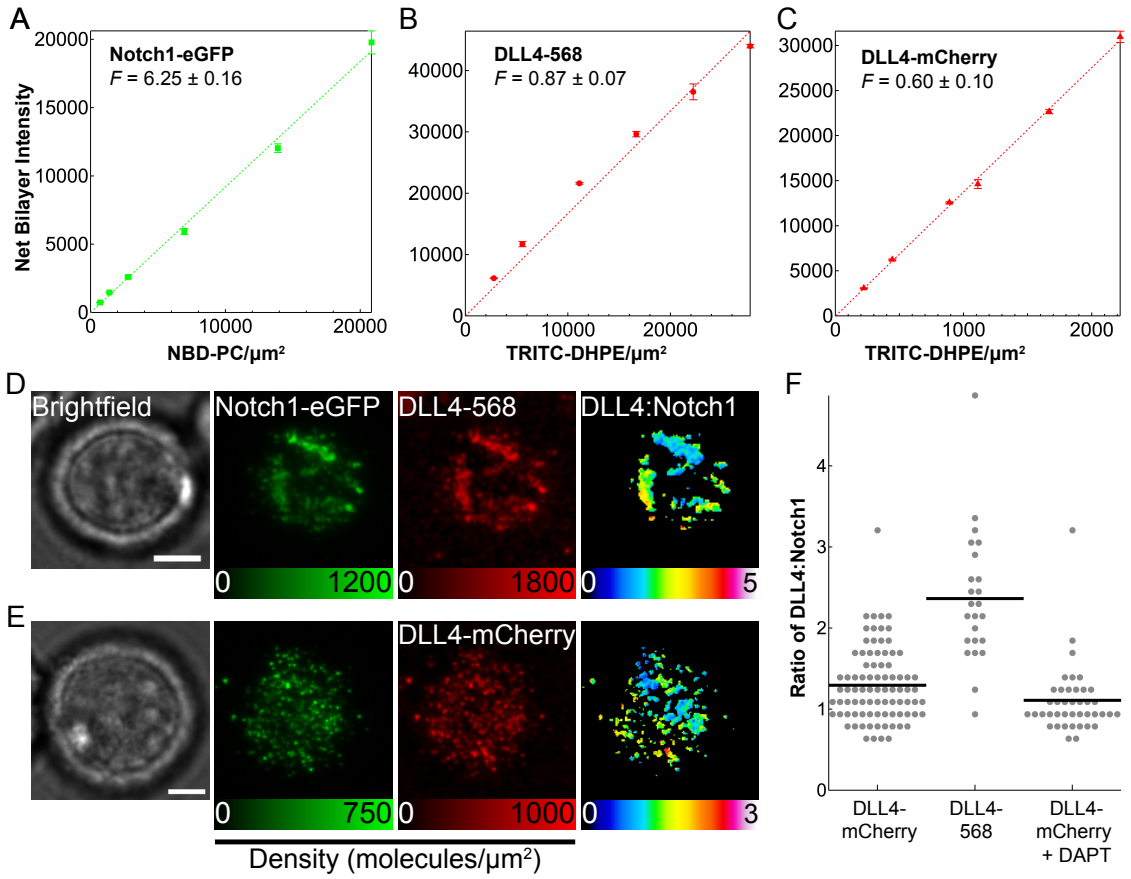

Figure 3.9. Bilayer calibration curves and calculation of binding ratio. (A) Intensity of NBD-PC bilayer at different molecular densities with the *F* factor comparing brightness of Notch1-eGFP and NBD-PC. (B) Calibration curve and *F* factor relating TRITC-DHPE and DLL4-568. (C) Calibration curve and *F* factor relating TRITC-DHPE and DLL4-mCherry. Representative quantitative fluorescence images of Notch1-eGFP expressing

cells engaged to supported lipid membrane surfaces with (D) DLL4-mCherry and (E) DLL4-568 ligand. Each series includes images collected in brightfield, surface density maps of Notch1-eGFP and ligand (calibration bar in molecules/μm^2), and a masked ratio (DLL4:Notch1) heat map. Scale bar = 5 μm. (F) Scatter plot of the ratio of DLL4:Notch1 determined from quantitative fluorescence analysis. Each dot indicates the ratio value from a single cell, and the horizontal line indicates the average value of all measurements.

Ligand and receptor densities in live cell experiments were determined after allowing the Notch1-eGFP cells to incubate on DLL4 functionalized membranes for 30 min. Representative brightfield, Notch1-eGFP and DLL4 images are shown in **Fig. 3.9** *D-E*. The fluorescence intensity in each channel was converted into a surface density map, which displays the density of ligand and receptor molecules within individual clusters. A summary of the image analysis procedure is provided in **Fig. 3.10**. To determine the binding ratio, the DLL4 image was divided by the Notch1-eGFP image to generate a heat map of ratio values (DLL4:Notch1). In order to identify individual clusters, a mask was applied to the ratio image by selecting the regions of the cell expressing Notch1-eGFP. Analysis of these images showed an observed ratio value that varied from 0-5 under each cell, and the overall DLL4:Notch1 ratio was generally lower for DLL4-mCherry than for DLL4-568 ligand.

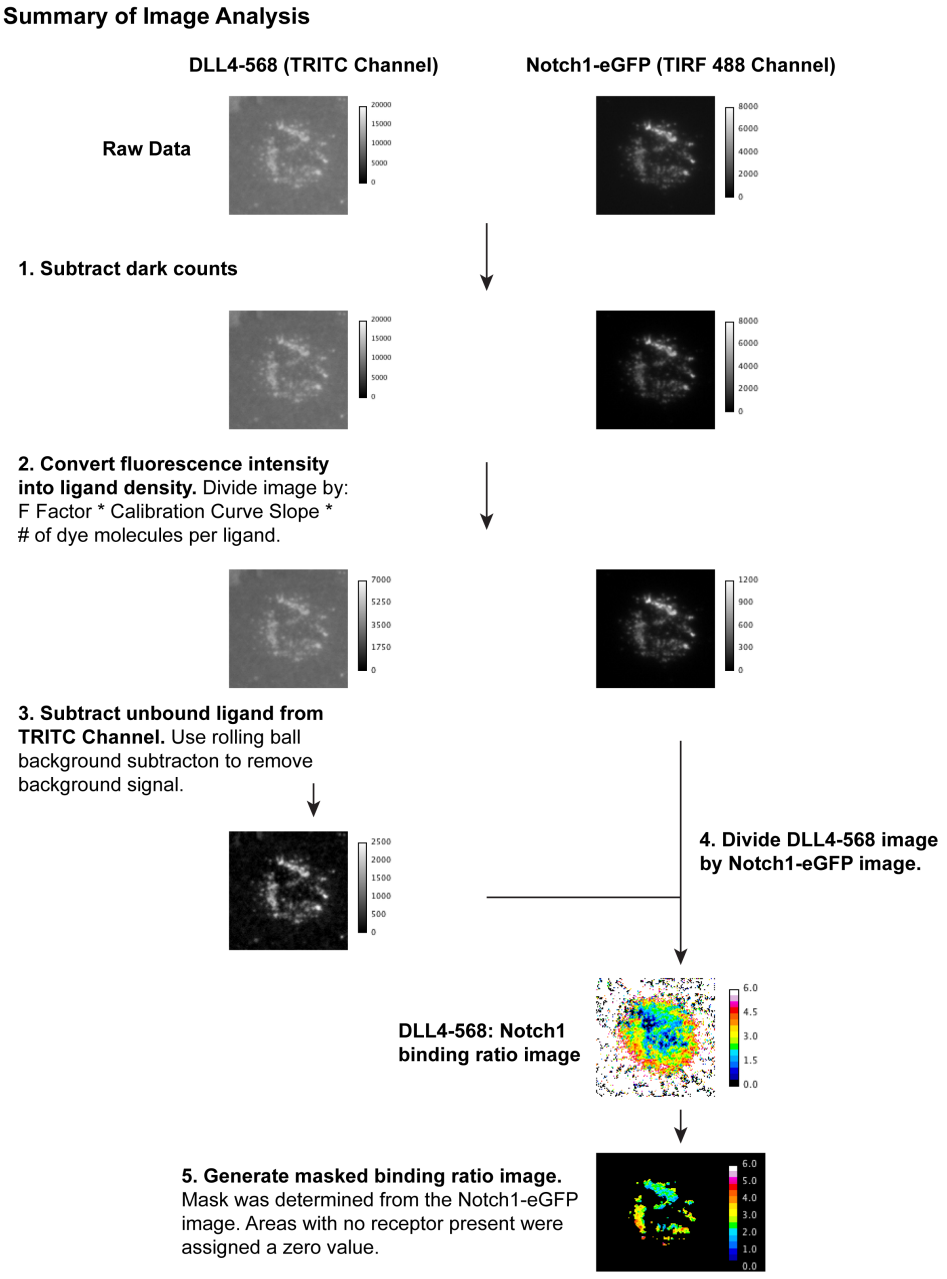

Figure 3.10. Summary of image analysis to determine the binding ratio between DLL4 and Notch1.

To compare ratio values across a statistically meaningful population of cells, a total of 40 to 85 cells were analyzed for each type of ligand. A summary of ratio values is provided in **Fig. 3.9** *F* and **Table 3.1**. These values were obtained from histograms of

ratio distributions fit with a Gaussian function (**Fig. 3.11**). The binding stoichiometry was calculated to be 1.3 ± 0.5 for DLL4-mCherry:Notch1 and 2.4 ± 0.8 for DLL4-568:Notch1. In order to explain the higher DLL4-568:Notch1 value, we hypothesized that a fraction of labeled, but unbound ligand was present within ligand-receptor clusters due to the higher initial density on the membrane surface. We tested this idea by tuning the ligand concentration on the membrane by lowering the percentage of Ni^{2+}-NTA lipid molecules within the bilayer and observing the effect on the DLL4:Notch1 ratio, as shown in **Fig. 3.12**. As the density of DLL4-568 was decreased from 3700 to 300 molecules per μm^2, the stoichiometry of DLL4-568:Notch1 decreased from 2.4 ± 0.8 to 1.6 ± 0.4, nearing the value obtained with DLL4-mCherry. The minimum amount of ligand required for cell adhesion was determined to be near 0.25 mol% or 20 molecules per μm^2 (**Fig. 3.13**).

Ligand	**Ratio DLL4:Notch1**	**Average receptor-bound DLL4 density**	**Average Notch1 density**	**N**	**mol% Ni^{2+}-DOGS-NTA**	**Initial surface density (ligand/μm^2)**
DLL4-mCherry	1.3 ± 0.5	490	420	85	2	1400
DLL4-mCherry + DAPT	1.1 ± 0.4	520	500	41	2	1100
DLL4-568	2.4 ± 0.8	820	390	24	2	3700
DLL4-568	2.2 ± 0.5	970	480	11	1	1500
DLL4-568	2.0 ± 0.5	1000	560	14	0.75	1000
DLL4-568	1.6 ± 0.4	700	510	11	0.5	300

Table 3.1. DLL4-Notch1 ratio determined from quantitative fluorescence analysis. Average density values for DLL4 and Notch1 refers to the average pixel value for all clusters of a single cell. See Methods for details on data analysis.

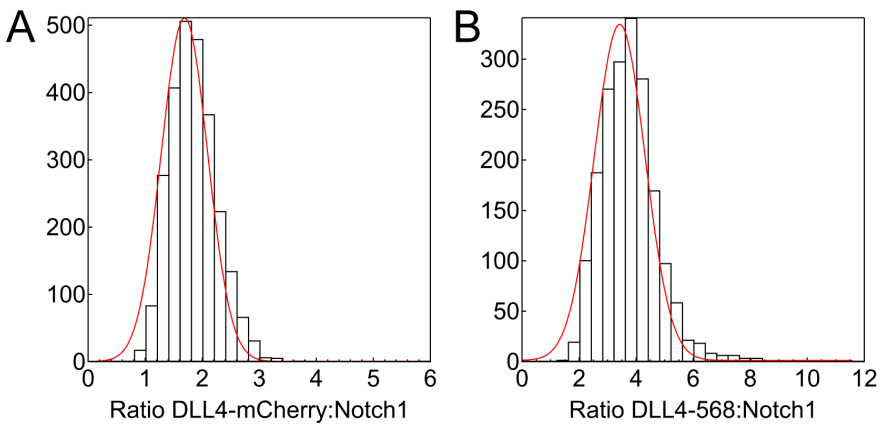

Figure 3.11. Representative histograms of ratio values. The histograms were fit with a Gaussian for binding of (A) DLL4-mCherry to Notch1-eGFP or (B) DLL4-568 to Notch1-eGFP.

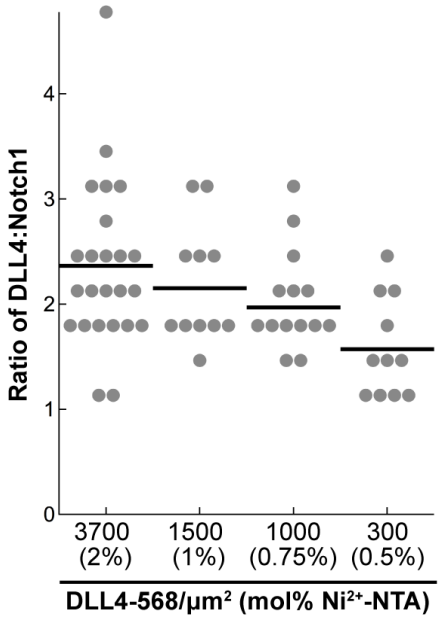

Figure 3.12. Determining the stoichiometry of DLL4 to Notch1 binding at live cell-supported lipid membrane junctions. The stoichiometry of binding was plotted as a function of ligand density. In these experiments, mole percent of Ni^{2+}-NTA lipid was reduced from 2% to 0.5% and resulted in a lower binding ratio between DLL4-568 and Notch1. Each circle represents binding between a single cell and the membrane containing tethered ligand, and the mean ratio is indicated with a horizontal line.

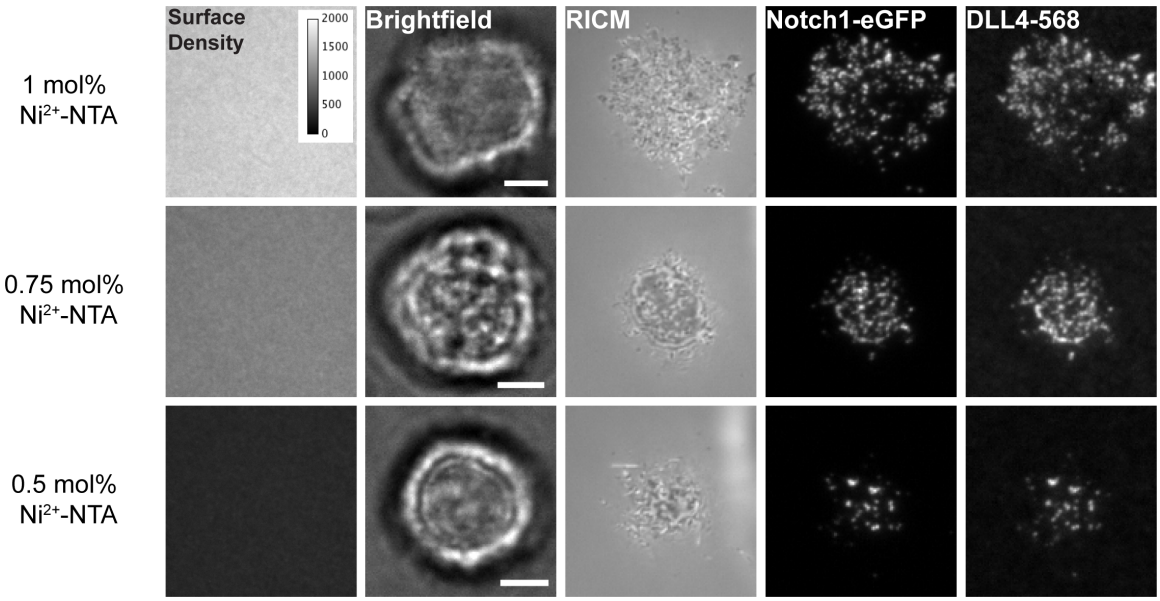

Figure 3.13. Effect of DLL4-568 density on Notch1 binding. Surfaces with varying densities of DLL4-568 were produced (left panel) and Notch1-eGFP expressing cells were incubated for 30 min prior to imaging. The strength of cell contact is seen in RICM and diminishes as the amount of available surface ligand is reduced. Ni^{2+}-NTA lipid concentrations below 0.5 mol% resulted in no cell attachment (data not shown). Scale bar = 5 μm.

Another possible explanation for the slightly elevated amount of DLL4 is due to the fact that the eGFP is fused to the NICD on the cytoplasmic portion of the receptor. Therefore, the ratio values reported more accurately relate NICD density to DLL4, and it is possible that S2 cleaved DLL4-Notch1 complexes remain trapped within the cell-supported membrane junction, while the S3 cleaved NICD diffuses away from the plasma membrane. Diffusion of membrane proteins surrounded by other proteins within the bilayer is highly hindered and would support this hypothesis [30]. In order to test this idea, cells were treated with DAPT to prevent S3 cleavage, and the stoichiometry of DLL4:Notch1 was determined to be 1.1 ± 0.4, **Fig. 3.9** *F*. The similarity of the values for DAPT treated and untreated populations suggests that the presence of the inhibitor does not affect binding between the ligand and receptor. While this measurement establishes

the ratio of ligand to receptor molecules, it is not sufficiently sensitive to be used as an assay of Notch activation by reporting changes in the ratio value.

3.2.4 Biological activity of surface tethered DLL4

To quantify the biological activity of different forms of the membrane-bound ligand, two independent methods were used to measure Notch activity levels. The first strategy employed a reporter cell line engineered by Sprinzak et al. to monitor Notch1 activation through the expression of a citrine (YFP) reporter, which was controlled by the 12XCSL promoter.[31] Supported lipid membranes were prepared with histidine-tagged, DLL4, DLL4-mCherry or DLL4-568, and the fluorescence intensity of the YFP reporter was measured after 48 h of cell incubation to maximize reporter expression. Reporter fluorescence was normalized to cells treated with the γ-secretase inhibitor, DAPT (N-[N-(3,5-difluorophenacetyl-L-alanyl)]-S-phenylglycine t-butyl ester). For Notch reporter cells engaged with the DLL4-functionalized membrane, the reporter signal intensity within the nucleus was 2.5 ± 0.5 times greater than the control (**Fig. 3.14** *A*, DLL4). In addition, DLL4-568 and DLL4-mCherry membranes showed slightly lower activation levels when compared to deca-histidine DLL4 that was not fluorescently tagged (**Fig. 3.14** *A*, DLL4-mC and DLL4-568). Variation in activation levels for different ligand types is attributed to fluctuations in the ligand surface density as well as ligand efficacy. The average surface density was calculated to be ~3700 DLL4-568 per μm^2 compared with ~1400 DLL4-mCherry per μm^2 (**Table 3.1**). However, as mentioned previously, it is likely that chemical modification of critical lysine residues in the receptor-binding domain of the DLL4-568 molecule alters its binding affinity.

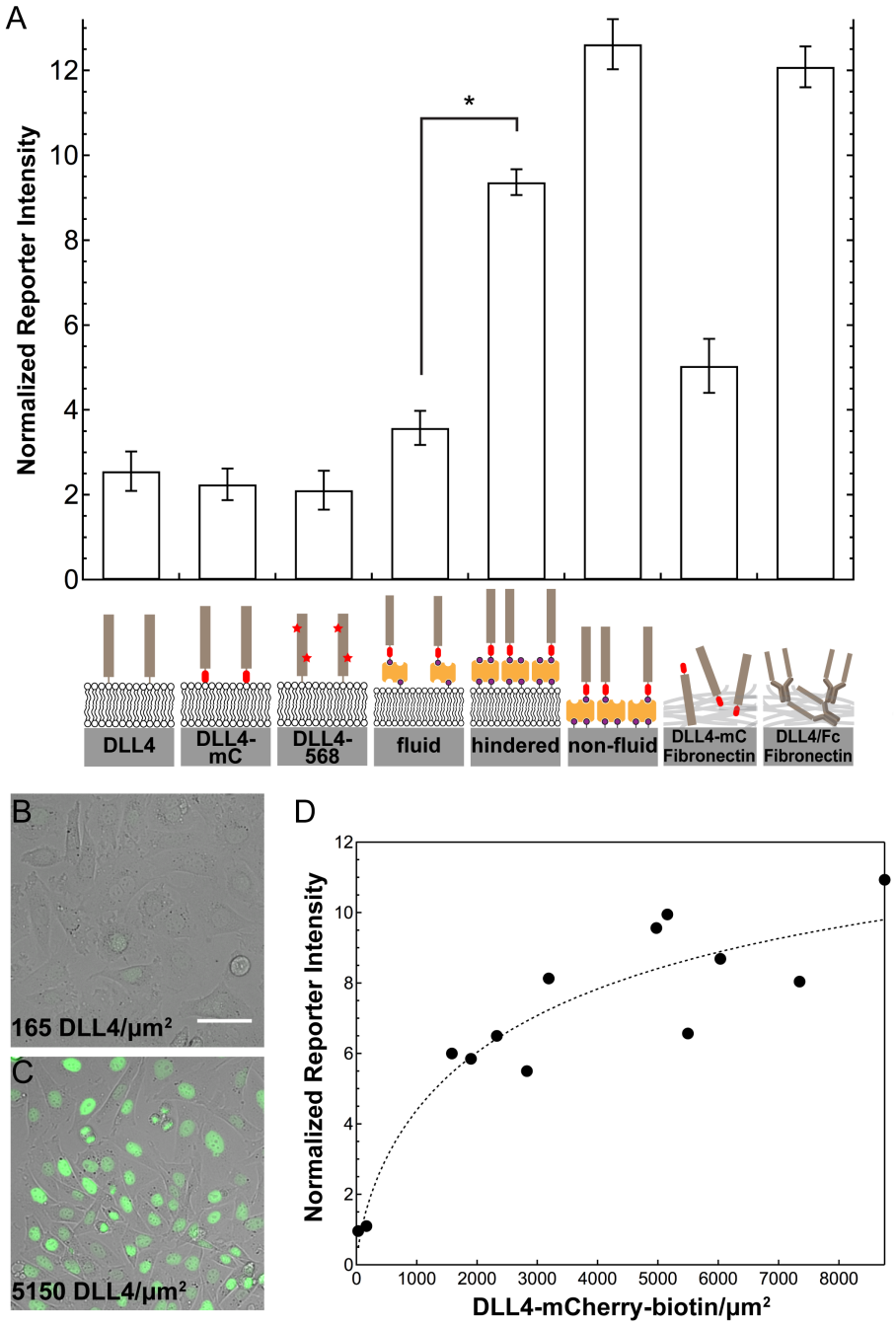

Figure 3.14. Role of ligand tether and lateral mobility on Notch activation levels. A reporter cell line engineered by Sprinzak et al. containing full length Notch1 and a YFP reporter controlled by a synthetic 12XCSL promoter was used to measure Notch activation levels. (A) Mean fluorescence intensity of reporter cells was measured after 48 h for the following surface types (left to right): supported membrane with histidine-tagged variants of DLL4, supported membrane with laterally mobile DLL4-mCherry-biotin (fluid), supported membrane with hindered DLL4-mCherry-biotin (hindered), functionalized glass with non-fluid DLL4-mCherry-biotin (non-fluid), DLL4-mCherry physisorbed with fibronectin, and DLL4/Fc physisorbed with fibronectin, *P < 0.001.

Error bars represent SEM for experiments performed in triplicate. Orange rectangles represent streptavidin and purple circles represent biotin moieties. Abbreviations for mCherry = mC; biotin = bio. Representative images of Notch reporter cells on supported membranes with (B) 165 molecules/μm^2 of non-fluid DLL4-mCherry-biotin and (C) 5150 molecules/μm^2 of non-fluid DLL4-mCherry-biotin. Scale bar = 10 μm. (D) Calibration of reporter cell line response to different surface densities of non-fluid DLL4-mCherry-biotin. The data was fit to a Hill function, which is indicated by the dashed line.

To reaffirm the biological activity of these ligands, we used a second readout by immunostaining for the NICD to visualize proteolytically cleaved receptor within the nucleus. Surfaces were prepared in a similar manner as described above and Notch1-eGFP cells were incubated on the surfaces for 3 h. The cells were fixed, permeabilized and treated with a primary antibody specific for cleaved NICD (Val1744). Representative fluorescence images of either DAPT treated or untreated Notch1-eGFP expressing cells with DAPI stained nuclei and antibody stained NICD on an unlabeled DLL4 functionalized membrane are shown in **Fig. 3.15**. To quantify activation levels, the nucleus was identified using the DAPI signal, and the mean NICD intensity was measured within each nucleus (**Fig. 3.15**). The trends in Notch activation levels were consistent with those observed with the reporter cell line.

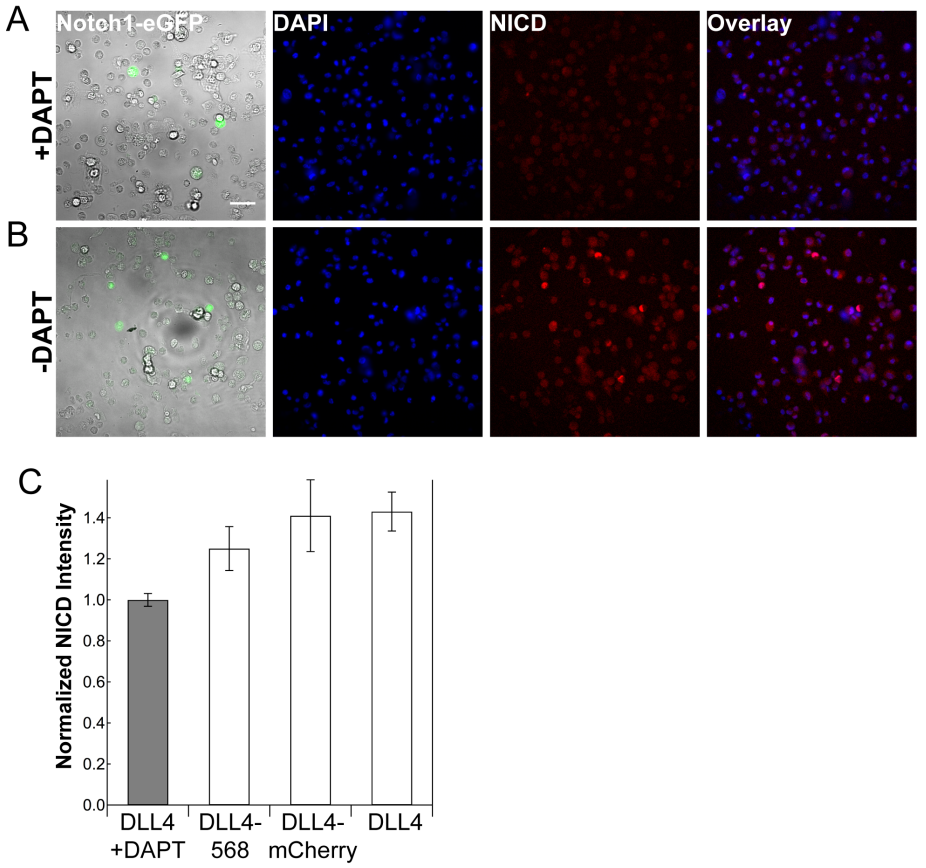

Figure 3.15. Activation of the Notch signaling pathway using the supported membrane platform. (A) DAPT treated or (B) untreated Notch1-eGFP cells were engaged to DLL4-functionalized membranes for 3 h and fixed and stained prior to imaging. Fluorescence images of Notch1-eGFP (green) overlayed with the brightfield view, nuclear stain with DAPI (blue), cleaved NICD (Val1744) (red), and an overlay of the DAPI and NICD channels showing translocation of the NICD into the nucleus. Scale bar = 50 μm. (C) Quantitative analysis of average nuclear localization of the NICD as visualized through antibody staining, which is a measure of Notch activation. As a negative control, cells were treated with 25 μM DAPT during the course of the experiment (shaded bar). Error bars represent the standard error of the mean (SEM) for experiments performed in triplicate.

Another key factor that may influence activation levels of the Notch receptor is the stability of the ligand tether to the supported lipid membrane. For this reason, we designed a biotin ligase-modified DLL4-mCherry. The biotin-streptavidin association (K_d ~ 4 x 10^{-14} M)[32] provides a more stable anchor to the membrane surface when compared with histidine-NTA binding (K_d ~ 10 x 10^{-6} M).[33] While the overall DLL4 structure

remains unchanged, use of a biotin tether increased the Notch activation levels to 3.6 ± 0.4 fold over the control (**Fig. 3.14** *A*, fluid). This result indicates that if the ligand remains firmly associated with the membrane surface, then Notch activation levels increase.

It is unlikely that the observed increase in activation is due to formation of ligand dimers on tetrameric streptavidin. First, streptavidin is attached to the membrane surface through head-modified biotin lipid molecules; therefore two of the binding sites are unavailable to the ligand (**Fig. 3.14** *A*, fluid).[34] In addition, the density of fluorophore labeled streptavidin on a fluid biotin-DPPE surface was measured to be ~730 molecules per μm^2. The density of DLL4-mCherry-biotin was calculated to be ~770 molecules per μm^2 suggesting that there is close to one ligand molecule per streptavidin. In addition, it is sterically unfavorable for two ligand molecules to be bound to the same streptavidin molecule. The two binding sites of streptavidin (on the same face) are separated by ~2.0 nm,[35, 36] and the diameter of the mCherry beta-barrel is approximately 3.0 nm,[37] leaving little room for both ligand molecules to bind to the same side of the streptavidin.

3.2.5 Role of lateral ligand mobility on Notch activation

An important advantage of the supported membrane platform is that lateral mobility of the DLL4 ligand is dictated by the fluidity of the supported lipid membrane. Therefore, synthetic membrane surfaces can be tuned to present chemically identical DLL4 ligands that differ only by their lateral diffusion coefficient (*D*). To alter the lateral mobility of ligand molecules, the percentage of biotin-DPPE lipids doped into DOPC vesicles was varied from 0.1 to 4 mol%. At 0.1 mol% biotin-DPPE, membrane-tethered ligand molecules remain fluid, but at 4 mol% biotin-DPPE the ligand displays hindered

long range diffusion (**Fig. 3.16**) as the surface nears the packing density limit of streptavidin.[38, 39] Line scans over the photobleached areas qualitatively indicate the difference in lateral mobility of DLL4-mCherry-biotin (**Fig. 3.16**). The ligand density of the 4 mol% biotin-DPPE membrane was reduced to match the ligand density of the 0.1 mol% biotin-DPPE surface by titration with free D-biotin (**Fig. 3.17**). When Notch reporter cells were cultured on these surfaces and the activation levels quantified, the hindered DLL4-mCherry-biotin ligand displayed significant enhancement in activation (2.6-fold) over the fully fluid ligands ($P < 0.001$), **Fig. 3.16** *A* (compare fluid to hindered).

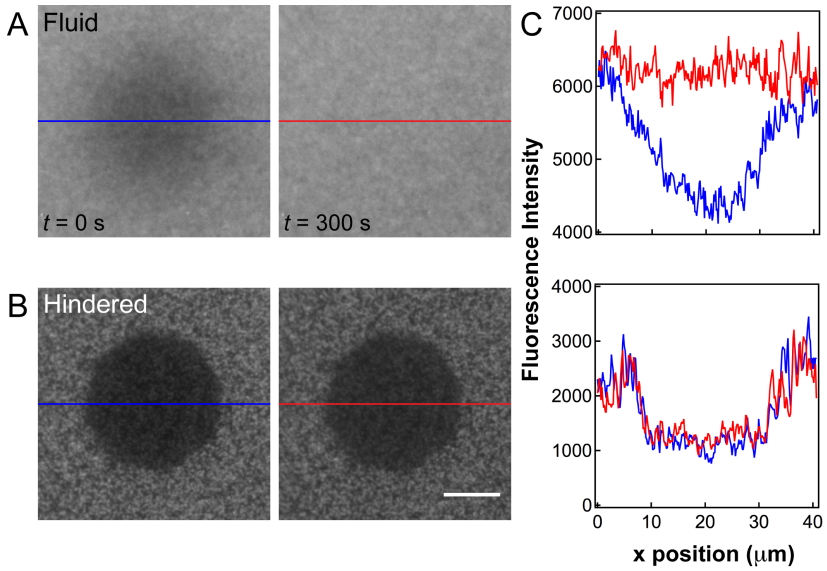

Figure 3.16. Lateral mobility of supported membranes with tethered DLL4 ligand. FRAP assay of (A) fluid and (B) hindered DLL4-mCherry-biotin functionalized lipid membranes that were photobleached and allowed to recover for 5 min. Scale bar = 10 μm. (C) Lines scans of fluorescence intensity over the indicated areas of images (A) and (B).

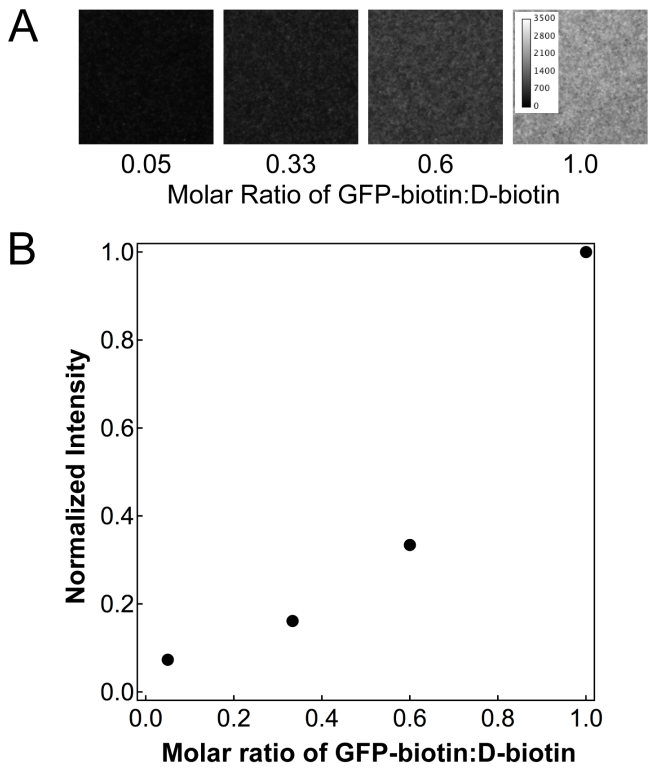

Figure 3.17. Competitive binding experiment between GFP-biotin and D-biotin on a lipid membrane. In this experiment, GFP-biotin was selected as a model ligand in place of DLL4-mCherry-biotin. The goal was to titrate different molar ratios of biotinylated (fluorescent) ligand to D-biotin on a membrane surface and to observe the effect on fluorescence intensity. First, eGFP α-thioester (expressed and purified using the IMPACT kit from New England Biolabs, Ipswich, MA) was site specifically modified with cysteine-biotin (Carbosynth, San Diego, CA) using expressed protein ligation [40]. The resulting GFP-biotin was incubated on a streptavidin functionalized 0.1 mol% biotin-DPPE membrane at a series of molar ratios of GFP-biotin to D-biotin. The total biotin concentration was maintained at 250 nM. (A) Representative epifluorescence images of biotin-DPPE membranes incubated with different molar ratios of GFP-biotin to D-biotin. (B) Plot illustrating the fluorescence intensity as a function of the molar ratio of GFP-biotin to D-biotin. This plot was used to make an initial estimate for the amount of free D-biotin needed to produce a 4 mol% biotin-DPPE bilayer with the same ligand density (fluorescence intensity) as a 0.1 mol% biotin-DPPE surface.

Given that the 4 mol% biotin-DPPE membrane presented a small fraction of lipid molecules that remained mobile and some lipid dissociation from the membrane occurs over the 48 h incubation time, we next sought to test the activity of covalently

immobilized ligand. Accordingly, DLL4-mCherry was fully immobilized using two different strategies (see Materials and Methods). First, a mixture of fibronectin and DLL4-mCherry or DLL4/Fc was adsorbed onto a glass substrate. This resulted in a normalized reporter response of 5.0 ± 0.6 and 12.1 ± 0.5 (**Fig. 3.14** *A* DLL4-mC and DLL4/Fc Fibronectin), respectively. This approach has been reported in the literature and results in randomly oriented ligand molecules within a thin film of fibronectin. In the second strategy, the DLL4-mCherry-biotin ligand was directly anchored to the glass slide through biotin groups that were covalently attached to the glass slide. Following incubation with the reporter cells, Notch activation levels were 12.6 ± 0.6 times greater than the DAPT control, which was the highest level measured on any type of surface tested (**Fig. 3.14** *A*, non-fluid). This result confirms that proper ligand orientation coupled with non-labile surface immobilization lead to the most potent ligand activity. Taken together, this data shows that limiting lateral membrane fluidity can enhance receptor activation and lends support to the proposed mechanotransduction model of Notch receptor activation.[10] Moreover, the difference in activation between fluid and non-fluid ligand also indicates that there is a lateral component to Notch tension-driven activation, which may provide an additional level of spatio-mechanical regulation of receptor activation.

Given that the Notch transcriptional reporter generates a non-linear response to ligand density, we next aimed to develop a quantitative calibration relating the absolute molecular ligand density (input) with reporter YFP intensity (output). We quantified ligand densities using the fluorescence-based lipid membrane calibration and recorded the corresponding reporter response using a series of non-fluid DLL4-mCherry-biotin

functionalized surfaces, **Fig. 3.14** *B-D*. We found that the response of the reporter cell line to immobilized ligand molecules was steeply graded (**Fig. 3.14** *D*) as captured in the representative images shown in **Fig. 3.14** *B-C*. The shape of this plot is in agreement with prior literature precedent,[31] and indicates that the reporter response rapidly saturates when cells engage surfaces presenting densities greater than ~2000 DLL4-mCherry-biotin molecules per μm^2.

To better understand the interplay between DLL4 ligand density and *D,* and their role in modulating Notch activation, we performed a more detailed analysis using a set of membrane surfaces with *D* ranging from ~0 to 0.6 $\mu m^2/s$ and densities ranging from 120 to 26,000 molecules/μm^2. Although such parameters may exceed the range of physiological values, the absolute lateral mobility and surface density of ligands and receptors within living systems is not known. We quantified *D* of membrane tethered DLL4-mCherry-biotin by employing an established FRAP-based analysis method.[41] Interestingly, for surfaces with ligand densities of 1500 molecules per μm^2 or lower, activation of the Notch reporter showed a non-linear and sharp increase as *D* approached 0 (**Fig. 3.18** *A*). Although ligand density and *D* are not completely independent parameters, especially in densely packed membranes, high levels of reporter activation (> 5-fold over DAPT control) were observed as *D* approached 0 over a wide range of ligand densities (**Fig. 3.18** *B*). Both plots indicate that restricting the lateral mobility of DLL4 drastically increases Notch activation, while ligand density appears to be a less sensitive parameter for tuning activation. These results confirm that the mechanical properties of the ligand (lateral mobility) alter its biochemical activity in a highly non-linear fashion, which is suggestive of the mechano-regulatory model of Notch activation.

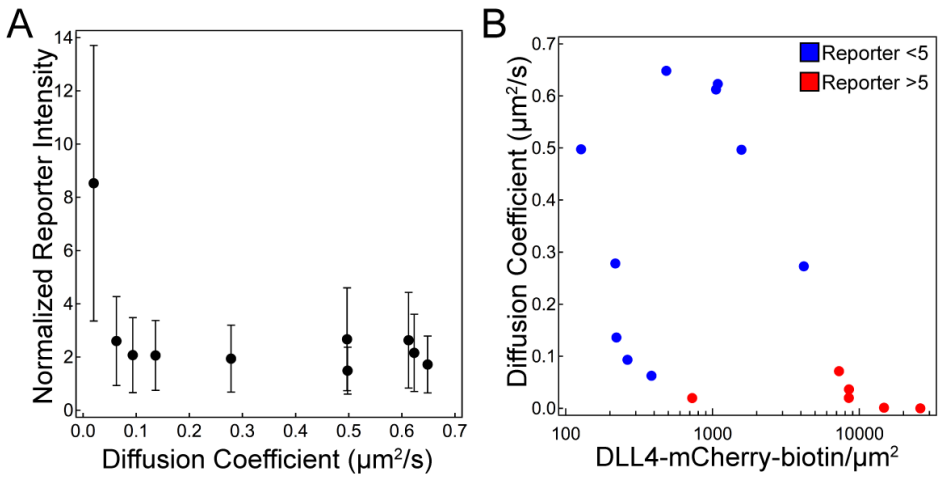

Figure 3.18. The effect of DLL4 lateral mobility, as characterized by diffusion coefficient (*D*), and density on Notch activation levels. (A) For membrane surfaces with less than 1500 DLL4-mCherry-biotin molecules per μm^2, *D* was varied from ~0 to 0.6 μm^2/s. Notch activation sharply increased as *D* approached 0. Error bars indicate the standard deviation in reporter intensity as measured from 1000 cells (or more) 48 h after plating. The average *D* for each surface was determined using a previously published FRAP assay.[41] (B) When the *D* and density were both varied, high levels of Notch activation (normalized reporter intensities > 5, red marker) were observed when *D* neared 0 and when ligand density was increased.

3.3 Conclusions

To study the molecular mechanisms of the Notch receptor pathway, where chemo-mechanical coupling within cellular junctions is increasingly appreciated, it is clear that new experimental strategies must be developed. The use of supported proteolipid membranes overcomes some of the limitations of other conventional methods for studying the Notch signaling pathway. We have demonstrated that DLL4-Notch1 binding can be recaptured at the interface between a cell membrane and supported lipid membrane surface. Using quantitative fluorescence microscopy, it was observed that ligand and receptors actively formed clusters on fluid membranes containing, on average, hundreds of molecules per μm^2. The stoichiometry of DLL4 to Notch1 within these clusters was approximately 1.3 ± 0.5, near the expected 1:1 value. Through live cell

imaging, the dynamic nature of ligand-receptor binding and clustering was captured including observation of coordinated loss of ligand and receptor molecules at the inter-membrane junction. Using epi-TIRFM, the NICD was observed to leave the cell-supported membrane interface but remain near the plasma membrane. Finally, the mechanical properties and lateral mobility of the ligand molecules play a significant role in modulating activation of the Notch receptor. More specifically, ligand activity increased drastically as it became hindered or non-mobile. Despite the limited evidence showing that cells modulate the lateral mobility of Notch ligands or receptors within the plasma membrane, this work points toward an unprecedented mechanism of physical regulation of Notch receptor activation by simply modulating lateral mobility. This work opens the door to investigating Notch mechanotransduction mechanisms,[42, 43] and for screening of targets that may alter Notch ligand-receptor mobility and internalization dynamics.

3.4 Materials and methods

3.4.1 Preparation of small unilamellar vesicles

Phospholipids (1,2-dioleoyl-*sn*-glycero-3-phosphocholine, DOPC; 1,2-dioleoyl-*sn*-glycero-3-[(N-(5-amino-1-carboxypentyl)iminodiacetic acid)succinyl], Ni^{2+}-NTA; 1-oleoyl-2-(6-[(7-nitro-2-1,3-benzoxadiazol-4-yl)amino]hexanoyl)-*sn*-glycero-3-phosphocholine, NBD-PC; and 1,2-dioleoyl-*sn*-glycero-3-phosphoethanolamine-N-(cap biotinyl), biotin-DPPE) were purchased from Avanti Polar Lipids (Alabaster, AL). Fluorescent lipid (N-(6-tetramethylrhodaminethiocarbamoyl)-1,2-dihexadecanoyl-*sn*-glycero-3-phosphoethanolamine), TRITC-DHPE was from Life Technologies (Grand Island, NY). To prepare small unilamellar vesicles, lipids were combined in a round

bottom flask at the desired molar ratio in chloroform and dried on a rotary evaporator to form a lipid film. The film was dried under a stream of N_2 for 15 min and then resuspended with Nanopure water to achieve a lipid concentration of 2 mg/ml. The lipid solution was frozen in a dry ice-acetone bath and thawed in a 40° C water bath three times. The vesicles were passed through a 100 nm polycarbonate filter (Whatman, Florham Park, NJ) 11 times using a high-pressure extruder (Northern Lipids, Burnaby, Canada) warmed to 45° C.

3.4.2 Assembly of supported lipid membranes

To prepare the glass surface, a 96 well plate with #1.5 glass (Greiner, Germany) was etched with 1 M NaOH for 1 h and rinsed with Nanopure water. A 0.5 mg/ml vesicle solution prepared in 10 mM Tris, 150 mM NaCl, pH 8.0 (for Ni^{2+}-NTA) or PBS (for biotin-DPPE) buffer was added to the glass for 20 min to form the bilayer. The surfaces were blocked with 0.1 mg/ml BSA for 30 min. For surfaces containing biotin-DPPE, the membranes were incubated with 36 nM streptavidin (Rockland Immunochemicals, Gilbertsville, PA) for 45 min. After rinsing unbound streptavidin, the surface was treated with 40 nM of c[RGDfK(biotin-PEG-PEG)] (Peptides International, Louisville, KY) or 50 nM of DLL4-mCherry-biotin for 1 h. For attachment of histidine tagged proteins, the surface was treated with a 10 mM Tris, 100 mM $Ni(II)Cl_2$, pH 8.0 solution for 5 min and then incubated overnight with either 66 nM of DLL4-568/647 or 60 nM DLL4-mCherry. Between each step of the supported membrane assembly, the wells were rinsed with 10 ml of 10 mM Tris, 300 mM NaCl, pH 8.0 (Ni^{2+}-NTA) or PBS (biotin-DPPE).

3.4.3 DLL4 ligand labeling with Alexa Fluor dye

Deca-histidine tagged recombinant human DLL4 (R&D Systems, Minneapolis, MN) was reconstituted in PBS, pH 7.4 to 0.8 μg/ml. A sodium bicarbonate solution was added to the protein solution at a final concentration of 0.1 M. Twenty fold molar excess of Alexa Fluor 568 or 647 NHS ester (Life Technologies) was resuspended in DMSO and added dropwise to the pH adjusted protein solution. The reaction proceeded for a total of 1 h and was quenched with the addition of 1 M Tris buffer (final concentration, 10 mM).

3.4.4 Design and expression of DLL4-mCherry

The cDNA sequence of the human DLL4 ECD (corresponding to residues Ser27-Pro524) was cloned into the pcDNA3 mammalian expression vector (Life Technologies). The fluorescent protein mCherry, biotin acceptor peptide (GLNDIFEAQKIEWHE) and deca-histidine tag were fused in frame to the C-terminus of DLL4 ECD. The final construct, pcDNA3-DLL4-mCherry, was sequence verified. HEK 293T cells were cultured to 70% confluency (following ATCC conditions) in 10 cm dishes and transfected with 10 μg of pcDNA3-DLL4-mCherry using $CaPO_4$. After 16 h, the media was removed and indicator- and serum-free Eagle's minimum essential medium (EMEM) was added, and the cells were cultured for an additional 5 days. The conditioned media containing secreted DLL4-mCherry protein was collected and concentrated. The ligand was purified using Ni-NTA magnetic agarose beads (Qiagen, Valencia, CA), buffer exchanged into 10 mM Tris, 300 mM NaCl, pH 8.0 and stored at 4 °C.

3.4.5 Biotin ligase modification of DLL4-mCherry

Purified DLL4-mCherry was concentrated and buffer exchanged into 10 mM Tris, 100 mM NaCl, pH 8.0. The substrate solution was combined with 10 mM ATP, 10 mM MgOAc, 50 μM D-biotin and 1.2 μg of biotin ligase in 50 mM bicine buffer, pH 8.3

(Genecopoeia, Rockville, MD). The reaction was incubated at 30° C for 5 h and purified by removing excess biotin using an Amicon Ultra 10k filter (Millipore, Billerica, MA) to yield DLL4-mCherry-biotin. The biotin ligase (BirA) site-specifically incorporates the biotin moiety at the lysine residue located in the biotin acceptor peptide sequence.[44, 45]

3.4.6 Live cell imaging

The stably transfected Notch1-eGFP C2C12 mouse (*Mus musculus*) myoblast cell line (provided by G. Weinmaster, UCLA) was maintained in Dulbecco's modified Eagle medium (DMEM) supplemented with 10% fetal bovine serum (FBS), 5% cosmic calf serum, 100 IU/ml penicillin, 100 μg/ml streptomycin, and 2 μg/ml puromycin (Cellgro, Manassas, VA). Cells were cultured overnight on a 10 cm dish and used for experiments the following day. The cells were pipetted off of the surface using PBS and pelleted. The functionalized lipid membrane surfaces were exchanged into warm cell imaging media (Hanks' balanced salts, 10 mM HEPES, pH 7.4). For quantitative fluorescence measurements, 25,000 cells were added into each well and incubated for 30 min at 37°C and 5% CO_2. Samples were imaged at 37°C for 30 min using a Nikon Ti Eclipse microscope equipped with an Evolve EM CCD (Photometrics, Tuson, AZ) and objective warmer (Warner, Hamden, CT). The excitation sources used included an Intensilight epifluorescence source and a TIRF launcher with two laser lines: 488 nm (10mW) and 638 nm (20mW). Images were collected using NIS Elements software and analyzed using ImageJ. To observe live cell dynamics, ~10,000 cells were added per membrane surface and individual cells were tracked as they attached to the membrane.

3.4.7 Binding specificity of DLL4 functionalized membranes

A portion of the human Notch1 receptor, including residues Ala19-Gln526 of the extracellular domain, was fused to human IgG_1 (Pro100-Lys330) through a 6 amino acid linker (R&D Systems, Minneapolis, MN). This chimera is present in its soluble form as a disulfide-linked homodimer. The protein was labeled with Alexa 647 NHS ester as described above and purified using Bio-Rad P-4 gel (Bio-Rad, Hercules, CA) to yield NECD-647. DLL4 functionalized membranes were incubated with 33 nM of NECD-647 for 45 min, rinsed and imaged.

3.4.8 Calibration curves and determination of F factor

To calibrate the fluorescence intensity, TRITC-DHPE surfaces ranging from 0 to 0.08 mol% and NBD-PC surfaces from 0 to 0.75 mol% were imaged under the same conditions as the live cell images. The number of fluorophore molecules per unit area was estimated from the footprint of DOPC, which was determined to be 0.72 nm^2.[46] In order to use the calibration curves, the intensity of the ligand molecules was compared with the lipid-fluorophore standards to obtain the *F* factor. The *F* factor is defined as:

$F = \frac{I_{sol(ligand)}}{I_{sol(lipid)}}$, where $I_{sol(ligand)}$ and $I_{sol(lipid)}$ are the intensity of the ligand or lipid molecules in solution after being normalized for concentration. These values were measured on the fluorescence microscope by moving the focal plane (~100 μm) into the center of the sample. It is important to note that for DLL4-568 unconjugated dye was thoroughly removed from the sample by purification with Ni-NTA magnetic agarose beads prior to measuring the *F* factor value.

3.4.9 Data analysis for stoichiometry measurements

To calculate the protein density, the fluorescence images were background subtracted and then quantified by dividing each image by the *F* factor and calibration curve slope. In the ligand channel, the unbound ligand was subtracted as this represented ligand molecules that were present on the membrane surface but not bound to receptor molecules. A correction factor was introduced to account for the 28% of ligand binding to untagged Notch homologs measured in the parental cell line, *vide infra*. The ligand image was then divided by the receptor image to generate the ratio image (DLL4:Notch1). A threshold was applied to the receptor image to determine areas where Notch receptors were located, and all other areas were set to zero. This mask was applied to the ratio image and each non-zero pixel value was binned into a histogram fit with a single Gaussian. The peak value for each histogram, representing an individual cell, was determined and averaged for a population of 40-80 cells.

3.4.10 Activation of Notch reporter cell line

Following assembly and imaging of the supported membrane or physisorbed surfaces, Notch1 reporter cells were trypsinized from the cell culture flask and 10,000 cells were distributed onto each surface. Activation of the reporter was measured by epifluorescence microscopy 48 h after plating. Cells were maintained in Alpha MEM Earle's Salts (Irvine Scientific, Santa Ana, CA) supplemented with 10% FBS, 100 IU/ml of penicillin, 100 μg/ml streptomycin, 400 μg/ml Zeocin, 10 μg/ml Blasticidin and 600 μg/ml Geneticin (Life Technologies).

3.4.11 Immunostaining and analysis of NICD localization

Membrane surfaces with histidine-tagged DLL4 were prepared as described and 30,000 cells, which were either treated with 25 μM DAPT (Calbiochem, Billerica, MA)

(negative control) or DMSO for 16 h, were added into each well. After 3 h with continued drug or vehicle treatment, the cells were rinsed with cold PBS, fixed with 4% paraformaldehyde for 12 min and permeabilized with 0.1% (v/v) Triton X-100 for 5 min. The samples were blocked with a 1% (w/v) BSA in PBS solution overnight. The primary antibody for cleaved NICD (Cell Signaling Technology, Danvers, MA) was diluted 1:200 in 1% BSA and incubated for 1 h. After rinsing, the secondary antibody labeled with Alexa Fluor 647 (Life Technologies) was diluted 1:1000 and incubated for 30 min. Lastly, DAPI (Life Technologies) was added at a concentration of 300 nM for 5 min. To determine the intensity of the NICD within the nuclei, the DAPI signal was used to locate the nucleus and then the signal intensity from the secondary antibody within these areas was measured.

3.4.12 Biotin-functionalized glass for non-fluid DLL4 surfaces

All glass substrates (25 mm diameter, #2 coverslips, VWR, Radnor, PA) were sonicated in Nanopure water and piranha etched (H_2O_2:H_2SO_4; 1:3; v:v) for 15 min. (Caution: piranha solution is an extremely strong oxidant and can become explosive if mixed with organics). After rinsing with copious amounts of water, the glass substrates were dried under nitrogen and immersed in toluene. The substrates were incubated for 1 h at room temperature in a 0.4% (v/v) solution of 3-aminopropyltriethoxysilane (Gelest, Morrisville, PA) in toluene. The substrates were rinsed with ethanol and dried under nitrogen. The amine-functionalized slides were reacted with 500 ml per slide of 0.05% (w/v) sulfo-NHS-LC-biotin (Pierce, Rockford, IL) and 5% (w/v) mPEG-NHS, MW 2000 (Nanocs, Boston, MA) in 0.1 M sodium bicarbonate overnight. The slides were rinsed with water, dried and placed into an Attofluor chamber (Life Technologies) for further

functionalization (beginning with BSA blocking), see assembly of supported lipid membrane section for details.

3.4.13 Physisorbed DLL4 on glass

A solution of 12.5 μg/ml DLL4/Fc (Sino Biological, China) or DLL4-mCherry and 5 μg/ml fibronectin in PBS was incubated on a glass bottom 96 well plate for 1 h while shaking at 250 rpm. Excess fibronectin and ligand were rinsed away with 5 ml of PBS. The DLL4/Fc protein is composed of the extracellular domain of DLL4 (Ser27-Pro524) fused to the Fc region of human IgG_1 at the C-terminus. This recombinant human protein is present as a disulfide-linked homodimer.

3.4.14 Measurement of ligand diffusion coefficient

DLL4 diffusion coefficients were measured on a Nikon Ti Eclipse inverted microscope (Nikon, Melville, NY) with a 100X N.A. 1.49 CFI Apo TIRF objective lens. A small spot (d ~20 μm) of the membrane tethered DLL4 surface was photobleached with a 561 nm laser until the fluorescence intensity neared dark count levels. Fluorescence recovery was captured over 2 min with images taken in 2 s intervals. A series of 10 prebleach images was also collected to correct for the non-uniform illumination profile of the Intensilight excitation source. Images were acquired with an EM-CCD camera iXon DU897 (Andor, Belfast, UK) through the use of Nikon's NIS Elements and analyzed using ImageJ (NIH, Bethesda, MD). For a detailed description of the photobleaching analysis method, please see reference.[41]

3.5 References

1. Fagotto, F.; Gumbiner, B. M., Cell contact-dependent signaling. *Dev. Biol.* **1996,** *180* (2), 445-454.

2. Gordon, W. R.; Arnett, K. L.; Blacklow, S. C., The molecular logic of Notch signaling - a structural and biochemical perspective. *J. Cell Sci.* **2008,** *121* (Pt 19), 3109-3119.

3. Cordle, J.; Johnson, S.; Tay, J. Z. Y.; Roversi, P.; Wilkin, M. B.; de Madrid, B. H.; Shimizu, H.; Jensen, S.; Whiteman, P.; Jin, B.; Redfield, C.; Baron, M.; Lea, S. M.; Handford, P. A., A conserved face of the Jagged/Serrate DSL domain is involved in Notch trans-activation and cis-inhibition. *Nat. Struct. Mol. Biol.* **2008,** *15* (8), 849-857.

4. Gordon, W. R.; Roy, M.; Vardar-Ulu, D.; Garfinkel, M.; Mansour, M. R.; Aster, J. C.; Blacklow, S. C., Structure of the Notch1-negative regulatory region: implications for normal activation and pathogenic signaling in T-ALL. *Blood* **2009,** *113* (18), 4381-4390.

5. Stephenson, N. L.; Avis, J. M., Direct observation of proteolytic cleavage at the S2 site upon forced unfolding of the Notch negative regulatory region. *Proc. Natl. Acad. Sci. U. S. A.* **2012,** *109* (41), E2757-65.

6. Meloty-Kapella, L.; Shergill, B.; Kuon, J.; Botvinick, E.; Weinmaster, G., Notch ligand endocytosis generates mechanical pulling force dependent on dynamin, epsins, and actin. *Dev. Cell* **2012,** *22* (6), 1299-1312.

7. Shergill, B.; Meloty-Kapella, L.; Musse, A. A.; Weinmaster, G.; Botvinick, E., Optical tweezers studies on notch: single-molecule interaction strength is independent of ligand endocytosis. *Dev. Cell* **2012,** *22* (6), 1313-1320.

8. Chen, J.; Zolkiewska, A., Force-induced unfolding simulations of the human Notch1 negative regulatory region: possible roles of the heterodimerization domain in mechanosensing. *PLoS One* **2011,** *6* (7), e22837.

9. Varnum-Finney, B.; Wu, L.; Yu, M.; Brashem-Stein, C.; Staats, S.; Flowers, D.; Griffin, J. D.; Bernstein, I. D., Immobilization of Notch ligand, Delta-1, is required for induction of notch signaling. *J. Cell Sci.* **2000,** *113* (23), 4313-4318.

10. Parks, A.; Klueg, K. M.; Stout, J.; Muskavitch, M. A., Ligand endocytosis drives receptor dissociation and activation in the Notch pathway. *Development* **2000,** *127* (7), 1373-1385.

11. Nichols, J. T.; Miyamoto, A.; Olsen, S. L.; D'Souza, B.; Yao, C.; Weinmaster, G., DSL ligand endocytosis physically dissociates Notch1 heterodimers before activating proteolysis can occur. *J. Cell Biol.* **2007,** *176* (4), 445-458.

12. Tiyanont, K.; Wales, T. E.; Aste-Amezaga, M.; Aster, J. C.; Engen, J. R.; Blacklow, S. C., Evidence for Increased Exposure of the Notch1 Metalloprotease Cleavage Site upon Conversion to an Activated Conformation. *Structure* **2011,** *19* (4), 546-554.

13. Wang, X.; Ha, T., Defining single molecular forces required to activate integrin and notch signaling. *Science* **2013,** *340* (6135), 991-994.

14. Carroll-Portillo, A.; Spendier, K.; Pfeiffer, J.; Griffiths, G.; Li, H.; Lidke, K. A.; Oliver, J. M.; Lidke, D. S.; Thomas, J. L.; Wilson, B. S.; Timlin, J. A., Formation of a mast cell synapse: Fc epsilon RI membrane dynamics upon binding mobile or immobilized ligands on surfaces. *J. Immunol.* **2010,** *184* (3), 1328-1338.

15. Hsu, C.-J.; Hsieh, W.-T.; Waldman, A.; Clarke, F.; Huseby, E. S.; Burkhardt, J. K.; Baumgart, T., Ligand mobility modulates immunological synapse formation and T cell activation. *PLoS One* **2012,** *7* (2), e32398.

16. Tsai, J.; Kam, L. C., Lateral Mobility of E-cadherin Enhances Rac1 Response in Epithelial Cells. *Cell. Mol. Bioeng.* **2010,** *3* (1), 84-90.

17. Salaita, K. S.; Nair, P. M.; Petit, R. S.; Neve, R. M.; Das, D.; Gray, J. W.; Groves, J. T., Restriction of receptor movement alters cellular response: physical force sensing by EphA2. *Science* **2010,** *327* (5971), 1380-1385.

18. Luty, W. H.; Rodeberg, D.; Parness, J.; Vyas, Y. M., Antiparallel segregation of notch components in the immunological synapse directs reciprocal signaling in allogeneic Th : DC conjugates. *J. Immunol.* **2007,** *179* (2), 819-829.

19. Rebay, I.; Fleming, R. J.; Fehon, R. G.; Cherbas, L.; Cherbas, P.; Artavanis-Tsakonas, S., Specific EGF repeats of Notch mediate interactions with Delta and Serrate: implications for Notch as a multifunctional receptor. *Cell* **1991,** *67* (4), 687-699.

20. Toomre, D.; Steyer, J. A.; Keller, P.; Almers, W.; Simons, K., Fusion of constitutive membrane traffic with the cell surface observed by evanescent wave microscopy. *J. Cell Biol.* **2000,** *149* (1), 33-40.

21. Merrifield, C. J.; Feldman, M. E.; Wan, L.; Almers, W., Imaging actin and dynamin recruitment during invagination of single clathrin-coated pits. *Nat. Cell Biol.* **2002,** *4* (9), 691-698.

22. Mattheyses, A. L.; Simon, S. M.; Rappoport, J. Z., Imaging with total internal reflection fluorescence microscopy for the cell biologist. *J. Cell Sci.* **2010,** *123* (21), 3621-3628.

23. Tarassishin, L.; Yin, Y.; Bassit, L.; Li, Y., Processing of Notch and amyloid precursor protein by gamma-secretase is spatially distinct. *Proc. Natl. Acad. Sci. U. S. A.* **2004,** *101* (49), 17050-17055.

24. Sorensen, E. B.; Conner, S. D., γ -secretase-dependent cleavage initiates notch signaling from the plasma membrane. *Traffic* **2010,** *11* (9), 1234-1245.

25. Gupta-Rossi, N.; Six, E. M.; LeBail, O.; Logeat, F.; Chastagner, P.; Olry, A.; Israël, A.; Brou, C., Monoubiquitination and endocytosis direct gamma-secretase cleavage of activated Notch receptor. *J. Cell Biol.* **2004,** *166* (1), 73-83.

26. Tagami, S.; Okochi, M.; Yanagida, K.; Ikuta, A.; Fukumori, A.; Matsumoto, N.; Ishizuka-Katsura, Y.; Nakayama, T.; Itoh, N.; Jiang, J.; Nishitomi, K.; Kamino, K.; Morihara, T.; Hashimoto, R.; Tanaka, T.; Kudo, T.; Chiba, S.; Takeda, M., Regulation of Notch signaling by dynamic changes in the precision of S3 cleavage of Notch-1. *Mol. Cell. Biol.* **2008,** *28* (1), 165-176.

27. Hicks, C.; Ladi, E.; Lindsell, C. E.; Hsieh, J. J. D.; Hayward, S. D.; Collazo, A.; Weinmaster, G., A secreted Delta1-Fc fusion protein functions both as an activator and inhibitor of Notch1 signaling. *J. Neurosci. Res.* **2002,** *68* (6), 655-667.

28. Galush, W. J.; Nye, J. A.; Groves, J. T., Quantitative fluorescence microscopy using supported lipid bilayer standards. *Biophys. J.* **2008,** *95* (5), 2512-2519.

29. Nye, J. A.; Groves, J. T., Kinetic control of histidine-tagged protein surface density on supported lipid bilayers. *Langmuir* **2008,** *24* (8), 4145-4149.

30. Lippincott-Schwartz, J.; Snapp, E.; Kenworthy, A. K., Studying protein dynamics in living cells. *Nat. Rev. Mol. Cell Biol.* **2001,** *2* (6), 444-456.

31. Sprinzak, D.; Lakhanpal, A.; LeBon, L.; Santat, L. A.; Fontes, M. E.; Anderson, G. A.; Garcia-Ojalvo, J.; Elowitz, M. B., Cis-interactions between Notch and Delta generate mutually exclusive signalling states. *Nature* **2010,** *465* (7294), 86-90.

32. Green, N. M., Avidin and streptavidin. *Methods Enzymol.* **1990,** *184*, 51-67.

33. Lata, S.; Gavutis, M.; Tampé, R.; Piehler, J., Specific and stable fluorescence labeling of histidine-tagged proteins for dissecting multi-protein complex formation. *J. Am. Chem. Soc.* **2006,** *128* (7), 2365-2372.

34. Lou, C.; Wang, Z.; Wang, S.-W., Two-dimensional protein crystals on a solid substrate: effect of surface ligand concentration. *Langmuir* **2007,** *23* (19), 9752-9759.

35. Hendrickson, W. A.; Pähler, A.; Smith, J. L.; Satow, Y.; Merritt, E. A.; Phizackerley, R. P., Crystal structure of core streptavidin determined from multiwavelength anomalous diffraction of synchrotron radiation. *Proc. Natl. Acad. Sci. U. S. A.* **1989,** *86* (7), 2190-2194.

36. Ren, C.-L.; Carvajal, D.; Shull, K. R.; Szleifer, I., Streptavidin-biotin binding in the presence of a polymer spacer. A theoretical description. *Langmuir* **2009,** *25* (20), 12283-12292.

37. Yang, F.; Moss, L. G.; Phillips, G. N., The molecular structure of green fluorescent protein. *Nat. Biotechnol.* **1996,** *14* (10), 1246-1251.

38. Mao, H.; Yang, T.; Cremer, P. S., Design and characterization of immobilized enzymes in microfluidic systems. *Anal. Chem.* **2002,** *74* (2), 379-385.

39. Nguyen, T. T.; Sly, K. L.; Conboy, J. C., Comparison of the energetics of avidin, streptavidin, neutrAvidin, and anti-biotin antibody binding to biotinylated lipid bilayer examined by second-harmonic generation. *Anal. Chem.* **2012,** *84* (1), 201-208.

40. Muralidharan, V.; Muir, T. W., Protein ligation: an enabling technology for the biophysical analysis of proteins. *Nat. Methods* **2006,** *3* (6), 429-438.

41. Jönsson, P.; Jonsson, M. P.; Tegenfeldt, J. O.; Höök, F., A method improving the accuracy of fluorescence recovery after photobleaching analysis. *Biophys. J.* **2008,** *95* (11), 5334-5348.

42. Stabley, D. R.; Jurchenko, C.; Marshall, S. S.; Salaita, K. S., Visualizing mechanical tension across membrane receptors with a fluorescent sensor. *Nat. Methods* **2012,** *9* (1), 64-67.

43. Liu, Y.; Yehl, K.; Narui, Y.; Salaita, K. S., Tension sensing nanoparticles for mechano-imaging at the living/nonliving interface. *J. Am. Chem. Soc.* **2013,** *135* (14), 5320-5323.

44. Beckett, D.; Kovaleva, E.; Schatz, P. J., A minimal peptide substrate in biotin holoenzyme synthetase-catalyzed biotinylation. *Protein Sci.* **1999,** *8* (4), 921-929.

45. Chen, I.; Howarth, M.; Lin, W.; Ting, A. Y., Site-specific labeling of cell surface proteins with biophysical probes using biotin ligase. *Nat. Methods* **2005,** *2* (2), 99-104.

46. Vacklin, H. P.; Tiberg, F.; Thomas, R. K., Formation of supported phospholipid bilayers via co-adsorption with beta-D-dodecyl maltoside. *Biochim. Biophys. Acta* **2005,** *1668* (1), 17-24.

Chapter 4: Tension Sensing in the Notch Signaling Pathway

4.1 Mechanotransduction: Translating force into an intracellular message

4.1.1 Introduction

Mechanotransduction is broadly defined as the process by which cells detect and convert physical forces into biochemical information. The ability to sense and respond to force is a process used by all phyla, from mammals to bacteria. In higher order organisms, these processes are responsible for the proper development and function of systems within the body including the heart, lung, skin and muscle as well as the maintenance of bone and cartilage.[1, 2] Physical forces also play an important role in controlling an organism's sense of hearing and touch. For these reasons, dysregulation of force sensing components is an important but often overlooked factor in human diseases including asthma, osteoporosis, atherosclerosis and heart failure.[3]

In many cases, the precise molecular mechanism of how signals are transduced across the cell membrane remains unknown. This is especially true in the case of mechanotransduction where there are few tools available to apply and measure molecular forces and to determine the biological consequences of these stimuli. Mechanotransduction differs from the classical 'stimulus-response' coupling where a signaling molecule (e.g., hormone, growth factor or cytokine) in solution binds with its cognate receptor and initiates a molecular signal within the cell. Instead, cells are exposed to a variety of mechanical inputs, which are experienced as substrate stiffness, fluid shear and compressive strain.[4-7] Usually, these mechanical forces work by exposing cryptic binding sites buried within the structure of a mechanosensitive molecule. Despite these fundamental differences, there is mounting experimental evidence that mechanical

cues are as critical and potent as chemical cues in the regulation of complex cellular functions.[2]

In spite of their universality, only a small number of mechanosensitive systems have been thoroughly investigated, and the accrued results have led to the conclusion that there is unlikely a unifying mechanotransducer, which controls all mechanical response.[8] Instead, each system has developed a unique way to handle and respond to mechanical stimuli, highlighting the importance of studying many different types of mechano-sensitive molecules. The most well studied examples to date can be divided into two distinct categories. The first group consists of protein-mediated mechanoreceptors, specifically integrins and cadherins that directly (or indirectly through adaptor proteins) bind to the extracellular matrix (ECM) or neighboring cells. These receptors are directly connected to the cell cytoskeleton balancing external and internal forces. The second category to be discussed is lipid-bilayer mechanosensitive molecules. These ion channels and enzymes experience and adapt to membrane forces without a direct connection to the cytoskeleton. While it is generally accepted that force plays a role in activating cell surface receptors, there are many examples, such as the Notch receptor, for which the precise mechanism of force sensing remains unknown.

4.1.2 Cytoskeleton-associated mechanotransducers: Integrins and cadherins

In solid tissues, the ECM provides the basic framework for cell attachment, and the cell-ECM association is made through cell surface receptors called integrins. There are 24 types of integrins with each heterodimer composed of an α and β subunit. There are 18 different α subunits and 8 β subunits, and the specific combination of subunits determines substrate specificity for ECM ligands such as fibronectin, collagen or

laminin.[9] Upon binding to the ECM scaffold, the receptor undergoes a conformational change revealing binding sites on the cytoplasmic tails of the integrin.[10] A recent super-resolution microscopy study has stratified the ~40 nm region between the plasma membrane and actin cytoskeleton into 3 distinct layers, see **Fig. 4.1** *A*.[11] The first set of cytoplasmic proteins rapidly binds to the activated integrin and includes members such as focal adhesion kinase and paxillin. The intermediate force transduction layer is composed of proteins such as talin and vinculin. The final level completing the connection to the actin cytoskeleton includes zyxin, vasodilator-stimulated phosphoprotein and α-actinin.

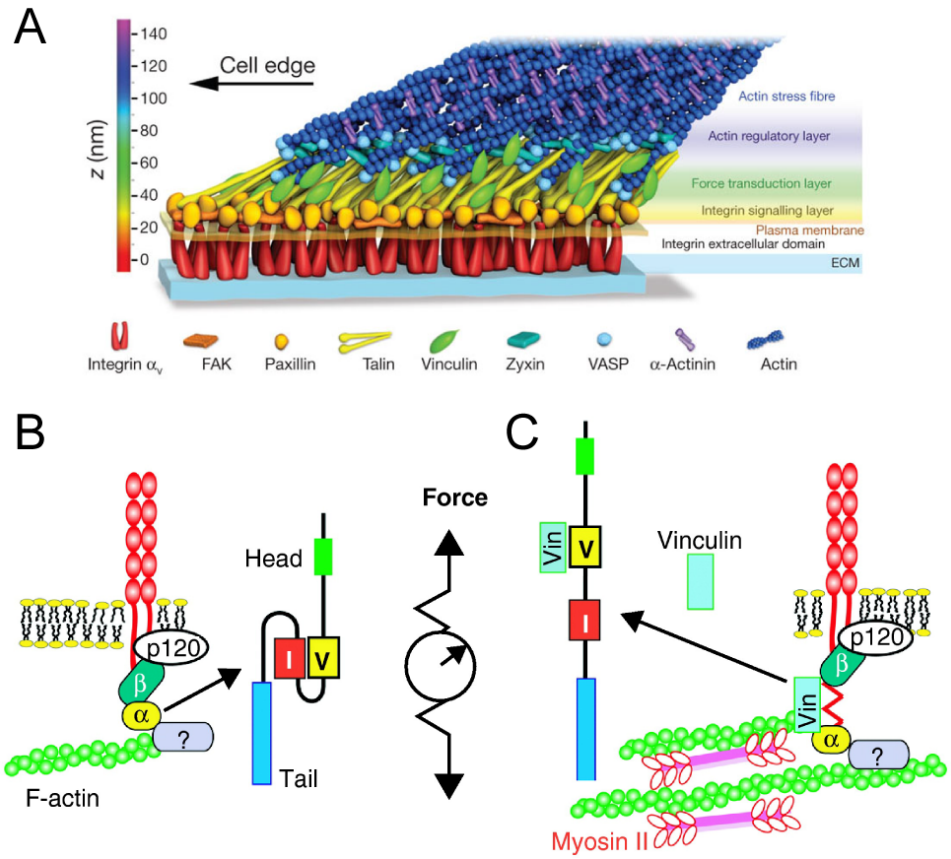

Figure 4.1. Examples of protein-mediated mechanotransducers. (A) Scheme depicting the nanoscale architecture of a focal adhesion. Z-positions were determined experimentally using interferometric photoactivated localization microscopy (iPALM). The model does not depict protein stoichiometry. Reproduced with permission from Reference 10. (B) Proposed molecular components involved in cadherin mechanosensing

in the absence of tension. (C) After tension is applied, the structure of α-catenin opens to reveal a vinculin binding site. Reproduced with permission from Reference 15.

Although not individually identified here, there are a total of 180 different types of proteins that play a role in the cell-ECM interaction and contribute to the formation of higher order structures called focal adhesions.[12] This complex network of proteins creates a connection from the outside environment of the cell to the internal cellular machinery. By creating such a link, cells are able to readily distribute mechanical forces throughout the entire cell body and dynamically respond to stimuli. In addition, mechanical force can travel in both directions, either from the outside-in or from the inside-out (in the case of cell-generated force). There are important elements in the pathway that are designed to sense and transduce mechanical signals. In a 2009 study, del Rio et al. conclusively identified talin as a key mechanotransducer of the integrin pathway whose structure revealed a cryptic binding site for vinculin when mechanically stretched.[13] While many components in cell-ECM adhesions have been identified, the search continues for other potential tension-sensitive molecules in this pathway as well as a complete picture of how cell response to mechanical inputs is regulated.

While integrins are certainly the most studied example of a mechanosensitive system, cell-cell junctions formed by interacting cadherins have emerged as another important model.[14, 15] Cadherins are a family of Ca^{2+} dependent membrane proteins that join together neighboring cells through the formation of adherens junctions, which are similar to focal adhesions. After binding to cadherins on an adjacent cell, p120 catenin, β-catenin, α-catenin and other potential actin-binding proteins localize on the cytoplasmic side of the cadherin molecule, see **Fig. 4.1** *B*.[16] Vinculin, also found in focal

adhesions, forms a link between α-catenin and the actomyosin cytoskeleton.[17] One model has proposed that mechanical tension leads to exposure of a buried vinculin binding site within α-catenin although this has yet to be verified experimentally, **Fig. 4.1** *C*. The process of force transduction through cadherins is likely not as straightforward as described, for instance, when vinculin knockout cells are tested the mechanoresponse is attenuated but not abolished.[18] This result implies that there are multiple mechanotransduction mechanisms utilized within cell-cell adhesions. In summary, cell-cell adhesions composed of cadherins and associated proteins have been established as a new class of mechanosensors. While there are shared members with cell-ECM adhesions, the full network of regulatory molecules has yet to be elucidated, and the cell-cell junction continues to provide a challenging environment to investigate.

4.1.3 Lipid-bilayer mediated mechanosensing: Mechanosensitive ion channels

In contrast to the adhesion-based examples, there is another category of mechanosensing molecules that has emerged, which exclusively relies on the interactions between lipid molecules and embedded proteins (e.g., ion channel). When the membrane experiences a force, the lateral pressure in the lipid bilayer increases, and this pressure favors the open state of the channel due to its larger cross-sectional area.[19] This is balanced by the free energy term associated with unfavorable membrane-protein interactions. These competing contributions determine whether the channel will be found in the open or closed state and demonstrate how protein conformation can be modulated by tension without pulling by the cytoskeleton and associated proteins.[20]

Two of these mechanosensitive ion channels were initially identified in the plasma membrane of *E. coli*, MscL (Mechanosensitive channel of Large conductance)

and MscS (Mechanosensitive channel of Small conductance). The primary function of these channels is to protect cells from lysis upon hypoosmotic shock.[20] These channels confirmed that cells are able to sense and respond to force within the lipid bilayer.[21] The role of mechanosensitive ion channels in eukaryotes is less clear, but the possible connection to sensations such as hearing and touch make them intriguing targets to study. In the auditory system, hair cells of the inner ear possess a flexible bundle of stereocilia that are arranged in a graded fashion.[8] These stereocilia are able to detect subnanometer deflections caused by sound waves or head movement within a few microseconds. The hair bundles are interconnected by a set of fine molecular filaments called tip links, which are hypothesized to transduce mechanical force to mechanosensitive ion channels.[22] To date, the identity of the mechanosensitive ion channel involved in this process remain unknown, although transmembrane channel-like protein 1 and 2 (TMC1 and TMC2) have recently emerged as strong candidates,[23] making it difficult to determine whether the forces associated with hearing are transmitted directly or indirectly to the ion channel.

4.2 Current methods to measure and study cellular forces

In order to understand how mechanical inputs affect specific signaling proteins, there must be a collection of tools available for the precise application and measurement of pN forces in living cells. Among the most well established techniques are atomic force microscopy (AFM) and optical and magnetic tweezers. These single molecule methods are commonly used to apply specific forces to cell surface receptors and to record force-extension curves and rupture forces.[24] To address the serial nature of single molecule methods, our group and others have developed fluorescent force reporters that aim to

quantitatively image tension experienced by individual molecules within living cells at both intracellular and extracellular locations. The general strategy employs a flexible linker that is connected to a solid support at one end and a ligand molecule at the other end. For example in the molecular tension-based fluorescence sensor, the PEG linker acts as an entropic spring whose behavior can be predicted using the worm-like chain model. From this relationship, it is possible to infer the force by measuring the extension of the flexible linker and displacement of the fluorophore away from the quencher. This is not an exhaustive list of techniques (**Table 4.1**) but is instead meant to highlight the methods that are relevant for uncovering the role of force in the Notch signaling pathway.

Technique	Force Range Sensitivity	Spatial Resolution	Dynamics	Throughput
Atomic Force Microscopy	10-10^4 pN	single molecule	N/A	low
Optical Tweezers	0.1-100 pN	single molecule	N/A	low
Magnetic Tweezers	0.01-100 pN	single molecule	N/A	low
Genetically Encoded Tension Sensors	1-6 pN	<1 μm	ms	high
Molecular Tension-based Fluorescence Sensors	0.5-25 pN	<1 μm	ms	high

Table 4.1. Techniques used for the characterization of molecular forces.

4.2.1 Atomic force microscopy (AFM)

Atomic force microscopy was originally developed for sub-nanometer resolution imaging of non-conductive surfaces. It is now commonly used for single-molecule force spectroscopy measurements.[25] The instrument consists of a cantilever (spring constant, k ~ 1 and 10^5 pN nm^{-1}) with a sharp tip that is held above a piezoelectric scanning stage.[26]

A low power laser is reflected off the back of the cantilever onto a position-sensitive detector, which monitors changes in the tip position. When used to measure inter- and intramolecular forces, the biomolecule of interest is attached to the stylus at one end and the stage on the other. When the stage is extended away from the tip, in the axial direction, force information is obtained from deflection of the cantilever and extension curves reveal the distance that the molecule is stretched.

Previous AFM studies were used to measure the adhesion forces at the interface between individual Delta and Notch expressing cells.[27] More recently, Stephenson et al. applied force to a single repeat of human Notch2 NRR and directly observed metalloprotease cleavage at the S2 site.[28] In order to pull on the Notch2 NRR fragment, the sequence was modified to incorporate an N-terminal poly-lysine tag for attachment to an N-hydroxysuccinimide (NHS) functionalized gold surface and a C-terminal hexa-histidine tag for attachment to a Ni^{2+}-NTA modified tip. Results from the AFM experiments showed that NRR unfolding occurred at two different force regimes. At low force (~179 pN), LNR-A and B begin to unfold and reveal the S2 cleavage site. At high force (~372 pN), the larger HD domain and possibly the LNR-C begin to unfold. Molecular dynamics simulations verify that LNR-A and B restrict access to the S2 site and are exposed early on in the mechanical unfolding of the NRR structure. Interestingly, when the applied force was maintained at 200 pN leaving the S2 site solvent accessible, addition of the metalloprotease TACE resulted in cleavage of nearly half the samples tested. While the magnitude of tension applied was not physiologically relevant, it did suggest a sensitivity of the NRR towards cleavage in a force-dependent manner. The details uncovered from simulations and experiments reveal that the extracellular Notch2

NRR is resistant to full unfolding of its individual domains especially when coordinated with metal ions. This evidence supports the mechanotransduction model of Notch activation where ligand binding is followed by escape from the autoinhibited conformation of the NRR.

4.2.2 Optical tweezers

Optical tweezers are a versatile tool capable of stably trapping dielectric particles such as single cells, lipid vesicles, and polystyrene or silica microspheres.[24] To form an optical trap, light from a near-infrared laser is focused into a diffraction-limited spot using a high numerical aperture (NA) objective.[29] When objects approach the laser's electric field, they develop an electric dipole moment, which is influenced by two types of forces. The first are gradient forces located near the focal point that draw in objects, and the second is radiation pressure of the beam that moves objects along the direction of light propagation. When the gradient force dominates, a particle can become trapped in three dimensions near the laser focal point. The stiffness of the optical trap varies from 0.005-1 pN nm^{-1} and depends on parameters such as laser power, particle size and refractive index.

Using optical tweezers, Shergill et al. trapped polystyrene beads functionalized with Notch1 fused to the Fc domain of human IgG to investigate the strength of ligand-receptor binding.[30] Cells expressing Dll1 were brought into contact with the Notch1 beads and moved away leading to rupture of the molecular interaction as characterized by a sudden change in cell position. Based upon repeated measurements, the average rupture force for a single Dll1-Notch1 interaction was determined to be 19 pN.[30] The rupture force sets an upper limit for the amount of tension that the ligand-receptor bond can

withstand because higher values would result in dissociation of the ligand-receptor contact before causing a significant conformational change in the receptor structure. Utilizing a similar experimental setup, forces mediated by the Dll1 expressing cell were measured to be ~2.8 pN.[31] To generate such a force, the ligand cell used an alternative type of clathrin mediated endocytosis that requires dynamin, epsins and actin. Together, these studies quantitatively described the strength of the Dll1-Notch1 interaction and proposed a mechanism by which ligand cell pulling promotes activating proteolysis of the Notch receptor. These studies suffer from the inherent limitations of single molecule studies, and do not consider multiple ligand-receptor interactions (oligomerization), which may alter the forces measured.

4.2.3 Magnetic tweezers

Magnetic tweezers use permanent magnets or electromagnets positioned above the objective of an inverted microscope to create a magnetic field gradient (compared with an electric field gradient for optical tweezers). Super-paramagnetic beads tethered to a glass surface experience small and stable forces based upon their position within the magnetic field. This technique is able to apply such small forces due to the characteristic low force constant values of the tweezers ranging from 10^{-3} to 10^{-6} pN nm^{-1}. Additionally, magnetic tweezers are relatively straightforward to assemble, and the magnets are easily rotated allowing the sample to experience both force and torque. These properties make magnetic tweezers an ideal candidate for studying properties of DNA such as the elasticity of individual strands[32] and for directly observing and measuring topoisomerase activity on supercoiled DNA.[33]

4.2.4 Genetically encoded FRET force sensors

The aforementioned force techniques have all involved the use of specialized equipment in order to apply pN forces to biological samples. New approaches have been established that use fluorescence, specifically fluorescence resonance energy transfer (FRET), to report on the forces experienced by mechanosensitive molecules. The only type of instrument required for such experiments is a standard epifluorescence microscope, although optical tweezers and a FLIM system are necessary for more quantitative measurements. FRET is a widely used technique to investigate the structure and dynamics of biomolecules because non-radiative energy transfer occurs at distances between 10-100 Å.[34-36] The efficiency of energy transfer is generally defined as (1):

$$E = \frac{R_0^6}{\left[R_0^6 + r^6\right]} = 1 - \frac{I_{DA}}{I_D} \qquad (1)$$

where r is the donor-acceptor distance, R_0 is the characteristic distance where the efficiency of energy transfer is 50%, I_{DA} is the fluorescence intensity of the donor in the presence of the acceptor, and I_D is the donor intensity in the absence of the acceptor. Each donor-acceptor or donor-quencher pair possesses a unique Förster radius or R_0 value (in units of Å), which is described as (2):

$$R_0 = \left[8.785 \times 10^{-5} \cdot \frac{\kappa^2 \cdot \phi_D \cdot J(\lambda)}{\eta^4}\right]^{1/6} \qquad (2)$$

where κ^2 is an orientation factor relating the donor and acceptor dipoles (estimated to be 2/3), ϕ_D is the quantum yield of the donor molecule in the absence of the acceptor, $J(\lambda)$ is the overlap integral between donor and acceptor and η is the index of refraction of the sample (estimated to be 1.4). The overlap integral is expressed as (3):

$$J(\lambda) = \int F_D(\lambda) \cdot \varepsilon_A(\lambda) \cdot \lambda^4 \cdot d\lambda \qquad (3)$$

where F_D represents the overlap of donor emission with acceptor excitation and ε_A is the molar extinction coefficient of the acceptor (in units of M^{-1} cm^{-1}). Therefore, experimental measurements of fluorescence in conjunction with knowledge of R_0 provide molecular distances, which in turn are used to infer cellular forces.

Grashoff and co-workers developed a calibrated *in vivo* intramolecular tension sensor, which was successfully incorporated into vinculin.[37] The tension sensor module consists of a fluorescent protein FRET pair - cyan and yellow fluorescent protein (CFP and YFP) - that are connected by a flagelliform linker sequence, $(GPGGA)_8$, derived from a spider silk protein. One of the significant advances of this method is that it allows for intracellular imaging of tension, which requires that the tension sensor module to be genetically encoded between the head and tail domains of vinculin. When minimal tension is present, the donor and acceptor are in close proximity to one another and the sensor readout will indicate a high FRET efficiency. However, when vinculin experiences increased cellular tension, the elastic linker extends, separating the donor and acceptor and leading to a decrease in FRET efficiency. The authors calibrated the intracellular fluorescence signal and determined that the tension transduced by vinculin found in stable focal adhesions was ~2.5 pN.

The versatility of this tension sensor was recently demonstrated through its incorporation into another mechanotransducing molecules. Borghi et al. used the tension sensing module to determine if E-cadherins are direct mediators of force in cell-cell adhesion.[38] In this case, the sensor was fused between the transmembrane domain and catenin-binding domain on the intracellular portion of the membrane protein. Surprisingly, the results showed that E-cadherins are always under tension whether or not

they are present in cell-cell junctions. This leads to the possibility that E-cadherins are primed and ready to act as a link between the actomyosin cytoskeleton and external mechanical inputs. Importantly, the genetically encoded tension probe must be incorporated into a robust protein that can tolerate significant re-engineering. Therefore, it is unlikely to work well with transmembrane proteins such as Notch.

4.2.5 Molecular tension-based fluorescence microscopy (MTFM)

Cell surface receptors are among the first molecules to sense and respond to physical inputs experienced by the cell. While genetically encoded tension sensors are an excellent choice for investigating forces inside of the cell, they are less compatible for probing membrane proteins. Engineering membrane proteins fused to fluorescent proteins remains a challenge for several reasons. The size of the fluorescent protein is significant at ~ 27 kDa, which means that it could interfere with proper ligand recognition. Addition of the fluorescent protein can also lead to improper folding or modification of the receptor. For these reasons, our lab recently developed a sensor for characterizing the forces involved in epidermal growth factor receptor (EGFR) uptake after binding to EGF.[39] This fluorescent sensor was designed with a donor-quencher pair linked together with a polyethylene glycol (PEG) polymer. One end of the sensor was attached to a glass surface through a biotin-streptavidin linkage while the other end was conjugated to a single EGF molecule. Binding of the ligand to the receptor was followed by extension of the flexible PEG linker and resulted in an enhancement of the fluorescence signal or 'turn-on' response. The mechanical properties of the PEG polymer can be accurately described using the extended worm-like chain model, which permits conversion of FRET efficiency into force response. Fluorescent puncta, representing clusters of the extended

ligand, were captured and showed a force response of up to 4 pN in the initial moments leading to ligand internalization.

The dynamic range of any FRET-based sensor is fundamentally limited by the distance dependence of the energy transfer. In order to overcome this limitation, our group fabricated a gold nanoparticle (AuNP)-based molecular tension sensor where the quencher molecule was replaced with a 15 nm AuNP.[40] Fluorescence quenching by noble metal nanoparticles follow a $1/r^4$ distance dependence compared with $1/r^6$ relationship for FRET where r is the dye-particle or inter-dye distance. In turn, this increases the dynamic range of the AuNP-based sensor to 25 pN (**Table 4.1**). As a proof of principle, the force exerted by integrins upon binding with a cyclic Arg-Gly-Asp-D-Phe-Lys (cRGDfK) modified sensor was found to range from 1 to 15 pN. The magnitude of force reported represents the minimum force exerted per molecule as a diffraction limited spot in a high magnification fluorescence image may contain multiple sensors.

The previously discussed examples relied upon PEG to serve as an entropic spring, however, molecules that display even greater sensitivity to mechanical force may provide additional details into the process of mechanotransduction. To this end, several groups have used ssDNA,[41] dsDNA[42] or DNA hairpins[43] in place of the spider silk protein or PEG polymer. Recently, Wang et al. developed a tension gauge tether composed of a DNA duplex designed to rupture at a critical force. Furthermore, the gauges were modified with ligand molecules including cRGDfK and the Notch receptor ligand, DLL1.[44] For integrins, the cell was found to universally apply 40 pN of force per ligand-receptor interaction (as defined by the force needed to rupture the tether within 2 s) during the initial stages of adhesion. In the case of Notch receptors, the force exerted by

the cells was less than 12 pN but could not be specified any further due to limitations in the sensing technique. Current work in our group focuses on using DNA hairpins as digital sensors of pN forces, see **Fig. 4.2**.[45] This modular system is composed of two DNA arms connected by a DNA hairpin where one arm is modified with the ligand molecule and the second arm anchors the entire sensor construct. One advantage of this system is that the sensor can be multiplexed using hairpins with different dye-quencher pairs to monitor the extension of the hairpin set to different force thresholds. Also, importantly, this sensor is highly modular and consistently achieves QE values above 95%, which is an improvement over the PEG-based sensor.

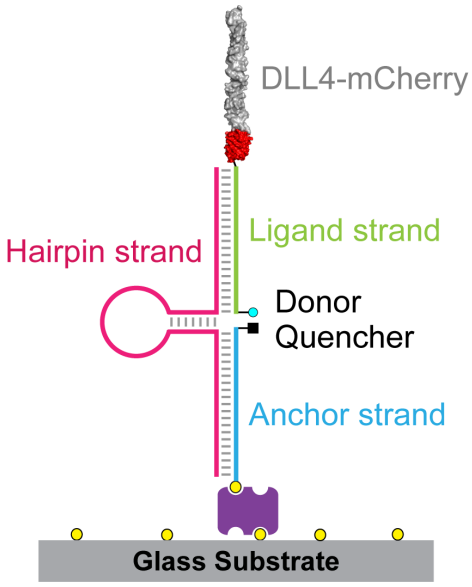

Figure 4.2. Scheme of DLL4 DNA hairpin sensor. The anchor strand (blue) is modified with a quencher molecule and attaches the sensor to the surface. The tension threshold is tuned by incorporating different hairpin strands (magenta) into the sensor. The ligand strand (green) is used to attach the molecular binding partner of the receptor of interest, in this case, the DLL4 ligand.

4.2.6 Comparing different methods for measuring force

In summary, several different strategies were presented for measuring forces involved in mechanotransduction. The key characteristics of each of these techniques are

outlined in **Table 4.1**. The first criteria to consider is the force range of each method, which is directly related to the stiffness of the spring or the spring constant, *k*. Magnetic tweezers are able to access the lowest forces at 0.01 pN while AFM is able to reach the highest forces at 10^4 pN. In addition, high spatial and time resolution are required to capture dynamic biological events that often occur on the millisecond or shorter time scales. Most of the methods presented are able to meet this requirement, although in some cases high resolution is not required in both domains. Most importantly, AFM, optical and magnetic tweezers are not suitable for force imaging, due to their serial nature.

There are fundamental limitations that restrict the use of these methods under certain experimental circumstances. AFM, optical and magnetic tweezers are serial methods where each force measurement provides details about a single interaction, whether this is the unfolding of a single protein domain or the rupture of a ligand-receptor contact. Many individual measurements are pooled together to describe average molecular behavior, but this type of data collection is time consuming and does not measure dynamics across the cell membrane. On the other hand, genetically encoded tension sensors and MTF probes are able to report forces across the entire cell for a large number of cells. The encoded sensor requires straightforward cloning to insert the tension sensor module into a target protein such that biological activity is not adversely affected. MTF probes require the modification of ligand molecules to include a flexible PEG linker and a surface anchor. However, the MTF sensor is more modular giving researchers more flexibility in the type of ligand that can be conjugated and in the selection of commercially available organic dye and quencher pairs that can be incorporated. In many ways, the genetically encoded tension sensors and MTF sensors provide complementary

information as the former is well suited for probing intracellular mechnotransducers and the latter is more appropriate for probing the molecular interface between the cell surface receptor and its surrounding environment.

Another important difference is that the genetically encoded sensor and MTF probes are able to accurately capture how the location and magnitude of force changes as a function of time. This type of information is critical for understanding processes such as cell adhesion and migration. For example, Liu et al. observed the initial moments of integrin binding to cRGDfK and noticed that the MTF signal quickly moves from the center of the cell to the cell edge.[40] Experiments of long duration, on the time scale of days, remain a challenge for any force sensor. In the case of the oligonucleotide probes, use of the sensor is limited to several hours due to degradation by cell-generated nucleases. While each type of probe has its benefits and limitations, ultimately the biological question will determine which sensor is best suited for the needs of the researcher.

4.3 Results and discussion

4.3.1 Designing a Notch tension sensor

The mechanotransduction model of Notch activation proposes that after ligand binding a mechanical force causes a significant conformational change in the NRR leading to proteolysis of the NICD. The source of this mechanical force remains unknown, although there is experimental evidence suggesting that the force originates from endocytosis of receptor bound ligand molecules.[46-48] In order to determine the origins and magnitude of the force and its role in Notch activation, both genetically encoded and MTF sensors were incorporated into the cognate Notch ligand, Delta-like

protein 4 (DLL4). For site-specific modification of DLL4, several bioconjugation strategies were employed including expressed protein ligation and Sortase A (SrtA) mediated ligation.

4.3.2 Incorporation of genetically encoded tension sensor into DLL4

From a chemical synthesis perspective, the most straightforward sensor design involves genetically encoding the repeating GPGGA flagelliform linker into the expressed DLL4 molecule. The DLL4 ligand was modified with a biotin moiety near the C-terminus using biotin ligase for surface attachment, **Fig. 4.3**. The original CFP-YFP FRET pair was replaced due to spectral overlap with eGFP-tagged Notch1 receptor in the C2C12 cell line. To replace this pair, mCherry was genetically encoded on one end of the elastic linker and QSY9 was conjugated to the anchoring streptavidin molecule. Selection of the quencher molecule was determined by measuring the quenching efficiency of the sensor in the resting state (no tension applied) on a supported lipid membrane. For the mCherry-QSY9 pair, the quenching efficiency (QE) was calculated to be 54% with a theoretical Förster radius (R_0) of 3.9 nm. This R_0 value was calculated using eq. 2 (defined above) and estimating that κ^2 is 2/3, $\phi_{mCherry}$ is 0.22, and η is 1.4.

MAAASRSASGWALLLLVALWQQRAAGSGVFQLQLQEFINERGVLASGRPCEPGCRTFFR
VCLKHFQAVVSPGPCTFGTVSTPVLGTNSFAVRDDSSGGGRNPLQLPFNFTWPGTFSLI
IEAWHAPGDDLRPEALPPDALISKIAIQGSLAVGQNWLLDEQTSTLTRLRYSYRVICSD
NYYGDNCSRLCKKRNDHFGHYVCQPDGNLSCLPGWTGEYCQQPICLSGCHEQNGYCSKP
AECLCRPGWQGRLCNECIPHNGCRHGTCSTPWQCTCDEGWGGLFCDQDLNYCTHHSPCK
NGATCSNSGQRSYTCTCRPGYTGVDCELELSECDSNPCRNGGSCKDQEDGYHCLCPPGY
YGLHCEHSTLSCADSPCFNGGSCRERNQGANYACECPPNFTGSNCEKKVDRCTSNPCAN
GGQCLNRGPSRMCRCRPGFTGTYCELHVSDCARNPCAHGGTCHDLENGLMCTCPAGFSG
RRCEVRTSIDACASSPCFNRATCYTDLSTDTFVCNCPYGFVGSRCEFPVGLPMVSKGEE
DNMAIIKEFMRFKVHMEGSVNGHEFEIEGEGEGRPYEGTQTAKLKVTKGGPLPFAWDIL
SPQFMYGSKAYVKHPADIPDYLKLSFPEGFKWERVMNFEDGGVVTVTQDSSLQDGEFIY
KVKLRGTNFPSDGPVMQKKTMGWEASSERMYPEDGALKGEIKQRLKLKDGGHYDAEVKT
TYKAKKPVQLPGAYNVNIKLDITSHNEDYTIVEQYERAEGRHSTGGMDELYKGPGGAGP
GGAGPGGAGPGGAGPGGAGPGGAGPGGAGPGGAMVSAGLNDIFEAQKIEWHEHHHHHHH
HHH

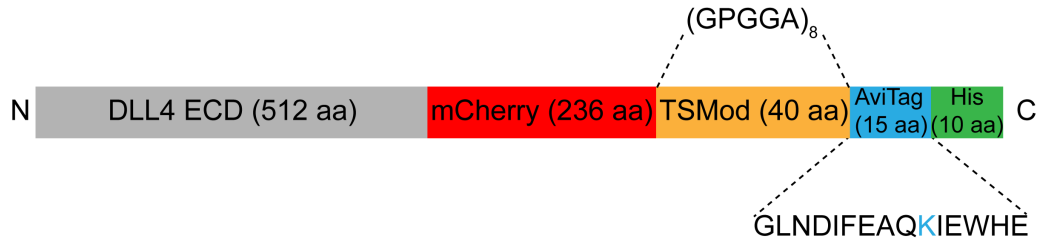

Figure 4.3. Amino acid sequence of DLL4 incorporating portions of the tension sensor module developed by Grashoff et al. DLL4 extracellular domain sequence consists of 512 amino acid and is fused with mCherry (236 amino acids in red). This is followed by the flagelliform linker $(GPGGA)_8$ (underlined), short connecting linker, AviTag sequence (15 amino acids in blue) and deca-histidine purification tag (green). Domains of the genetically encoded DLL4 tension sensor.

To observe cell exerted forces upon ligand binding, glass substrates covalently modified with biotin and passsivated with mPEG (MW~2000) were incubated with QSY9 labeled streptavidin and DLL4 (see Materials and Methods). When Notch1-eGFP cells were seeded onto the surface, ligand binding was clearly observed due to strong cell adhesion, but there was no observable tension signal, **Fig. 4.4**. One explanation for this result is the poor initial QE (54%) between mCherry and QSY9. The QE is low because the mCherry chromophore is buried within the β-barrel of mCherry by ~2 nm (based upon the crystal structure PDB:2H5Q), and the resting state of the spider silk protein adds additional distance. Taken together, the inter-dye distance between mCherry and QSY9 approaches the theoretical Förster radius. When the QE at the resting state is near 50%, a maximum of a 2-fold increase in the fluorescence intensity can be expected when the sensor is fully extended. To improve the sensor properties, it was necessary to place the donor and quencher in closer proximity to increase the resting state QE.

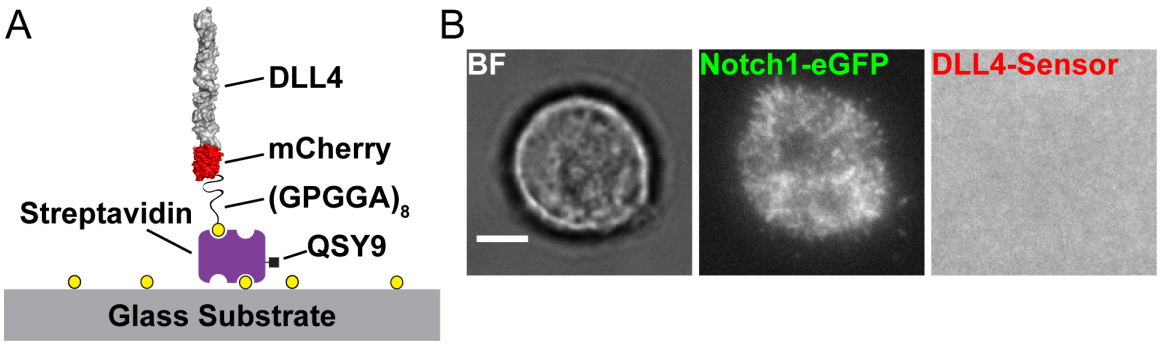

Figure 4.4. Genetically encoded DLL4 tension sensor. (A) Scheme showing the DLL4 ligand fused to mCherry and the elastic linker $(GPGGA)_8$ tethered to a glass substrate through a biotin-streptavidin interaction. Energy transfer between mCherry (donor) and QSY9 (quencher) results in quenched donor fluorescence in the resting state (as depicted). Cell applied force extends the linker resulting in an increase of donor fluorescence. (B) Representative images of Notch1-eGFP cells bound to DLL4 with genetically encoded tension sensor. Abbreviation: brightfield, BF. Scale bar represents 5 μm.

4.3.3 Semi-synthetic tension probes

4.3.3.1 Expressed protein ligation: DLL4 α-thioester and Cys-PEG_{24}-biotin

The goal for the next generation of force sensors developed in our lab was to reposition the quencher molecule site-specifically to the opposite terminus of the entropic spring, thereby increasing the QE in the resting state and thus increasing sensitivity and dynamic range. The first strategy was a semi-synthetic approach where the extracellular domain of the ligand was expressed using an insect expression system, and the sensor portion was chemically synthesized using solid phase peptide synthesis. These two components were joined together *in vitro* using expressed protein ligation (EPL), an extension of native chemical ligation, **Fig. 4.5**. To isolate the DLL4-mCherry-α thioester, the C-terminus of the ligand was fused to a self-splicing protein, called an intein, from the *Mycobacterium xenopi* DNA gyrase A (Mxe GyrA). This modified intein was engineered for thiolysis in the presence of a variety of thiols.[49] The intein tag includes a

chitin binding domain (CBD) that serves as an affinity tag for purification of the protein of interest. Formation of the α-thioester occurs when the captured ligand is treated with any of a variety of thiols including sodium 2-mercaptoethanesulfonate (MESNa). The ligand reacts with the N-terminal cysteine modified PEG tension sensor joining together the two polypeptides with a native amide backbone.

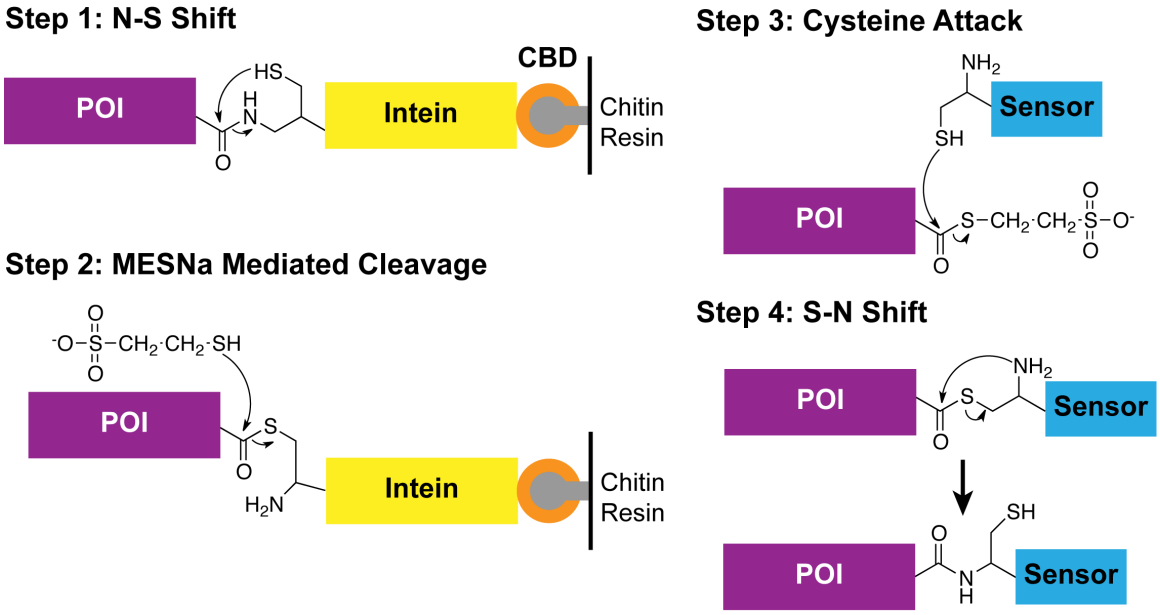

Figure 4.5. Strategy using expressed protein ligation to join a protein of interest (POI) with the tension sensor. The protein of interest can be expressed in any type of expression system before binding to the chitin resin. The Mxe GyrA intein and CBD are composed of a total of 236 amino acids.

As a proof of principle, mCherry-α thioester was expressed in *E. coli*, purified and ligated with a Cys-PEG_{24}-biotin, see **Fig. 4.6** *A* for structure. For these initial experiments, the quencher molecule was located on the streptavidin, however, an increase in the quenching efficiency is expected when the quencher is moved onto the PEG spring. The quenching efficiency between mCherry and QSY21 was determined to be 50%, **Fig. 4.7**. Both QSY9 (λ_{max}= 562 nm) and QSY21 (λ_{max}= 660 nm) are adequate quenchers of

mCherry fluorescence, but neither precisely matches the peak emission wavelength of 610 nm. One inherent difficultly in working with a donor-quencher pair instead of a traditional donor-acceptor pair is the hydrophobic nature of quencher molecules compared with traditional fluorophores. This property makes quencher molecules and their conjugates insoluble in certain aqueous conditions and at high concentration.

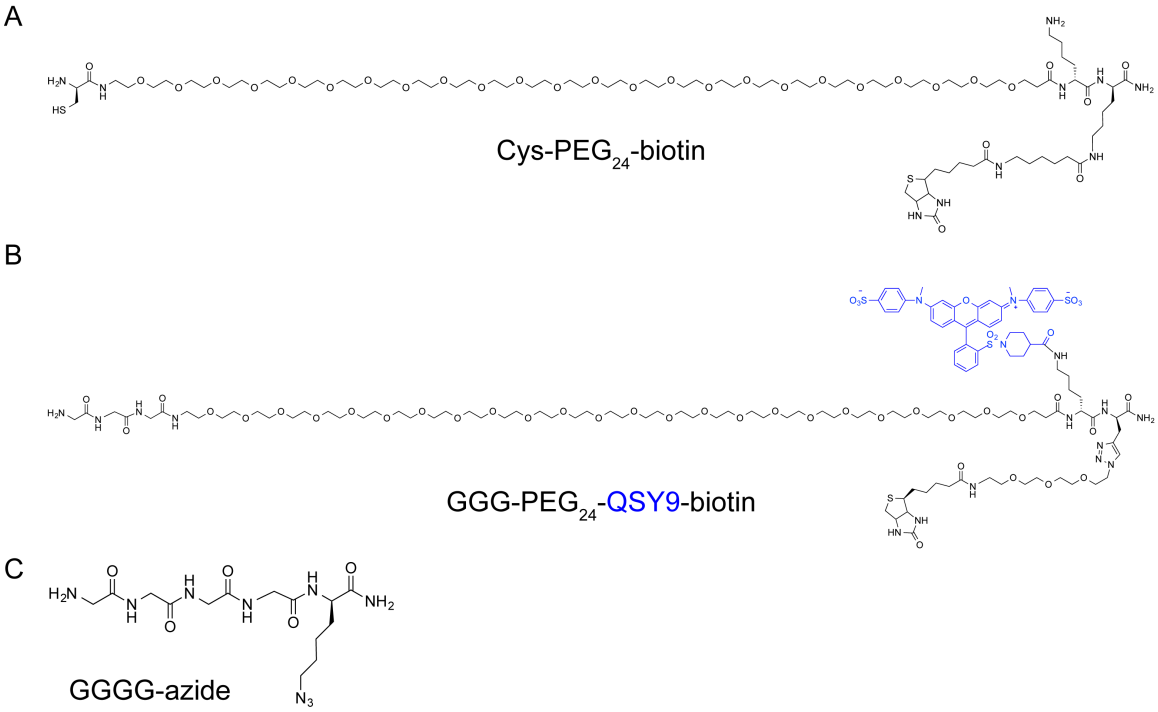

Figure 4.6. Chemical structure of linkers used in this work generated by solid phase peptide synthesis. (A) Cys-PEG_{24}-biotin used in EPL. (B) GGG-PEG_{24}-QSY9-biotin and (C) GGGG-azide used in Sortase A mediated ligation.

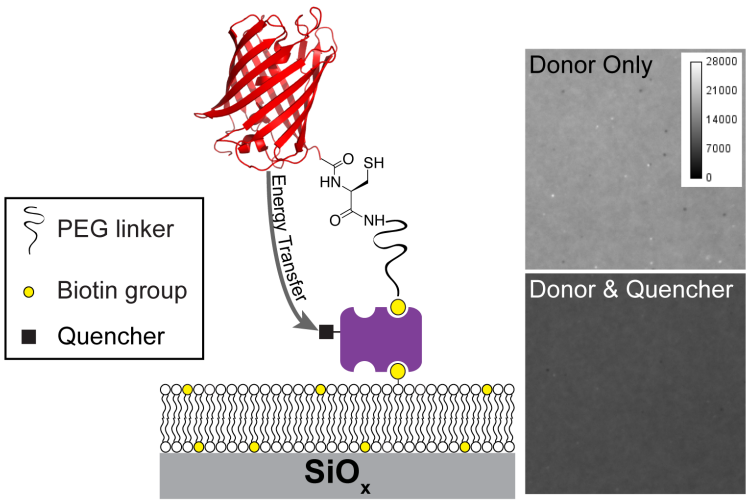

Donor/Quencher	QE	Theoretical R_0
mCherry/QSY21	50%	5.6 Å

Figure 4.7. Quenching efficiency of mCherry-α thioester and QSY21 labeled streptavidin measured on a supported lipid membrane.

Another challenge of this approach is achieving high expression yield of the DLL4-mCherry α-thioester. Overall, insect cells can produce between 10 μg-10 mg of recombinant protein per 10^7 cells, which is a modest amount when compared with bacterial expression systems.[50] Efficient ligation requires the target protein to be present at high μM or even mM concentration. As observed for other semi-synthetic molecules, *in vivo* or premature cleavage of the intein domain remains a problem and reduces yield of the recombinant protein.[51, 52] In addition, the rate of cleavage from the chitin column can be slow and inefficient taking up to 40 h to achieve 70-95% cleavage from the column at 4 °C. For these reasons, it was not possible to isolate enough purified DLL4-mCherry-α-thioester to utilize EPL to produce the Notch tension sensor.

4.3.3.2 Sortase mediated ligation:DLL4-mCherry-LPXTG and GGG-PEG$_{24}$-QSY9-biotin

The second semi-synthetic strategy employed a transpeptidase, Sortase A (SrtA), to site-specifically modify the DLL4-mCherry ligand with a PEG-based force sensor. SrtA is an enzyme present in most Gram-positive bacteria that covalently links proteins to the cell wall.[53] When used as a tool in chemical biology, SrtA (206 amino acids) is trunctated to remove 59 residues at the N-terminus that anchor the enzyme to the membrane. The transpeptidase recognizes the sequence LPXTG, and a cysteine residue (Cys184) in the active site catalyzes cleavage of the amide bond between threonine and glycine, **Fig 4.8**.[54, 55] Formation of the acyl-enzyme intermediate is followed by nucleophilic attack of the threonine carboxyl group by the N-terminus of an oligoglycine peptide resulting in the ligation of the two peptides. Using this strategy, we expressed a version of the DLL4-mCherry ligand containing the SrtA motif fused at the C-terminus (**Fig. 4.9**) and combined it with a triglycine peptide modified PEG_{24} with a quencher (QSY9) and biotin group.

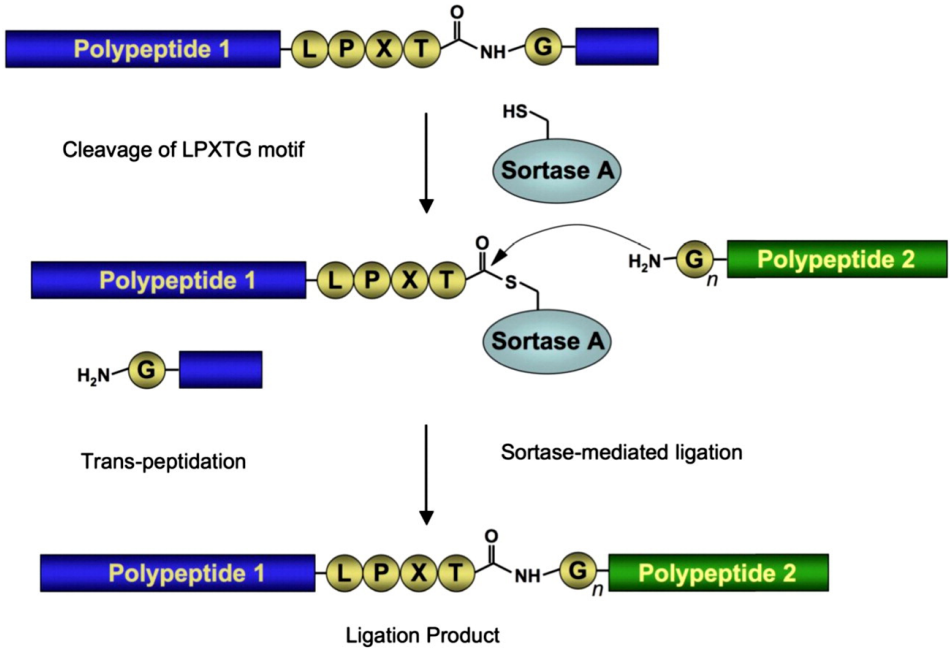

Figure 4.8. Mechanism of Sortase A mediated ligation. Reprinted from Reference 54, with permission from Elsevier.

MAAASRSASGWALLLLVALWQQRAAGSGVFQLQLQEFINERGVLASGRPCEPGCRTFFR
VCLKHFQAVVSPGPCTFGTVSTPVLGTNSFAVRDDSSGGGRNPLQLPFNFTWPGTFSLI
IEAWHAPGDDLRPEALPPDALISKIAIQGSLAVGQNWLLDEQTSTLTRLRYSYRVICSD
NYYGDNCSRLCKKRNDHFGHYVCQPDGNLSCLPGWTGEYCQQPICLSGCHEQNGYCSKP
AECLCRPGWQGRLCNECIPHNGCRHGTCSTPWQCTCDEGWGGLFCDQDLNYCTHHSPCK
NGATCSNSGQRSYTCTCRPGYTGVDCELELSECDSNPCRNGGSCKDQEDGYHCLCPPGY
YGLHCEHSTLSCADSPCFNGGSCRERNQGANYACECPPNFTGSNCEKKVDRCTSNPCAN
GGQCLNRGPSRMCRCRPGFTGTYCELHVSDCARNPCAHGGTCHDLENGLMCTCPAGFSG
RRCEVRTSIDACASSPCFNRATCYTDLSTDTFVCNCPYGFVGSRCEFPVGLPMVSKGEE
DNMAIIKEFMRFKVHMEGSVNGHEFEIEGEGEGRPYEGTQTAKLKVTKGGPLPFAWDIL
SPQFMYGSKAYVKHPADIPDYLKLSFPEGFKWERVMNFEDGGVVTVTQDSSLQDGEFIY
KVKLRGTNFPSDGPVMQKKTMGWEASSERMYPEDGALKGEIKQRLKLKDGGHYDAEVKT
TYKAKKPVQLPGAYNVNIKLDITSHNEDYTIVEQYERAEGRHSTGGMDELYKGLNDIFE
AQKIEWHE LPETGHHHHHHHHHH

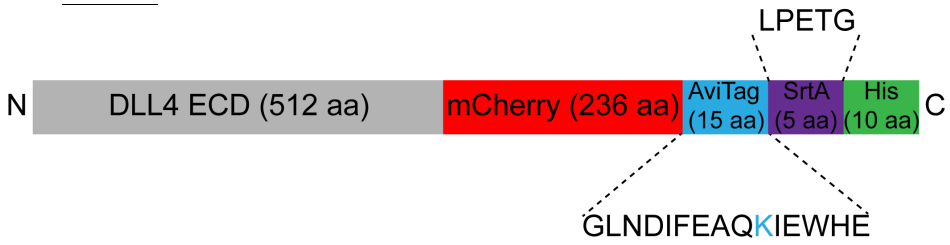

Figure 4.9. Amino acid sequence of DLL4 incorporating the Sortase motif. DLL4 extracellular domain sequence consists of 512 amino acid and is fused with mCherry (236 amino acids in red). This is followed by the AviTag sequence (15 amino acids, blue), the Sortase A motif (underlined) and deca-histidine purification tag (green). Domains of the semi-synthetic DLL4 PEG tension probe.

DLL4-mCherry-LPXTG was successfully ligated to the GGG-PEG_{24}-QSY9-biotin (structure shown in **Fig. 4.6** *B*) through use of SrtA. This was verified by Western Blot analysis through detection of the biotin group using HRP-conjugated streptavidin, see **Fig. 4.10**. While the exact yield of the SrtA ligation is unknown for this specific reaction, typical yields reported by researchers range from 30-85%.[56] The QE of the DLL4 tension sensor in the resting state was 73%. To ensure that modification of the DLL4 ligand did not adversely affect biological function, ligand-receptor binding was verified for supported membrane tethered DLL4. Notch1-eGFP cells were incubated on the laterally mobile ligand surface and binding was verified through co-localization of

ligand and receptor fluorescence, **Fig. 4.11** *A*. The behavior of the ligand with a PEG-based tension sensor appears indistinguishable to cases where the ligand does not contain a flexible linker.

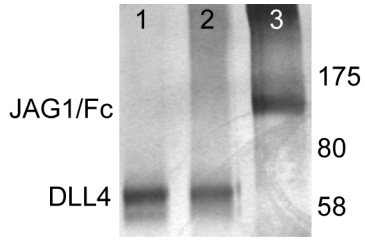

Figure 4.10. Western blot verifying conjugation of DLL4-mCherry ligand with PEG-based sensor. Lane 1: Sortase conjugated DLL4-mCherry and GGG-PEG$_{24}$-QSY9-biotin, Lane 2: Repeats of 1, Lane 3: Biotinylated JAG1/Fc.

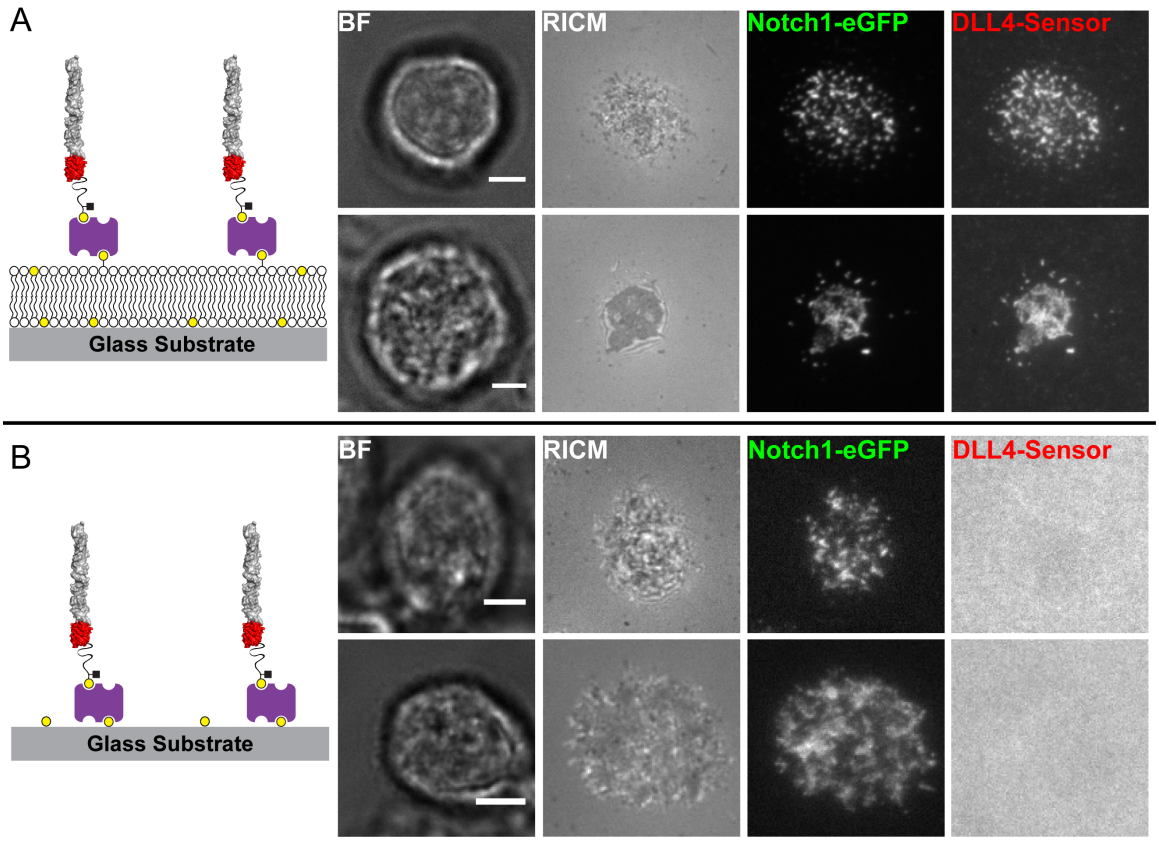

Figure 4.11. Notch1-eGFP binding to DLL4 ligand with PEG-based sensor on different surface types. (A) Notch1-eGFP cells bind specifically to supported membrane tethered DLL4 and form large clusters of ligand and receptor due to the lateral mobility of the DLL4 molecules (i.e. no resistance to cell applied tension). (B) Notch1-eGFP cells bind

to immobilized DLL4 ligand as confirmed by the tight contact to the substrate (RICM), but no sensor signal is observed.

In order to measure cell applied forces, the DLL4 ligand molecules must remain immobilized on the surface. The main reason for this is that the lateral mobility of the membrane tethered ligand leads to accumulation or clustering of DLL4 molecules in a process driven by receptor expressing cells, as seen in **Fig. 4.11** *A* and discussed in detail in Chapter 3. The increase in donor intensity is due to higher local density of ligand molecules and cannot be distinguished from signal caused by cell generated tension on the sensor. To remedy this, the modified DLL4-mCherry was bound to a covalently modified glass slide, where lateral movement of the ligand molecule is not possible. Therefore, any increase in fluorescence intensity is attributed to an applied force and not clustering. When cells were seeded onto such a surface, cell binding occurred, but there was no detectable increase in fluorescence signal that could be ascribed to force-induced extension of the flexible PEG linker, **Fig. 4.11** *B*.

There are several potential explanations for the failure to observer fluorescent response associated with Notch tension. One possibility is that Delta-Notch tension is sufficient to activate the sensor, but this event rarely transpires. There is evidence to support this hypothesis as release of the NICD at endogenous levels is known to be very low.[57] Additionally, it is important to emphasize that these are not single-molecule experiments and each pixel contains multiple sensors, which means that it may not be possible to detect the extension of an individual sensor. Combined with low incidence, the S2/S3 cleavage events may occur very rapidly, as the timescale of activation remains unknown. Therefore, it may be challenging to capture these transient events. The final explanation is that Delta-Notch tension is not sufficient enough for detection using

tension probes or non-existent. It is possible that a new type of sensor could address this issue - one that has higher sensitivity at lower applied force. It must also be considered that the mechanotransduction model may not accurately describe the mechanism of receptor activation.

4.3.3.3 Sortase mediated ligation:DLL4-LPXTG and DNA hairpin

As summarized previously, the force range of the PEG-based sensors is an improvement over the genetically encoded sensor (**Table 4.1**), but higher sensitivity can be achieved through the use of DNA hairpins. To this end, a DLL4-DNA conjugate was synthesized by coupling a donor-labeled, alkyne DNA strand with a GGGG-azide peptide (**Fig. 4.6** *C*) using standard click chemistry techniques. MALDI mass spectrometry was used to verify conjugation with an expected mass of 8603.2 amu for the Cy3B strand (**Fig. 4.12** *A*) and 8635.2 for the Cy5 strand (**Fig. 4.12** *B*). The peptide-DNA conjugate was joined to DLL4-mCherry-LPXTG ligand through SrtA mediated ligation. The DNA hairpin sensor was composed of three different components (see **Table 4.2** for sequences), as described earlier: the donor-modified ligand strand, the tension sensing hairpin and the quencher labeled anchor strand. The $F_{1/2}$ value is defined as the mean rupture force of the hairpin, which is comprised of two different free energy components. This first is the energy required to unfold the hairpin at zero force, and the second is the energy necessary to stretch ssDNA based upon the worm-like chain model.[58, 59] To verify correct assembly of the sensor onto the surface, the DNA strand complementary to the hairpin was hybridized in solution and on the surface. When the hairpin was opened in solution, an 11.5-fold increase in fluorescence intensity was observed, and when the hairpin was opened on the surface, a 5.2-fold increase was measured. The reduction in

hybridization efficiency is rationalized by restricted access of the complement to the hairpin when the sensor is anchored to a surface, **Fig. 4.13**.

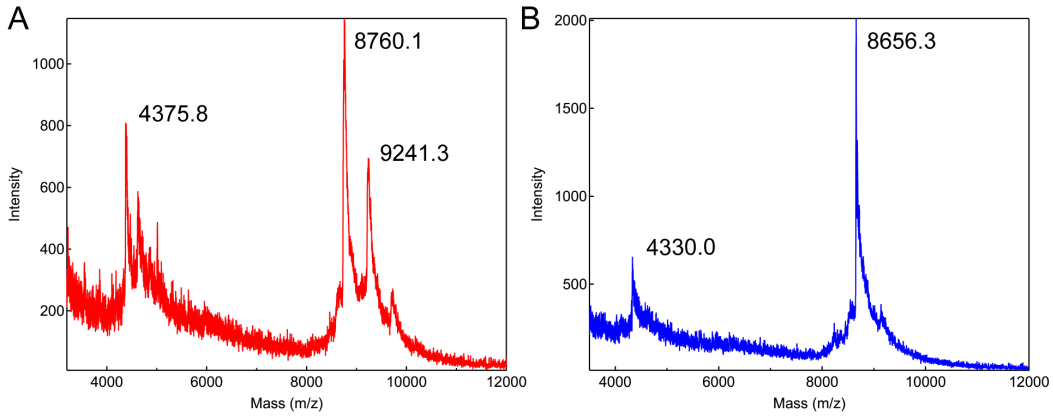

Figure 4.12. MALDI of donor labeled DNA ligand strand conjugated with GGGG-azide. The final mass was verified before ligation with the DLL4 ligand. (A) Click chemistry products of Cy3B labeled ligand strand with GGGG-azide after ethanol precipitation. (B) Click chemistry products of Cy5 labeled ligand strand with GGGG-azide.

DNA Description	$F_{1/2}$	Sequences
Ligand Strand	-	5′-A TTT GCT GGG CTA CGT GGC GCT CTT D-3'
Anchor Strand	-	5′-Q CGC ATC TGT GCG GTA TTT CAC TTT B-3′
Low Force Hairpin	2.4 pN	5′-GTG AAA TAC CGC ACA GAT GCG TTT CGA TAA CTT TTT TTT TTT TTT TTT TTT TTT TTG TTA TCG TTT AAG AGC GCC ACG TAG CCC AGC-3
Low Force Tension Threshold Probe	~2 pN	5′-GTG AAA TAC CGC ACA GAT GCG TTT CGA TAA CTT TTT TTT TTT rCrCrC TTT TTT TTT TTG TTA TCG TTT AAG AGC GCC ACG TAG CCC AGC-3
High Force Hairpin	16.0	5′-GTG AAA TAC CGC ACA GAT GCG TTT GCG CGC GCG CGC TTT TGC GCG CGC GCG CTT TAA GAG CGC CAC GTA GCC CAG C-3′
Low Force Complement	-	5'-AAA CGA TAA CAA AAA AAA AAA AAA AAA AAA AAA AAG TTA TCG AAA-3′

Table 4.2. Sequences of oligonucleotides used to construct the DNA hairpin tension sensor. Underlined portions of the sequence indicate the hairpin regions. Abbreviations used: A, alkyne; D, donor fluorophore; Q, quencher molecule; B, biotin moiety.

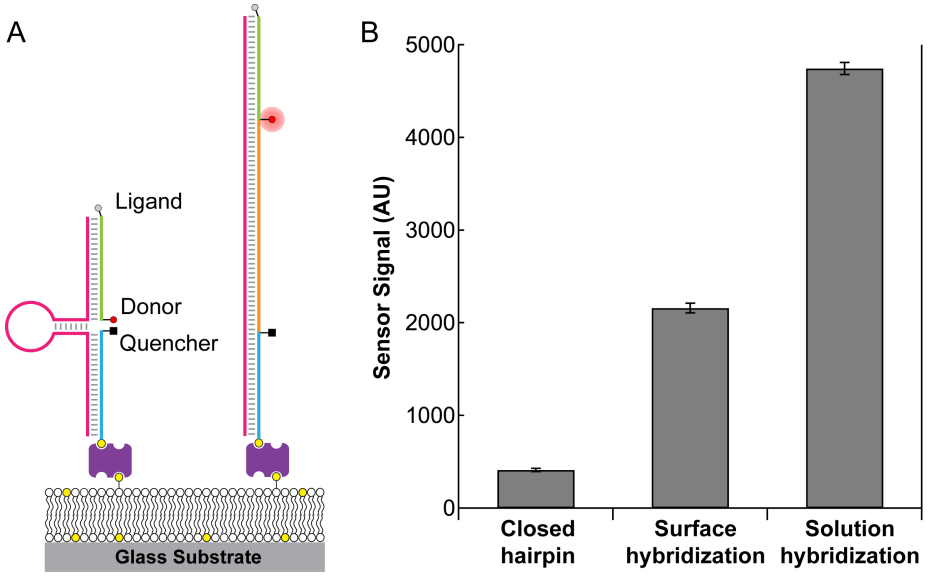

Figure 4.13. Opening of DNA hairpin DLL4 tension sensor. (A) Scheme of the DNA hairpin based tension sensor on a supported membrane. (B) Bar graph showing hairpin sensor response to opening with the complementary strand (orange in A). In this case, the hairpin strand had an $F_{1/2}$ value of ~2.4 pN. Error bars indicate the standard deviation of intensity from sampling at least 5 different areas of one surface.

Similar to the PEG-based sensor, the binding capability of the DLL4-DNA conjugate was verified on a supported membrane platform as shown in **Fig 4.14** *A*. While colocalization of the ligand and receptor signal was observed, the affinity was reduced due to the presence of ligand strand without DLL4 conjugated. As previously discussed, the tension applied to the DNA hairpin sensor before separation of donor and quencher is tuned by the sequence of the hairpin strand. The magnitude of applied force of the Notch expressing cells is unknown, therefore, two different hairpins were tested: 2.4 pN and 16 pN. When the DNA hairpin sensor was immobilized, ligand-receptor binding was still observed, however, there was no observable tension signal, **Fig. 4.14** *B* and *C*. To

promote tension signal, media was pipetted near ligand-bound cells to introduce turbulent flow and foster opening of the hairpin sensor, but no signal was noted. During this process, most cells detached from the surface indicating that the ligand and receptor dissociate before the sensor unfolds, **Fig. 4.15**. This result corroborates previous data that the tension threshold for activation is very low. Interestingly, activation of the Notch signaling pathway was verified for both surfaces containing non-mobile hairpin sensors using a Notch reporter cell line. The 2.4 pN hairpin sensor response was 7.0 fold over the DAPT control, and the 16 pN hairpin was 5.9 fold over the control. This result confirms that receptor proteolysis does occur and releases the NICD with the hairpin sensor present, but the cell-generated tension is not observed on an individual cell basis.

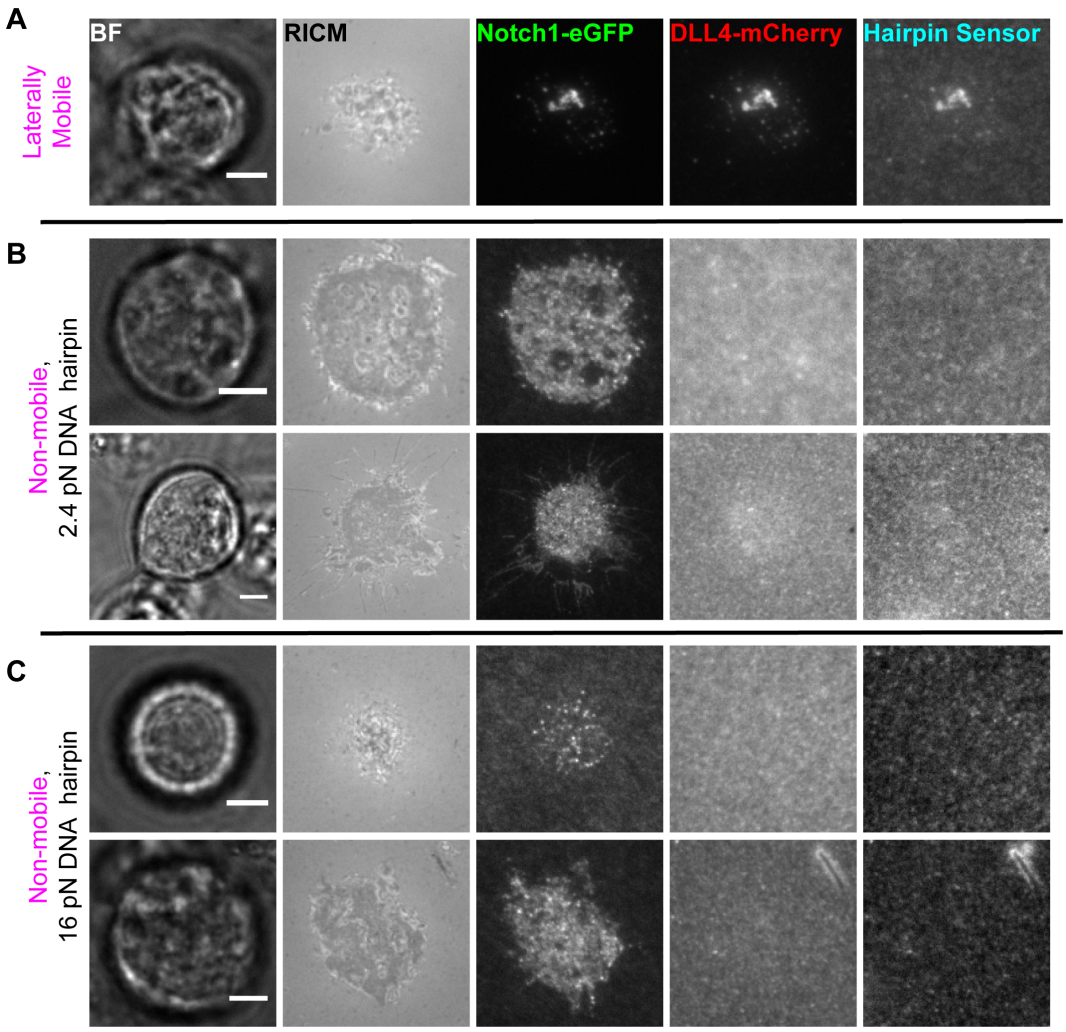

Figure 4.14. Representative images of Notch1-eGFP cells binding to DLL4-mCherry hairpin sensor. (A) When the sensor is tethered to a supported membrane and is laterally mobile, the cells bind and cluster ligand as expected. (B) Images of cells binding to non-mobile DLL4 sensor using a 2.4 pN hairpin sequence. (C) Same as (B) except the hairpin has an $F_{1/2}$ of 16 pN. Scale bar represents 5 μm.

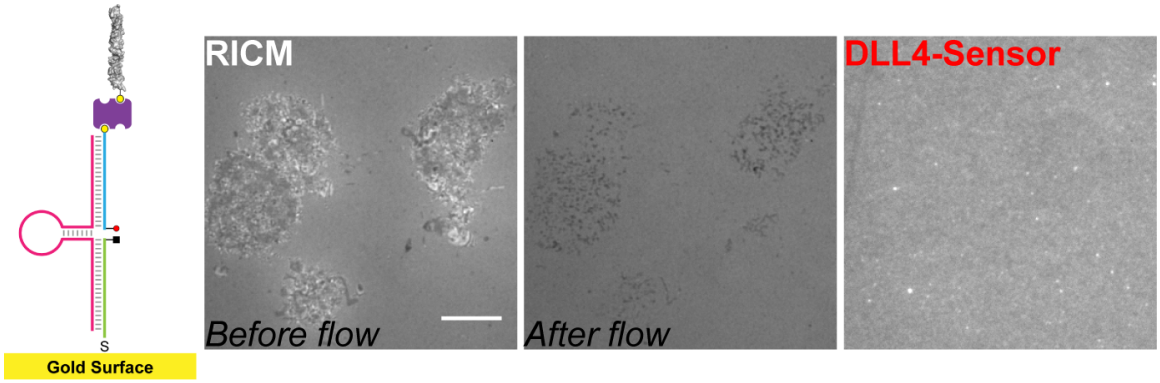

Figure 4.15. Use of turbulent flow to open the DNA hairpin sensor. The DNA hairpin sensor is tethered to the surface as depicted in the scheme. RICM images before and after the application of flow reveal cell detachment with no observable tension sensor signal.

As mentioned above, one possible reason for no tension signal could arise from a transient or rapid proteolysis event. To increase the likelihood of observing cell exerted tension, the Notch1 expressing cells were treated with a broad spectrum metalloprotease inhibitor, BB94. The rationale was that with this treatment the Notch receptor would continuously attempt to bind and pull the ligand molecule but would be unable to catalyze S2 cleavage. It appears that cell behavior was not affected by the presence of the BB94 and did not reveal any concealed tension signal, **Fig. 4.16**.

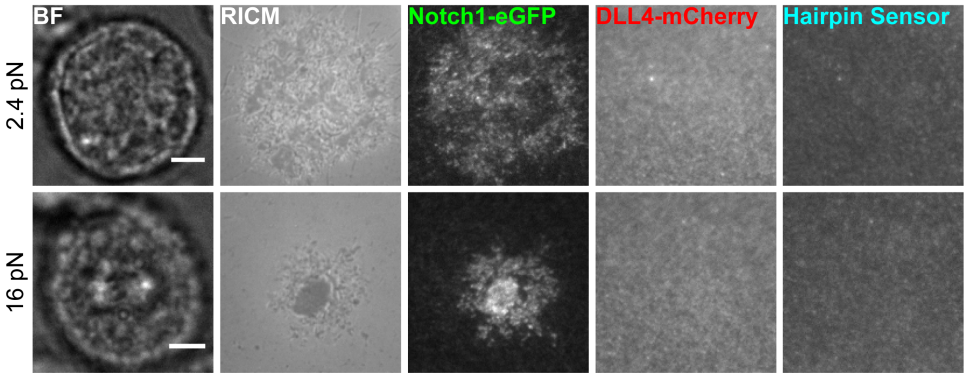

Figure 4.16. Notch1-eGFP expressing cells were treated with a metalloprotease inhibitor to block S2 cleavage. (Top row) Cells were seeded onto a non-mobile DLL4-mCherry ligand modified with a 2.4 pN DNA hairpin sensor. (Bottom row) Same as top panel

except DNA hairpin sensor was hybridized with a 16 pN hairpin. Scale bar represents 5 μm.

One important improvement made to the DNA hairpin tension sensor design was to eliminate any fluorescence signal not associated with the donor-quencher pair. The DLL4-mCherry ligand was used for initial experiments because the fluorescent tag facilitated expression, purification and visualization of the ligand on the surface. However, the spectral profile of mCherry overlaps with the ideal donor molecule, Cy3B. Therefore, mCherry was removed from the ligand sequence, and this version of the ligand was subsequently ligated to the Cy3B labeled ligand strand. The biological functionality of the ligand was confirmed with binding and clustering of the receptor on a supported membrane using a tethered, biotinylated DLL4, **Fig. 4.17**. Successful modification of the ligand strand with DLL4 was also observed, **Fig. 4.17**. This version of the tension sensor will be tested after removal of free (non-ligated) Cy3B DNA from the reaction mixture.

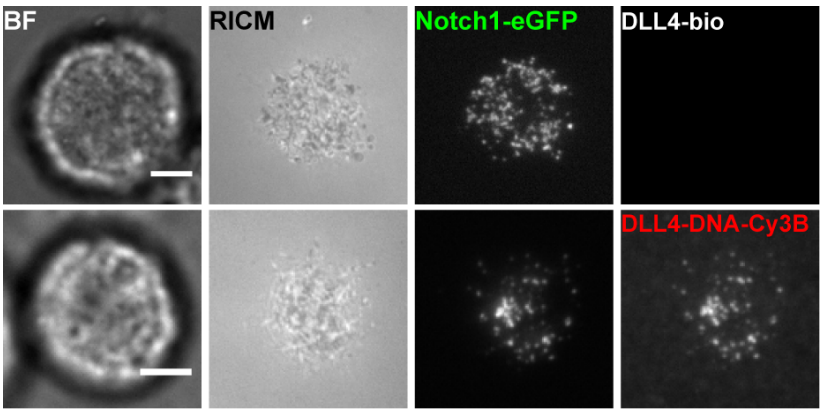

Figure 4.17. Comparison of Notch1-eGFP cell binding to different types of expressed DLL4 ligand functionalized onto a fluid 0.1 mol% biotin DPPE supported lipid membrane. (Top row) DLL4-biotin ligand was modified with biotin ligase reaction to site-specifically introduce a biotin moiety at the C-terminus. This ligand does not contain the mCherry fluorescent protein. (Bottom row) DLL4-DNA-Cy3B is a protein-DNA conjugate produced from Sortase-mediated ligation of DLL4 ligand containing the

Sortase A motif and polyglycine modified Cy3B labeled DNA. Scale bar represents 5 μm.

4.4 Conclusions

In summary, the overall goal of this work was to determine the role of force on Notch receptor activation. Currently, the data suggest that the force exerted by Notch receptors at the cell surface is either very low or does not exist. Regardless of the type of sensor used, tension was not observed. This opens up the possibility for the development of a new sensor that is more sensitive in the low pN regime. However, it may be difficult to push the boundary much lower because thermal fluctuations begin to play an important role at such low force (for example, spontaneous hairpin opening or PEG extension can occur). One strategy presently being pursued is the design of a tension threshold sensor (see **Table 4.2**), which leads to a permanent fluorescence signal when the cell pulls the ligand strand and does not return. This can be achieved by modifying the DNA hairpin to include RNA bases in the loop region that are readily cleaved by RNase A, **Fig. 4.18**. Ultimately, a conformational change of the Notch receptor must take place, and it is just a matter of time before this event can be captured in real-time.

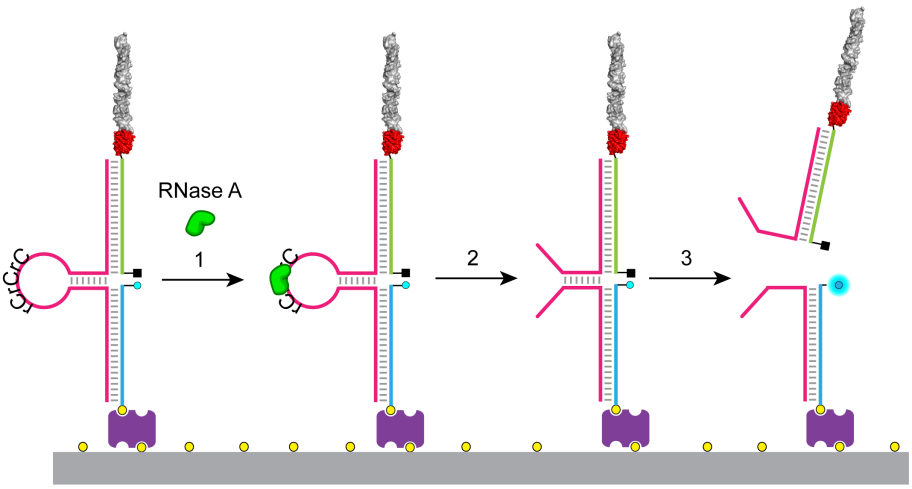

Figure 4.18. Scheme of tension threshold sensor. (1) The DNA hairpin is modified to contain several RNA bases. RNase A is added to selectively cleave the single stranded RNA in the hairpin. (2) After cleavage, the hairpin sensor is only held together by the DNA base pairs within the stem region. (3) Cell applied force will result in permanent loss of the ligand strand and the top half of the hairpin.

4.5 Materials and methods

4.5.1 Expression of DLL4 ligands

Each DLL4 ligand was expressed using a baculovirus expression vector system specifically designed for eukaryotic expression of recombinant proteins from BD Biosciences (San Diego, CA). The protein of interest was cloned into pVL1393, a baculovirus transfer vector, amplified and isolated for further use. A T25 flask of *Sf9* insect cells was grown at 27 °C in Sf-900 II media (Life Technologies, Grand Island, NY) supplemented with 10% fetal bovine serum (Corning, Manassas, VA) until reaching 50-70% confluency. After removing the growth media, the insect cells were treated with 1 mL of Transfection Buffer A (BD Biosciences). To generate DNA complexes, 5 µg of pVL1393-DLL4 vector and 0.5 µg of linearized baculovirus were combined for 5 min and mixed with 1 mL of Transfection Buffer B. The DNA solution was added dropwise onto the *Sf9* cells and incubated for 4 h at 27 °C. After 4 h, the cells were gently rinsed

with growth media and cultured for 4 days. Only successful recombination results in the production of viable virus and over-expression of the protein of interest. The virus was collected and further amplified by addition of 1.5 mL of the collected supernatant to a T225 flask of *Sf9* cells. Generally, one round of viral amplification is sufficient for proceeding to the protein expression phase, but if expression levels are low a second round of amplification may be required.

To isolate recombinant DLL4 ligand, 5 x T225 flasks of *Sf9* cells were cultured to 50-70% confluency and infected with 1.5 mL of the amplified viral stock. After 5 days, the cells and supernatant were collected and spun down at 4500 g. DLL4 ligand molecules were secreted and purified from the conditioned media (~200 mL) using the C-terminal deca-histidine tag. Briefly, 8 mL of Ni-NTA agarose (Qiagen, Valencia, CA) slurry was added to the conditioned media and placed onto a rocker for 1 h at 4°C. The agarose was rinsed with 2 x 10 mL of wash buffer (50 mM NaH_2PO_4, 300 mM NaCl, 20 mM imidazole, pH 8.0) and eluted with 2 x 10 mL of elution buffer (same as wash except with 250 mM imidazole). The eluted protein was concentrated and buffer exchanged into 1 x PBS or other suitable storage buffer using an Amicon Ultra-15 10 kDa filter (Millipore, Billerica, MA). All cloning and sequencing services were provided courtesy of Dr. Oskar Laur of the Emory Custom Cloning Core Facility.

4.5.2 Genetically encoded tension sensor

The genetically encoded tension sensor was obtained from Reference 36. The plasmid was acquired from Addgene #26021. Only the linker region $(GPGGA)_8$ from the tension sensor module (TSMod) was inserted into the DLL4 ligand as the CFP-YFP pair was not appropriate for the current experimental set-up.

4.5.3 Semi-synthetic tension probe

Solid phase peptide synthesis of PEG constructs including Cys-PEG_{24}-biotin, GGG-PEG_{24}-QSY9-biotin and GGGG-azide was completed by Yuan Chang. Modified DNA strands were obtained from IDT (Coralville, Iowa) and fluorophore/quencher coupling reactions were completed by Yun Zhang. Details on the preparation of covalently functionalized glass surfaces can be found in Chapter 3.

4.5.3.1 Expression and purification of mCherry α-thioester

To generate the C-terminal mCherry α-thioester, the fluorescent protein sequence was cloned into pTXB1 (New England Biolabs, Ipswich, MA). Importantly, the C-terminal residue immediately upstream of the intein cleavage site was alanine. This is critical for achieving efficient cleavage of the thioester from the chitin beads. The plasmid was transformed into BL21(DE3) and a single colony was used to inoculate a 5 mL culture of LB containing 100 μg/mL ampicillin. A 500 mL solution of 2 xYT media was inoculated with the 5 mL overnight culture and incubated at 37 °C until the OD_{600} reached 0.5. Protein expression was induced with IPTG at a final concentration of 0.3 mM, and the temperature was lowered to 30 °C for 3-6 h. The cells were centrifuged at 4000 g for 30 min at 4 °C, and the pellets were stored overnight at -80 °C. It is important to note that production of eGFP produces a green cell pellet, but expression of mCherry does not produces a reddish-purple pellet. The distinctive color does not appear until hours after cell lysis when the protein has had enough time to properly fold.

The cells pellets were resuspended in 20 mL of lysis buffer (50 mM Na_2HPO_4, 250 mM NaCl, 1 mM EDTA, 0.1% Triton X-100, pH 8.0) including 80 μl of protease inhibitor cocktail (Sigma, St. Louis, MO). A probe sonicator was used to lyse the cells

(total time 4 min, on for 10 s, off for 20 s). The lysate was clarified by spinning at 23,400 g for 30 min at 4 °C. During this time, the column was loaded with 10 mL of chitin bead slurry and washed with 10 column volumes (CVs) of wash buffer (50 mM Na_2HPO_4, 250 mM NaCl, pH 8.0). The lysate was loaded onto the beads and incubated on the rocker for 1 h at 4 °C. The flowthrough was collected and the column was washed with 20 CVs of column buffer followed by 3 CVs of cleavage buffer (50 mM Na_2HPO_4, 250 mM NaCl, 50 mM MESNa, pH 8.0). Lastly, the mCherry was cleaved from the column by incubating with 1 CV of cleavage buffer for 40 h at 4 °C. The purified protein was concentrated and buffer exchanged into PBS before aliquoting and storing at -80 °C. The final concentration of mCherry α-thioester was determined using λ_{max} = 587 nm and ε = 72,000 M^{-1} cm^{-1}.

4.5.3.2 Expressed protein ligation: mCherry a-thioester and Cys-PEG_{24}-biotin

The mCherry α-thioester was concentrated (50 μM) and buffer exchanged into ligation buffer (20 mM potassium phosphate, 50 mM MESNA, 3 mM TCEP, pH 7.5). Cys-PEG_{24}-biotin was added at a final concentration of 0.1-10 mM. The reaction mixture was incubated for 48 h at 4 °C. To purify the reaction, unreacted Cys-PEG_{24}-biotin was removed from the mixture by diafiltration using an Amicon Ultra 0.5 mL 10 kDa filter. The yield of the ligation was analyzed by SDS-PAGE on a 12% separating gel.

4.5.3.3 Expression and purification of Sortase A (SrtA)

Sortase A (SrtA) was expressed in BL21(DE3) competent *E. coli* and purified using the incorporated hexa-histidine tag. A 5 mL culture of LB media with ampicillin (100 μg/mL) was inoculated and grown overnight at 37 °C. A 500 mL solution of LB media with ampicillin was inoculated with the 5 mL overnight culture and grown to an

OD_{600} of approximately 0.6. SrtA expression was induced through the addition of IPTG to a final concentration of 1 mM and incubated for an additional 3 h. The cells were aliquoted and centrifuged at 4000 g for 30 min at 4 °C. The media was removed and the cell pellets were stored overnight at -80 °C.

To lyse the cells, a total of 20 mL of lysis buffer (50 mM NaH_2PO_4, 300 mM NaCl, 10 mM imidazole, pH 8.0) with 80 µl of protease inhibitor cocktail was used to resuspend the cell pellet. A probe sonicator was used to lyse the cells (total time 4 min, on for 10 s, off for 20 s). The lysate was clarified by spinning at 23,400 g for 30 min at 4 °C. To prepare the purification column, 5 mL of the Ni-NTA agarose slurry was rinsed with 5 mL of wash buffer. The clarified lysate was added directly to the agarose and incubated on a rocker for 1 h in the cold room. The column was washed with 25 mL of wash buffer and eluted with 10 mL of elution buffer. The purified SrtA was concentrated and buffer exchanged into 10 mM Tris, 300 mM NaCl, pH 8.0. The final yield was determined by UV-Vis (with an estimated extinction coefficient of 14,440 M^{-1} cm^{-1}) to be ~25-30 mg for a 500 mL culture. The pET-SrtA-ΔN vector was generously provided by Prof. Stefan Lutz.

4.5.3.4 Click chemistry reaction to produce oligoglycine modified DNA

Donor labeled ligand strand was resuspended in a 50 vol% DMSO solution (100 µM) and 2 M triethylammonium acetate, pH 7.0 was added to bring the final concentration to 0.2 M. Tetra-glycine azide (~100 µg) was resuspended in 10 µL of a 50 vol% DMSO solution. The azide and DNA strand were combined with ascorbic acid (0.5 mM) and copper(II)-TBTA solution in 50% DMSO (0.5 mM). The mixture was vortexed and incubated overnight at ambient temperature. The click reaction was stopped by

ethanol precipitation of the DNA using 1 part reaction mixture: 0.1 part 3 M NaCl: 2.5 parts ethanol. The solution was incubated at -20 °C for 30 min and centrifuged at 15,000 rpm for 1 hour at 4 °C. The supernatant was removed and the DNA pellet was dried down and resuspended in water. Addition of the tetra-glycine peptide leads to a 400 amu shift in the DNA peak as seen by MALDI-TOF mass spectrometry. Samples were spotted with 3-hydroxypicolinic acid matrix. Concentrations listed in parentheses are the final molar concentration in the reaction mixture.

4.5.3.5 Sortase mediated ligation: DLL4-mCherry-LPXTG and DNA hairpin

To synthesize the DLL4-DNA conjugate, the DLL4 ligand and SrtA were buffer exchanged into reaction buffer (50 mM Tris, 150 mM NaCl, 10 mM $CaCl_2$, pH 8.0). The tetra-glycine ligand strand was diluted with reaction buffer to a final concentration of 40 μM. This was added to the DLL4 ligand (10 μM) and SrtA (50 μM). The reaction mixture was incubated at 40 °C for 4 h and quenched with EDTA (10 mM). Concentrations listed in parentheses are final molar concentrations in the reaction mixture and reaction conditions are derived from previous work by Levary et al.[56] In order to remove the unligated DNA, the mixture was purified by size exclusion chromotagraphy using a Superdex 200 10/300 GL column (GE Healthcare, Piscataway, NJ) controlled by an ÄKTA FPLC system. Free DNA elutes from the column at a retention volume of 16.7 mL, and the larger DLL4-DNA molecule elutes at 13.6 mL.

4.6 References

1. Chicurel, M. E.; Chen, C. S.; Ingber, D. E., Cellular control lies in the balance of forces. *Curr. Opin. Cell Biol.* **1998,** *10* (2), 232-239.

2. Ingber, D. E., Mechanobiology and diseases of mechanotransduction. *Ann. Med.* **2003,** *35* (8), 564-577.

3. Jaalouk, D. E.; Lammerding, J., Mechanotransduction gone awry. *Nat. Rev. Mol. Cell Biol.* **2009,** *10* (1), 63-73.

4. Engler, A. J.; Sen, S.; Sweeney, H. L.; Discher, D. E., Matrix Elasticity Directs Stem Cell Lineage Specification. *Cell* **2006,** *126* (4), 677-689.

5. Geiger, B.; Spatz, J. P.; Bershadsky, A. D., Environmental sensing through focal adhesions. *Nat. Rev. Mol. Cell Biol.* **2009,** *10* (1), 21-33.

6. Vogel, V.; Sheetz, M., Local force and geometry sensing regulate cell functions. *Nat. Rev. Mol. Cell Biol.* **2006,** *7* (4), 265-275.

7. Tzima, E.; Irani-Tehrani, M.; Kiosses, W. B.; Dejana, E.; Schultz, D. A.; Engelhardt, B.; Cao, G.; DeLisser, H.; Schwartz, M. A., A mechanosensory complex that mediates the endothelial cell response to fluid shear stress. *Nat. Cell Biol.* **2005,** *437* (7057), 426-431.

8. Orr, A. W.; Helmke, B. P.; Blackman, B. R.; Schwartz, M. A., Mechanisms of Mechanotransduction. *Dev. Cell* **2006**.

9. Petit, V.; Thiery, J. P., Focal adhesions: structure and dynamics. *Biol. Cell* **2000,** *92* (7), 477-494.

10. Kim, M.; Carman, C. V.; Springer, T. A., Bidirectional transmembrane signaling by cytoplasmic domain separation in integrins. *Science* **2003,** *301* (5640), 1720-1725.

11. Kanchanawong, P.; Shtengel, G.; Pasapera, A. M.; Ramko, E. B.; Davidson, M. W.; Hess, H. F.; Waterman, C. M., Nanoscale architecture of integrin-based cell adhesions. *Nature* **2010,** *468* (7323), 580-584.

12. Wolfenson, H.; Lavelin, I.; Geiger, B., Dynamic regulation of the structure and functions of integrin adhesions. *Dev. Cell* **2013,** *24* (5), 447-458.

13. del Rio, A.; Perez-Jimenez, R.; Liu, R.; Roca-Cusachs, P.; Fernandez, J. M.; Sheetz, M. P., Stretching single talin rod molecules activates vinculin binding. *Science* **2009,** *323* (5914), 638-641.

14. Liu, Z.; Tan, J. L.; Cohen, D. M.; Yang, M. T.; Sniadecki, N. J.; Ruiz, S. A.; Nelson, C. M.; Chen, C. S., Mechanical tugging force regulates the size of cell–cell junctions. *Proc. Natl. Acad. Sci. U. S. A.* **2010**.

15. Ladoux, B.; Anon, E.; Lambert, M.; Rabodzey, A.; Hersen, P.; Buguin, A.; Silberzan, P.; Mège, R.-M., Strength dependence of cadherin-mediated adhesions. *Biophys. J.* **2010,** *98* (4), 534-542.

16. Leckband, D. E.; le Duc, Q.; Wang, N.; de Rooij, J., Mechanotransduction at cadherin-mediated adhesions. *Curr. Opin. Cell Biol.* **2011,** *23* (5), 523-530.

17. Yonemura, S.; Wada, Y.; Watanabe, T.; Nagafuchi, A.; Shibata, M., α -Catenin as a tension transducer that induces adherens junction development. *Nat. Cell Biol.* **2010,** *12* (6), 533-542.

18. le Duc, Q.; Shi, Q.; Blonk, I.; Sonnenberg, A.; Wang, N.; Leckband, D.; de Rooij, J., Vinculin potentiates E-cadherin mechanosensing and is recruited to actin-anchored sites within adherens junctions in a myosin II–dependent manner. *J. Cell Biol.* **2010**.

19. Phillips, R.; Ursell, T.; Wiggins, P.; Sens, P., Emerging roles for lipids in shaping membrane-protein function. *Nature* **2009,** *459* (7245), 379-385.

20. Haswell, E. S.; Phillips, R.; Rees, D. C., Mechanosensitive channels: what can they do and how do they do it? *Structure* **2011,** *19* (10), 1356-1369.

21. Kung, C.; Martinac, B.; Sukharev, S., Mechanosensitive channels in microbes. *Annu. Rev. Microbiol.* **2010**.

22. Ingber, D. E., Cellular mechanotransduction: putting all the pieces together again. *FASEB J.* **2006,** *20* (7), 811-827.

23. Pan, B.; Géléoc, G. S.; Asai, Y.; Horwitz, G. C.; Kurima, K.; Ishikawa, K.; Kawashima, Y.; Griffith, A. J.; Holt, J. R., TMC1 and TMC2 Are Components of the Mechanotransduction Channel in Hair Cells of the Mammalian Inner Ear. *Neuron* **2013,** *79* (3), 504-515.

24. Bustamante, C.; Macosko, J. C.; Wuite, G. J., Grabbing the cat by the tail: manipulating molecules one by one. *Nat. Rev. Mol. Cell Biol.* **2000,** *1* (2), 130-136.

25. Neuman, K. C.; Nagy, A., Single-molecule force spectroscopy: optical tweezers, magnetic tweezers and atomic force microscopy. *Nat. Methods* **2008,** *5* (6), 491-505.

26. Brenner, M. D.; Zhou, R.; Ha, T., Forcing a connection: impacts of single-molecule force spectroscopy on in vivo tension sensing. *Biopolymers* **2011,** *95* (5), 332-344.

27. Ahimou, F.; Mok, L.-P.; Bardot, B.; Wesley, C., The adhesion force of Notch with Delta and the rate of Notch signaling. *J. Cell Biol.* **2004,** *167* (6), 1217-1229.

28. Stephenson, N. L.; Avis, J. M., Direct observation of proteolytic cleavage at the S2 site upon forced unfolding of the Notch negative regulatory region. *Proc. Natl. Acad. Sci. U. S. A.* **2012,** *109* (41), E2757-65.

29. Grier, D. G., A revolution in optical manipulation. *Nature* **2003,** *424* (6950), 810-816.

30. Shergill, B.; Meloty-Kapella, L.; Musse, A. A.; Weinmaster, G.; Botvinick, E., Optical tweezers studies on notch: single-molecule interaction strength is independent of ligand endocytosis. *Dev. Cell* **2012,** *22* (6), 1313-1320.

31. Meloty-Kapella, L.; Shergill, B.; Kuon, J.; Botvinick, E.; Weinmaster, G., Notch ligand endocytosis generates mechanical pulling force dependent on dynamin, epsins, and actin. *Dev. Cell* **2012,** *22* (6), 1299-1312.

32. Smith, S. B.; Finzi, L.; Bustamante, C., Direct mechanical measurements of the elasticity of single DNA molecules by using magnetic beads. *Science* **1992,** *258* (5085), 1122-1126.

33. Strick, T. R.; Croquette, V.; Bensimon, D., Single-molecule analysis of DNA uncoiling by a type II topoisomerase. *Nature* **2000,** *404* (6780), 901-904.

34. Clegg, R. M., Fluorescence resonance energy transfer and nucleic acids. *Methods Enzymol.* **1992,** *211*, 353-388.

35. Wu, P.; Brand, L., Resonance energy transfer: methods and applications. *Anal. Biochem.* **1994,** *218* (1), 1-13.

36. Piston, D. W.; Kremers, G.-J., Fluorescent protein FRET: the good, the bad and the ugly. *Trends Biochem. Sci* **2007,** *32* (9), 407-414.

37. Grashoff, C.; Hoffman, B. D.; Brenner, M. D.; Zhou, R.; Parsons, M.; Yang, M. T.; McLean, M. A.; Sligar, S. G.; Chen, C. S.; Ha, T.; Schwartz, M. A., Measuring mechanical tension across vinculin reveals regulation of focal adhesion dynamics. *Nature* **2010,** *466* (7303), 263-266.

38. Borghi, N.; Sorokina, M.; Shcherbakova, O. G.; Weis, W. I.; Pruitt, B. L.; Nelson, W. J.; Dunn, A. R., E-cadherin is under constitutive actomyosin-generated tension that is increased at cell-cell contacts upon externally applied stretch. *Proc. Natl. Acad. Sci. U. S. A.* **2012,** *109* (31), 12568-12573.

39. Stabley, D. R.; Jurchenko, C.; Marshall, S. S.; Salaita, K. S., Visualizing mechanical tension across membrane receptors with a fluorescent sensor. *Nat. Methods* **2012,** *9* (1), 64-67.

40. Liu, Y.; Yehl, K.; Narui, Y.; Salaita, K. S., Tension sensing nanoparticles for mechano-imaging at the living/nonliving interface. *J. Am. Chem. Soc.* **2013,** *135* (14), 5320-5323.

41. Shroff, H.; Reinhard, B. M.; Siu, M.; Agarwal, H.; Spakowitz, A.; Liphardt, J., Biocompatible force sensor with optical readout and dimensions of 6 nm3. *Nano Lett.* **2005,** *5* (7), 1509-1514.

42. Albrecht, C.; Blank, K.; Lalic-Mülthaler, M.; Hirler, S.; Mai, T.; Gilbert, I.; Schiffmann, S.; Bayer, T.; Clausen-Schaumann, H.; Gaub, H. E., DNA: a programmable force sensor. *Science* **2003,** *301* (5631), 367-370.

43. Tarsa, P. B.; Brau, R. R.; Barch, M.; Ferrer, J. M.; Freyzon, Y.; Matsudaira, P.; Lang, M. J., Detecting force-induced molecular transitions with fluorescence resonant energy transfer. *Angew. Chem. Int. Ed.* **2007,** *46* (12), 1999-2001.

44. Wang, X.; Ha, T., Defining single molecular forces required to activate integrin and notch signaling. *Science* **2013,** *340* (6135), 991-994.

45. Zhang, Y.; Salaita, K. S., DNA-based "Digital" pN-range Tension Probes Reveal Early Cell Adhesion Mechanics at the Single Molecule Level. *Submitted*. **2013**.

46. Parks, A.; Klueg, K. M.; Stout, J.; Muskavitch, M. A., Ligand endocytosis drives receptor dissociation and activation in the Notch pathway. *Development* **2000,** *127* (7), 1373-1385.

47. Wang, W.; Struhl, G., Drosophila Epsin mediates a select endocytic pathway that DSL ligands must enter to activate Notch. *Development* **2004,** *131* (21), 5367-5380.

48. Le Borgne, R.; Bardin, A.; Schweisguth, F., The roles of receptor and ligand endocytosis in regulating Notch signaling. *Development* **2005,** *132* (8), 1751-1762.

49. Evans, T.; Benner, J.; Xu, M., Semisynthesis of cytotoxic proteins using a modified protein splicing element. *Protein Sci*. **1998,** *7* (11), 2256-2264.

50. Demain, A. L.; Vaishnav, P., Production of recombinant proteins by microbes and higher organisms. *Biotechnol. Adv*. **2009,** *27* (3), 297-306.

51. Muralidharan, V.; Muir, T. W., Protein ligation: an enabling technology for the biophysical analysis of proteins. *Nat. Methods* **2006,** *3* (6), 429-438.

52. Singla, N.; Himanen, J. P.; Muir, T. W.; Nikolov, D. B., Toward the semisynthesis of multidomain transmembrane receptors: modification of Eph tyrosine kinases. *Protein Sci*. **2008,** *17* (10), 1740-1747.

53. Mazmanian, S. K.; Liu, G.; Ton-That, H.; Schneewind, O., Staphylococcus aureus sortase, an enzyme that anchors surface proteins to the cell wall. *Science* **1999,** *285* (5428), 760-763.

54. Tsukiji, S.; Nagamune, T., Sortase-mediated ligation: a gift from Gram-positive bacteria to protein engineering. *ChemBioChem* **2009,** *10* (5), 787-798.

55. Sancheti, H.; Camarero, J. A., "Splicing up" drug discovery. Cell-based expression and screening of genetically-encoded libraries of backbone-cyclized polypeptides. *Adv. Drug Delivery Rev.* **2009,** *61* (11), 908-917.

56. Levary, D. A.; Parthasarathy, R.; Boder, E. T.; Ackerman, M. E., Protein-protein fusion catalyzed by sortase A. *PLoS One* **2011,** *6* (4), e18342.

57. Schroeter, E. H.; Kisslinger, J. A.; Kopan, R., Notch-1 signalling requires ligand-induced proteolytic release of intracellular domain. *Nature* **1998,** *393* (6683), 382-386.

58. Woodside, M. T.; Behnke-Parks, W. M.; Larizadeh, K.; Travers, K.; Herschlag, D.; Block, S. M., Nanomechanical measurements of the sequence-dependent folding landscapes of single nucleic acid hairpins. *Proc. Natl. Acad. Sci. U. S. A.* **2006,** *103* (16), 6190-6195.

59. Liphardt, J.; Onoa, B.; Smith, S. B.; Tinoco, I.; Bustamante, C., Reversible unfolding of single RNA molecules by mechanical force. *Science* **2001,** *292* (5517), 733-737.

Chapter 5: Conclusions and Perspectives

5.1 Summary

At first glance, the Notch signaling pathway appears extraordinarily simple, a pathway where a portion of the receptor (NICD) itself becomes the transcription factor. There are no known secondary messengers, yet activation of the Notch receptor controls a wide array of cellular functions. For this to be possible, the receptor must be incredibly sensitive to its physical environment and developmental state. Unlike traditional signaling paradigms, our group and others have hypothesized that the Notch receptor couple external mechanical cues to chemical signaling within the cell. To test this hypothesis, a new method was developed to manipulate the ability of the receptor to organize within the membrane. This strategy was able to overcome many of the limitations introduced through the use of e-beam nanopatterned grids. A supported lipid membrane platform was developed to tether Delta ligand and to examine the important factors leading to Notch receptor activation. Intriguingly, reducing the lateral mobility of the DLL4 molecules resulted in higher activation levels for surfaces with equivalent ligand density. Lastly, we searched for evidence of a conformational change in the structure of Notch through the use of different tension sensors. Our current results indicate that the cell applied force is less than 2.4 pN, which is consistent with other experimentally published results.[1]

5.2 Disrupting receptor spatial organization

Based upon the results presented in Chapters 2 and 3, understanding the role of receptor oligomerization in the Notch signaling pathway remains an intriguing biological question. Reducing ligand mobility has a similar effect as inhibiting the ability of the cell to form large clusters, and as discussed in Chapter 3 immobile ligand molecules lead to

enhanced receptor activation. It is reasonable to imagine that diffusion barriers located between areas of laterally mobile ligand would have a similar effect. The preliminary data showed no enhancement in Notch activation for cells located on the nanopatterned grid area. However, the number of cells able to fit on these areas was small, less than 200 per pattern. In order to increase the population of cells on the gridded area, the e-beam pattern was modified to introduce a single pattern of closely spaced lines (2 μm apart) with a total surface area of 1 mm^2, as shown in **Fig. 5.1**. We plan to use these new nanopatterns to take a closer look at how disruption of Notch clustering affects signaling, and we expect enhanced activation from cells on the patterned area.

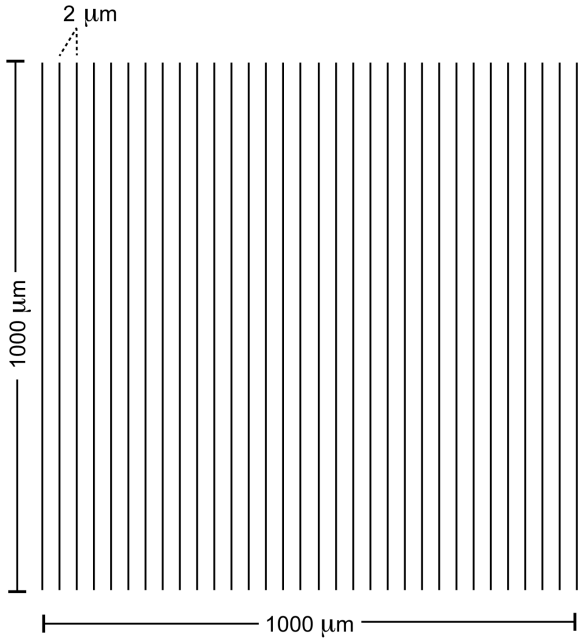

Figure 5.1. Modified e-beam nanopatterned grid. A series of chromium lines spaced 2 μm apart cover a total area of 1 mm^2. The line spacing is not drawn to scale.

5.3 What is the role of force?

Based upon current structural data and MD simulations,[2-6] a large conformational change is necessary to activate the Notch receptor. What remains unknown is how

exactly this change happens – if the structure is unraveled, then which side is pulling? While there is evidence to support that the ligand expressing cell generates force via endocytosis,[7-9] our results show that immobilization of the ligand is enough to lead to pathway activation. Currently, a flipped system is being produced where a fragment of the NECD is tethered to a surface (either on a membrane or directly to a solid support) and interacts with ligand expressing cells. In this case, there is no downstream signaling to observe, but force may be still be visualized using a fluorescent tension sensor. It is possible that the applied force could be highly directional rather simultaneous pulling by both the ligand and receptor.

One of the main challenges in studying the Notch receptor remains how to observe and measure activation. The best approach available is the reporter cell line developed by Sprinzak et al.,[10] but it suffers from several important drawbacks. The first is that the timescale for observing activation is too long. An initial indication of activation can be observed after 24 h, but generally 48 h is needed for full expression of the YFP reporter. This lags far behind transcriptional activation. In our hands, enhancements in Herp2 mRNA levels (a known downstream Notch target) are seen after 90 min of cell incubation, see **Fig 5.2**. This data clearly indicates that following ligand-receptor binding, proteolysis and transcriptional activation are rapid. However, what remains unclear is how much NICD is required to trigger this rapid downstream response. In the ideal circumstance, we would design a cell line that would generate a unique, fluorescent signal immediately upon NICD cleavage at S3. An alternative to this option is to instead use a luciferase complementation-based reporter that was recently developed by the Kopan group.[11] This cell line was obtained but not tested using our experimental

platform. Therefore, it is unclear if the bioluminescent reporter will be sensitive enough for detection on a single cell basis, but it remains a possible solution for quantifying real-time activation levels.

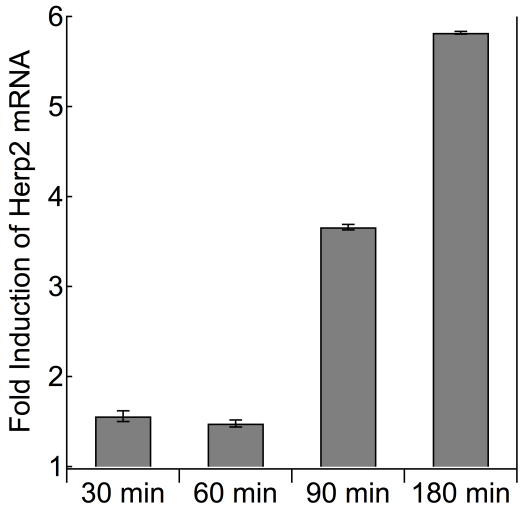

Figure 5.2. Notch activation as measured by RT-PCR. C2C12 cells expressing Notch1-eGFP were plated onto fibronectin surfaces with DLL4/Fc to obtain high levels of Notch activation. mRNA was isolated and quantitative PCR revealed an increase in Herp2 mRNA as a function of time. The maximum fold increase reached was 5.8-fold after 3 hours of surface incubation.

5.4 Future outlook

While the presence of a cell applied force remains elusive, there is still much to learn and understand about the Notch signaling pathway. As discussed in Chapter 4, the possibility that the activation of the Notch receptor is mainly lipid mediated should be considered. In addition, straightforward experiments such as measuring the Delta-Notch binding affinity in a two-dimensions will provide useful insight into the nature of the interaction. Ultimately, our goal is to obtain a molecular and quantitative picture of Notch receptor activation from initial ligand binding through proteolysis and finally transcriptional activation.

5.5 Other contributions and curriculum vitae

Although not specifically discussed in this thesis, I have made additional contributions to different projects within the group. A full list of publications is given below.

- Jurchenko, C.; Chang, Y.; Narui, Y.; Zhang, Y.; Salaita, K. S., Integrin generated forces lead to streptavidin-biotin unbinding in cellular adhesions. *Submitted*. **2013**.
- Narui, Y.; Salaita, K.S., Membrane tethered Delta activates Notch and reveals a role for spatio-mechanical regulation of the signaling pathway, *Biophys. J.* **2013,** *105* (12), 2655-2665.
- Liu, Y.; Yehl, K.; Narui, Y.; Salaita, K. S., Tension sensing nanoparticles for mechano-imaging at the living/nonliving interface. *J. Am. Chem. Soc.* **2013,** *135* (14), 5320-5323.
- Narui, Y.; Salaita, K. S., Dip-pen nanolithography of optically transparent cationic polymers to manipulate spatial organization of proteolipid membranes. *Chem. Sci.* **2012,** *3* (3), 794-799.
- Laroui, H.; Yan, Y.; Narui, Y.; Ingersoll, S. A.; Ayyadurai, S.; Charania, M. A.; Zhou, F.; Wang, B.; Salaita, K. S.; Sitaraman, S. V.; Merlin, D., L-Ala-γ-D-Glu-meso-diaminopimelic acid (DAP) interacts directly with leucine-rich region domain of nucleotide-binding oligomerization domain 1, increasing phosphorylation activity of receptor-interacting serine/threonine-protein kinase 2 and its interaction with nucleotide-binding oligomerization domain 1. *J. Biol. Chem.* **2011,** *286* (35), 31003-31013.

5.6 References

1. Wang, X.; Ha, T., Defining single molecular forces required to activate integrin and notch signaling. *Science* **2013,** *340* (6135), 991-994.

2. Gordon, W. R.; Vardar-Ulu, D.; Histen, G.; Sanchez-Irizarry, C.; Aster, J. C.; Blacklow, S. C., Structural basis for autoinhibition of Notch. *Nat. Struct. Mol. Biol.* **2007,** *14* (4), 295-300.

3. Gordon, W. R.; Roy, M.; Vardar-Ulu, D.; Garfinkel, M.; Mansour, M. R.; Aster, J. C.; Blacklow, S. C., Structure of the Notch1-negative regulatory region: implications for normal activation and pathogenic signaling in T-ALL. *Blood* **2009,** *113* (18), 4381-4390.

4. Tiyanont, K.; Wales, T. E.; Aste-Amezaga, M.; Aster, J. C.; Engen, J. R.; Blacklow, S. C., Evidence for Increased Exposure of the Notch1 Metalloprotease Cleavage Site upon Conversion to an Activated Conformation. *Structure* **2011,** *19* (4), 546-554.

5. Stephenson, N. L.; Avis, J. M., Direct observation of proteolytic cleavage at the S2 site upon forced unfolding of the Notch negative regulatory region. *Proc. Natl. Acad. Sci. U. S. A.* **2012,** *109* (41), E2757-65.

6. Chen, J.; Zolkiewska, A., Force-induced unfolding simulations of the human Notch1 negative regulatory region: possible roles of the heterodimerization domain in mechanosensing. *PLoS One* **2011,** *6* (7), e22837.

7. Parks, A.; Klueg, K. M.; Stout, J.; Muskavitch, M. A., Ligand endocytosis drives receptor dissociation and activation in the Notch pathway. *Development* **2000,** *127* (7), 1373-1385.

8. Wang, W.; Struhl, G., Drosophila Epsin mediates a select endocytic pathway that DSL ligands must enter to activate Notch. *Development* **2004,** *131* (21), 5367-5380.

9. Le Borgne, R.; Bardin, A.; Schweisguth, F., The roles of receptor and ligand endocytosis in regulating Notch signaling. *Development* **2005,** *132* (8), 1751-1762.

10. Sprinzak, D.; Lakhanpal, A.; LeBon, L.; Santat, L. A.; Fontes, M. E.; Anderson, G. A.; Garcia-Ojalvo, J.; Elowitz, M. B., Cis-interactions between Notch and Delta generate mutually exclusive signalling states. *Nature* **2010,** *465* (7294), 86-90.

11. Ilagan, M. X. G.; Lim, S.; Fulbright, M.; Piwnica-Worms, D.; Kopan, R., Real-time imaging of notch activation with a luciferase complementation-based reporter. *Sci. Signal.* **2011,** *4* (181), rs7.